

J.M. PITT
S. SCHLORHOLTZ
R.J. ALLENSTEIN
R.J. HAMMERBERG
TURGUT DEMIREL

SEPTEMBER 1983

FINAL REPORT

CHARACTERIZATION OF FLY ASH FOR USE IN CONCRETE

IOWA DOT PROJECT HR-225
ERI PROJECT 1485
ISU-ERI-AMES-84431

ENGINEERING RESEARCH INSTITUTE
IOWA STATE UNIVERSITY
AMES, IOWA 50011 USA

T. Demirel, Principal Investigator
J.M. Pitt, Principal Investigator
S.M. Schlorholtz, Research Associate
R.J. Allenstein, Research Assistant
R.J. Hammerberg, Research Assistant

FINAL REPORT

Characterization of Fly Ash
for Use in Concrete

Sponsored by the Iowa Department of
Transportation, Highway Division
and the Iowa Highway Research Board.

Iowa DOT Project HR-225
ERI Project 1485
ISU-ERI-Ames 84431

Department of Civil Engineering
Engineering Research Institute
College of Engineering
Iowa State University, Ames, IA

Introduction

Recent construction of new generation power plants burning western coal has within Iowa resulted in fly ash production on the order of 760,000 tons annually. Although fly ash has long been accepted as a valuable replacement for portland cement in concrete, most experience has been with fly ash generated from eastern bituminous coals. A few years ago, fly ash in Iowa was not a significant factor because production was small and economics dictated disposal as the better alternative than construction use. Today, the economic climate, coupled with abundance of the material, makes constructive use in concrete feasible. The problem is, however, fly ash produced from new power plants is different than that for which information was available. It seems fly ash types have outgrown existing standards.

The objective of this study was to develop fundamental information about fly ashes available to construction in Iowa such that its advantages and limitations as replacement to portland cement can be defined. Evaluative techniques used in this work involve sophisticated laboratory equipment, not readily available to potential fly ash users, so a second goal was preliminary development of rapid diagnostic tests founded on fundamental information. Lastly, Iowa Department of Transportation research indicated an interesting interdependency among coarse aggregate type, fly ash and concrete's resistance to freeze-thaw action. Thus a third charge of this research project was to verify and determine the cause for the phenomena.

TABLE OF CONTENTS

INTRODUCTION	i
TECHNIQUES FOR FLY ASH EVALUATION	1-19
Elemental Analysis	1
Quantitative Component Analysis	2
Hydration Reactions	12
EVALUATION OF SOME IOWA FLY ASHES	19-47
Variability in Elemental Composition	22
Crystalline Composition	26
Soundness of Fly Ash Concrete	31
Lime Pozzolanic Activity	37
Heat Evolution Test	42
FLY ASH AND RESISTANCE TO FROST ACTION	48-61
Durability Tests	48
Freeze-Thaw Durability	50
Durability and Pore Structure	58
PORE STRUCTURE EVALUATION	61-91
Mercury Porosimetry	63
Entrained Air in Hardened Mortar	75
Pore Distribution Along Aggregate Edge	80
Surface Activity	88
Flotation Test	89
SUMMARY AND CONCLUSIONS	91-93
RECOMMENDATIONS	94-95
ACKNOWLEDGEMENTS	95
REFERENCES	96-97
APPENDICES	98-138
Appendix A. Elemental Composition of Fly Ash	98
Appendix B. Expansion - Chemical Composition Data	102
Appendix C. Summary of Physical Tests	104
Appendix D. Mercury Porosimetry Data	108

Techniques for Fly Ash Evaluation

One objective of this project was to determine properties of Iowa fly ashes and evaluate their relevance to use of the material as an admixture of portland cement concrete. This phase of the research involved two approaches. The first involved the development of a rapid method for determining quantitative elemental composition while the second was aimed at both qualitative and quantitative determination of compounds.

Elemental Analysis

X-ray fluorescence techniques were adapted for rapid determination of elemental composition of fly ash. The analysis was performed using a Siemens SR-200 sequential x-ray spectrometer controlled by a PDP-11-03 microcomputer. The spectrometer was equipped with a ten sample specimen chamber and four interchangeable analyzing crystals. Unfiltered excitation radiation was generated using a chromium tube at 50 KV and 48 ma. Programs for the spectrometer were developed by the Siemens Corporation.

A sample of Lansing fly ash was selected to develop the fluorescence techniques where a qualitative determination of elements present was performed by determining characteristic wavelengths of fluorescent radiation. Quantitative determination of elements in fly ash was then accomplished by using the Siemens software. The software consists of interactive programs for the automatic operation of the spectrometer data collection and analysis. Programs for calibration and measurement of unknown concentrations are based on a multiple regression

(either quadratic or linear) of the characteristic radiation intensity on concentration. Methodology in the programs also takes into account absorption, enhancement and radiation overlaps as multiple variants and requires use of calibration standards.

To provide dependable results, the range of elemental composition for standards were selected to cover the expected concentrations of elements in unknown samples. Twenty standards prepared by blending six fly ashes of known elemental composition served as a basis for the calibration. The calibration was then checked against a National Bureau of Standards (NBS) fly ash standard and comparative results are shown in Table 1. Table 2 is a comparison of elemental analysis by x-ray fluorescence and conventional chemical analysis for the Lansing fly ash. In both cases it can be seen that the x-ray fluorescence technique offers an accurate assessment of elemental fly ash composition. The development of the fluorescence technique has not only made possible the study of variability and fly ash properties for this project, but has made possible the timely assessment of fly ash used in construction. X-ray fluorescence is now routinely being used to monitor most of Iowa's fly ash production.

Quantitative Component Analysis

A Siemens D-500 computer controlled x-ray diffractometer was used in development of quantitative techniques for determination of crystalline components (minerals) present in fly ash. The diffractometer was equipped with a graphite monochromator. A pulse-height analyzer for efficient monochromatization and monochromatic copper K_{α} radiation were used for all analyses. The diffractometer was

Table 1. Fluorescence Analysis of NBS Fly Ash Standard

	%, Measured	Known, %
Mg	.46	.46 ± .01
Na	.18	.17 ± .01
Fe	9.38	9.40 ± .10
Ti	.77	.80
Si	21.73	22.80 ± .80
Ca	.98	1.11 ± .01
Al	14.06	14
K	1.87	1.88 ± .06

Table 2. Comparison of Elemental Composition of Lansing Fly Ash

Elemental Oxide	Percentage ^a	Percentage ^b
SiO ₂	30.0	32.12
Al ₂ O ₃	19.7	18.06
Fe ₂ O ₃	5.9	5.34
Na ₂ O	1.8	1.77
K ₂ O	0.4	0.36
CaO	31.1	---
MgO	6.2	---
TiO ₂	1.3	---

^aBy x-ray fluorescence

^bASTM C-311 chemical analysis provided by Iowa DOT

controlled with a PDP-11-03 microcomputer. Operating software for the diffractometer was developed by the Siemens Corporation.

The first step in developing a methodology for quantitative assessment of crystalline compounds (minerals) present in fly ash was to qualitatively define mineral composition. This task was accomplished by performing conventional x-ray diffraction analyses on fly ashes from seven Iowa sources and comparing d-spacings with those listed in the Joint Committee on Powder Diffraction Standards (JCPDS) files. The first eight compounds listed in Table 3 are the crystalline components identified in all of the fly ashes and the top chart in Fig. 1 is typical of the x-ray analysis from the Lansing source.

The methodology for quantitative analysis of crystalline components was adapted from that independently developed by Chung (1) and Demirel (1a). This method involves development of a set of standard specimens consisting of compounds present in fly ash along with a reference compound. The reference compound cannot be a constituent of fly ash nor can it react with the host compounds. By mixing known quantities of the reference compound with a fly ash being analyzed and determining integrated x-ray intensities of selected diffraction peaks of the reference compound and the compound of interest. The weight fraction of the compound, W'_c , in the fly ash can be computed from:

$$W'_c = \left[\frac{(I_c/I_r)_{\text{unk.}}}{(I_c/I_r)_{\text{std.}}} \right] \left(\frac{W_c}{W_r} \right)_{\text{std.}} \left(\frac{W'_r}{1-W'_r} \right)_{\text{unk.}} \quad (1)$$

Table 3. Legend for Figures 1 and 2

Component	Abbreviation
Quartz (SiO ₂)	Q
Calcium Oxide (CaO)	C
Magnesium Oxide (MgO)	MgO
Magnetite (Fe ₃ O ₄)	M
Anhydrite (CaSO ₄)	A
Tricalcium Aluminate (Ca ₃ O·Al ₂ O ₆) (C ₃ A)	CA
Calcium Aluminum Sulfate (3CaO·3Al ₂ O ₃ ·CaSO ₄) (C ₄ A ₃ S)	CAS
Mullite (Al ₆ Si ₂ O ₁₃)	ML
Ettringite (6CaO·Al ₂ O ₃ ·3SO ₃ ·32H ₂ O) (C ₆ A ₃ S ₃ H ₃₂)	E
Monosulfoaluminate (Ca ₃ Al ₂ O ₆ ·CaSO ₄ ·13H ₂ O) (C ₄ A ₂ S ₁₃ H)	MSA
Gypsum (CaSO ₄ ·2H ₂ O)	G
Calcite (CaCO ₃)	Ct
Calcium Aluminum Silicate Hydrate (Ca ₂ Al ₂ SiO ₇ ·8H ₂ O)	CASH

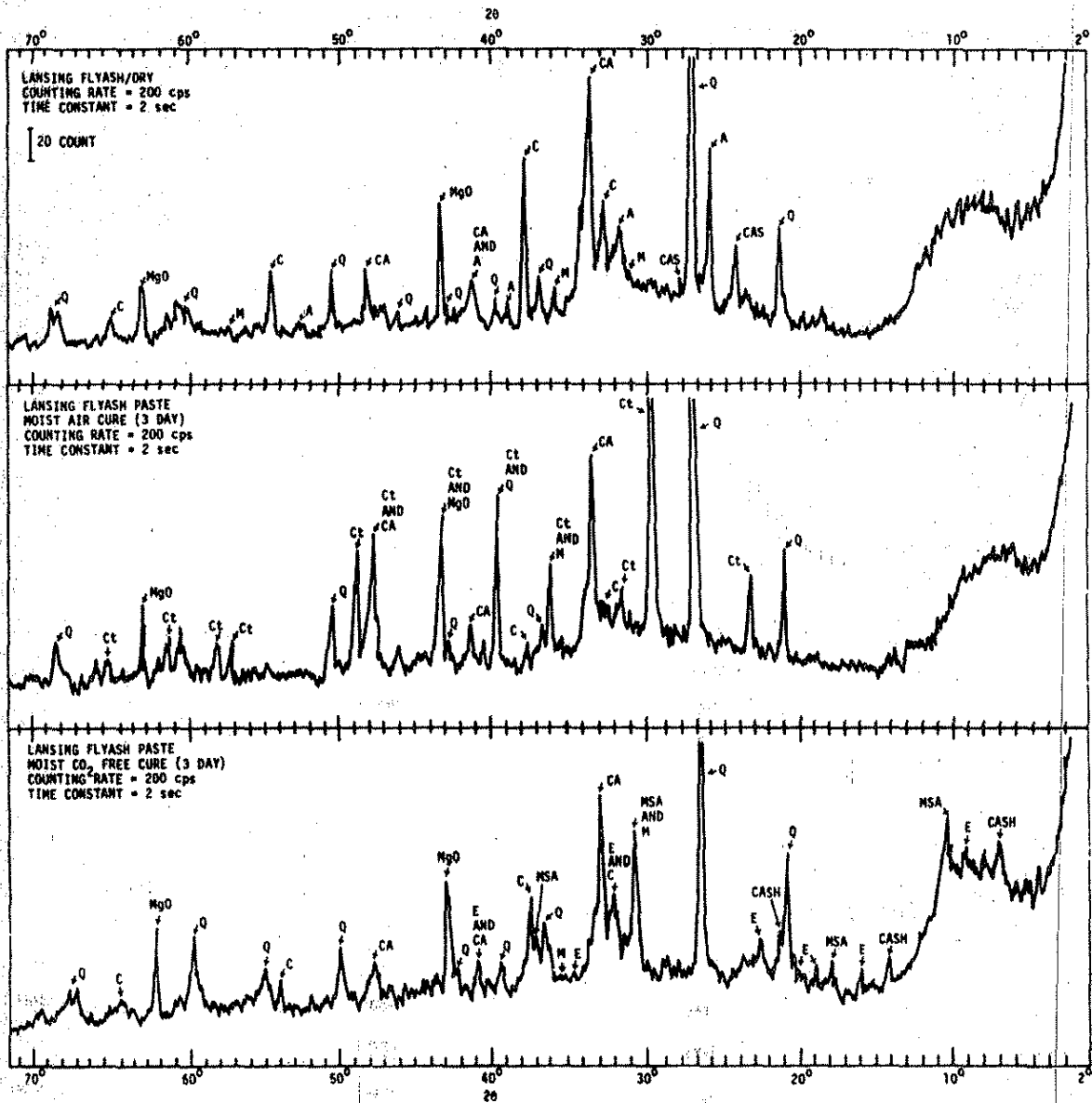


Figure 1. Diffraction Patterns of Lansing Ash
 Under Different Curing Conditions
 (See Table 3 for Legend).

where

$(I_c/I_r)_{\text{unk.}}$ = ratio of integrated intensities of the selected diffraction peaks of the compound of interest, and the reference compound measured from fly ash-reference compound mixture.

$(I_c/I_r)_{\text{std.}}$ = ratio of integrated intensities of the selected diffraction peaks of the compound of interest and the reference compound measured from the standard sample of known composition.

W_c = known weight fraction of the compound of interest contained in the standard sample.

W_r = known weight fraction of the reference compound contained in the standard sample.

W'_r = known weight of reference material added to the fly ash being investigated.

In concept, the application of Equation 1 is relatively simple. A calibration matrix for the x-ray intensity ratios of the standard is established by mixing known quantities of individual compounds known to be present in fly ash with a known quantity of a reference material and measuring integrated intensities of selected diffraction peaks. With such a calibration matrix established, quantities of compounds can be determined by adding a known amount of reference compound to the fly ash being evaluated and measuring integrated intensities of the selected diffraction peaks established during the calibration.

One task requisite to application of this approach to quantitative evaluation of fly ash is finding pure forms of all the constituent compounds required to develop the calibration. A second requisite is finding a reference compound which has no peak overlaps. Assuming the principle of superposition is applicable to peak overlaps, Equation 1 can be used for overlap corrections by making use of integrated intensities of other diffraction peaks. However, such adjustments tend to be cumbersome when interferences occur for several compounds. Among

several compounds tried sodium chloride was found to be the most suitable reference compound for fly ash analysis. Samples for diffraction analysis were prepared by combining measured amounts of sodium chloride with fly ash and then thoroughly mixing and grinding. Samples were pressed into plexiglas sample rings and to reduce the influence of crystal orientation, measurements were taken three times with the samples being rotated by 120 degrees. Integrated intensities were obtained for selected peaks using Siemen's Peak Integration program (2). Results of three determinations were averaged and the integrated intensities thus obtained were used in Equation 1 to compute concentrations.

To provide a check on the validity of this method of analysis two synthetic standards were prepared and analyzed. The results of the quantitative analysis are given in Table 4. Larger differences between known and measured quantities are thought to be due to crystal orientation which can cause an inaccurate intensity measurement, and it is suspected that this error can be reduced through use of the sample spinner which has recently been installed. X-ray diffraction charts of the synthetic standard No. 2 and the obsidian used in preparation are in Fig. 2 while the code for compound identification is the same as that previously presented.

Results of a quantitative compositional analysis of the Lansing fly ash are presented in Table 5. One explanation for the self-cementing properties of this particular fly ash is the fact that it contains a combined 7.5 percent of tricalcium aluminate and calcium aluminum sulfate, both of which are hydraulic cements. A second feature is that crystalline compounds comprise more than 26 percent of this fly ash

Table 4. Results of quantitative component analysis of synthetic standards.

Component	Actual weight percentage		Weight percentage from x-ray analysis	
	Std. No. 1	Std. No. 2	Std. No. 1	Std. No. 2
Tricalcium aluminate ($3\text{CaO}\cdot\text{Al}_2\text{O}_3$) (C_3A)	10.0	3.3	10.3	2.8 ± 0.6
Calcium aluminum sulfate ($3\text{CaO}\cdot 3\text{Al}_2\text{O}_3\cdot\text{CaSO}_4$) ($\text{C}_4\text{A}_3\bar{\text{S}}$)	15.0	5.0	14.8	8.0 ± 0.4
Quartz (SiO_2)	30.0	10.0	39.1	12.2 ± 1.9
Mullite ($\text{Al}_6\text{Si}_2\text{O}_{13}$)	10.0	3.3	9.5	2.5 ± 1.2
Magnetite (Fe_3O_4)	10.0	3.3	10.5	4.8 ± 0.93
Magnesium oxide (MgO)	15.0	5.0	15.5	5.0 ± 0.5
Calcium sulfate (CaSO_4)	5.0	0.0	4.90	0.06 ± 0.08
Calcium oxide (CaO)	5.0	0.0	5.07	0.2 ± 0.03
Glass ^a		67.0		65^b

^a Obsidian from Mt. St. Helens.

^b By difference

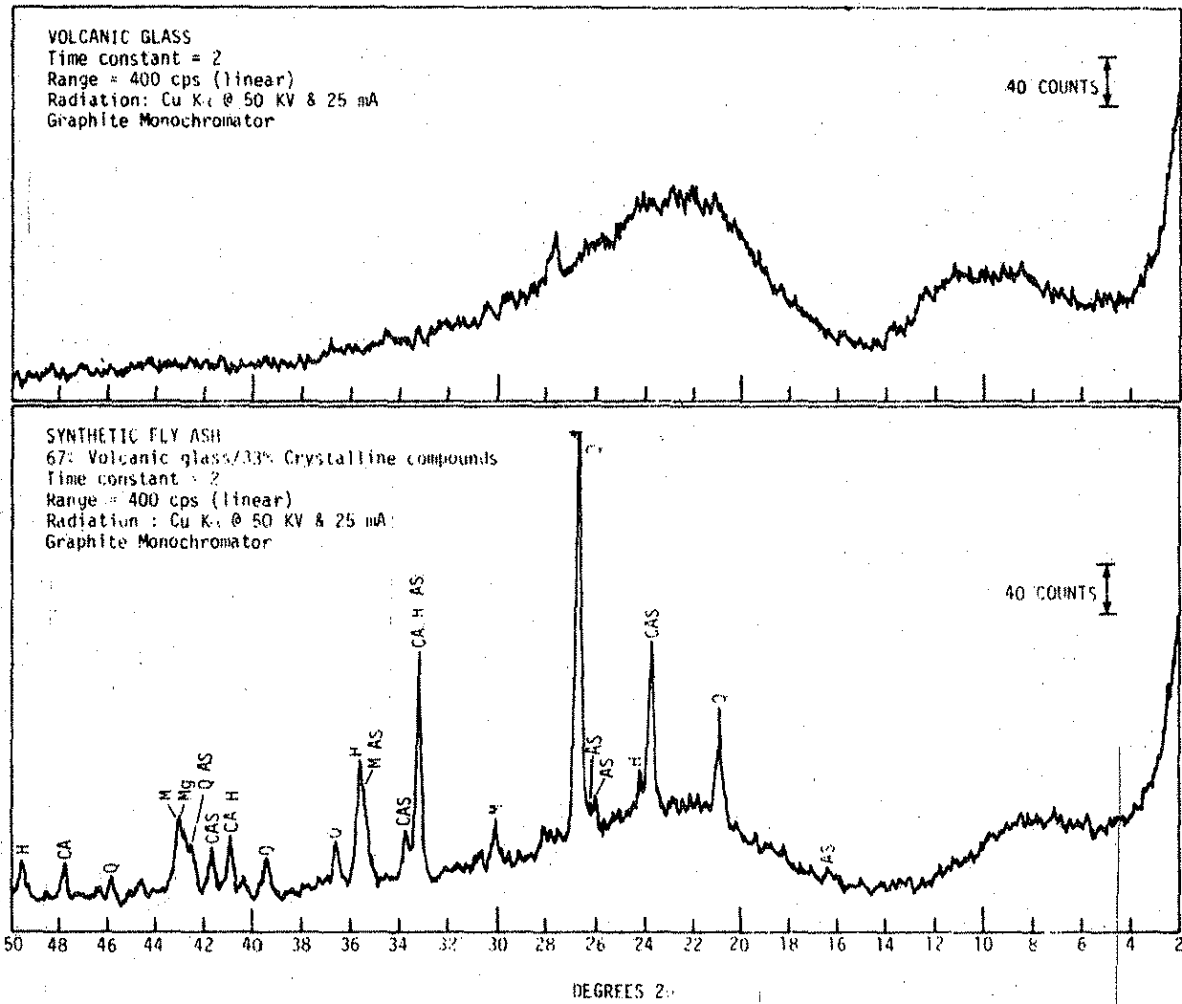


Figure 2. Diffraction Patterns of Synthetic
 Standard No. 2 and the Glassy Component.

Table 5. Crystalline Composition of Lansing Fly Ash

<u>Component</u>	<u>Percent</u>
Tricalcium aluminate (C ₃ A)	5.2
Calcium aluminum sulfate (C ₄ A ₃ S)	2.3
Calcium sulfate (CaSO ₄), (Anhydrite)	1.7
Calcium oxide (CaO)	2.1
Quartz (SiO ₂)	10.1
Mullite (Al ₆ Si ₂ O ₁₃)	0.9
Magnetite (Fe ₃ O ₄)	1.0
Magnesium Oxide (MgO), (Periclase)	2.8
Amorphous Contribution (glass) ^a	73.9

^a Estimated by subtracting sum of crystalline components from the total.

which could have a significant impact on pozzolanic reactions frequently considered to be the essence of fly ash reactions when used as a portland cement additive or in lime-fly ash stabilization of soils. An appreciable amount of this fly ash should contribute nothing to positive or detrimental reactions because about 12 percent of this fly ash are relatively stable compounds such as quartz, mullite, and magnetite. It is interesting to note that this "high-lime" fly ash having an elemental calcium composition expressed as oxide on the order of 30 percent contains only 2.1 percent free calcium oxide. In fact, the total calcium combined in crystalline compounds accounts for about one-sixth of that measured as elemental calcium. The remaining portions should be included in the amorphous phase. Depending on their nature, both free calcium and magnesium oxides could play a role in soundness of portland cement-fly ash concretes.

Hydration Reactions

To provide additional verification of composition and chemical properties of the constituents of a cementitious fly ash, the hydration mechanism of the Lansing fly ash was monitored using the oscillation capacity of the x-ray diffractometer. The oscillation feature allows rapid monitoring of crystalline compound growth and consumption by automatic repetitious scanning of the relevant portions of a diffraction pattern with time. This investigation consisted of preparing fly ash pastes at a 0.26 water/fly ash ratio, placing specimens into x-ray diffraction sample holders and starting the oscillating x-ray diffraction analysis. Extensive analysis was performed on fly ash pastes during the period from two minutes after the ash was mixed with

water until ninety minutes after mixing. Diffraction peaks selected for analysis of each compound are presented in Table 6. To provide information about the behavior of the aluminate compounds, three percent gypsum was added to some samples and to evaluate the behavior of CaO moist air and moist CO₂ free curing environments were used. The CO₂ free curing condition was achieved in a desiccator containing a 20 percent solution of NaOH.

The lower two diffraction patterns in Fig. 1 are for Lansing fly ash after three days curing in both environments and typical segments of oscillation diffraction patterns are in Fig. 3. Table 7 is a summary of the reactions and their status at various times. For each compound, a relative intensity of 100 is assigned to the highest intensity obtained during the period of analysis. A relative intensity of 100 corresponds to the largest amount of the compound present during the period of analysis. All other intensities of that compound are relative to 100 and correspond to its abundances during the hydration process.

Oscillation x-ray diffraction of the Lansing fly ash-water paste showed that calcium oxide was consumed during the period 7 to 38 minutes to a relative intensity of about 60% and then consumption leveled off. (Period refers to the time interval after the addition of water to fly ash.) Diffraction showed no calcium hydroxide formation during the period 2 to 90 minutes. Calcite formed in the period of 7 to 77 minutes and then leveled off. This data suggests that part of the calcite was formed from direct conversion of calcium oxide to calcite without an intermediate hydroxide stage. The atmosphere seemed to be a likely source of carbon dioxide for direct carbonation and proved to be so. This was determined when several samples which were cured in a carbon

Table 6. Diffraction Peaks for Oscillating
X-ray Analysis with Cu-K α Radiation.

Component	Peak selected for analysis	Oscillation range, 2θ (degrees)
Gypsum (CaSO ₄ ·2H ₂ O)	100%, d=7.56	8.5 - 13.5
Calcium Hydroxide (Ca(OH) ₂)	100%, d=2.63	33 - 35
Calcite (CaCO ₃)	100%, d=3.035	27 - 32
Calcium Oxide (CaO)	100%, d=2.405	36.5 - 38.5
Anhydrite (CaSO ₄)	100%, d=3.49	24.5 - 26.5
Calcium Aluminum Sulfate (3CaO·3Al ₂ O ₃ ·CaSO ₄)	100%, d=3.74	22.5 - 24.5
Ettringite (6CaO·Al ₂ O ₃ ·3SO ₃ ·32H ₂ O)	100%, d=9.67	8.5 - 13.5
Monosulfo-Aluminate (Ca ₃ Al ₂ O ₆ ·CaSO ₄ ·13H ₂ O)	100%, d=8.92	8.5 - 13.5
Calcium Aluminum Silicate Hydrate (Ca ₂ Al ₂ SiO ₇ ·8H ₂ O)	d=12.5	6.5 - 8.5

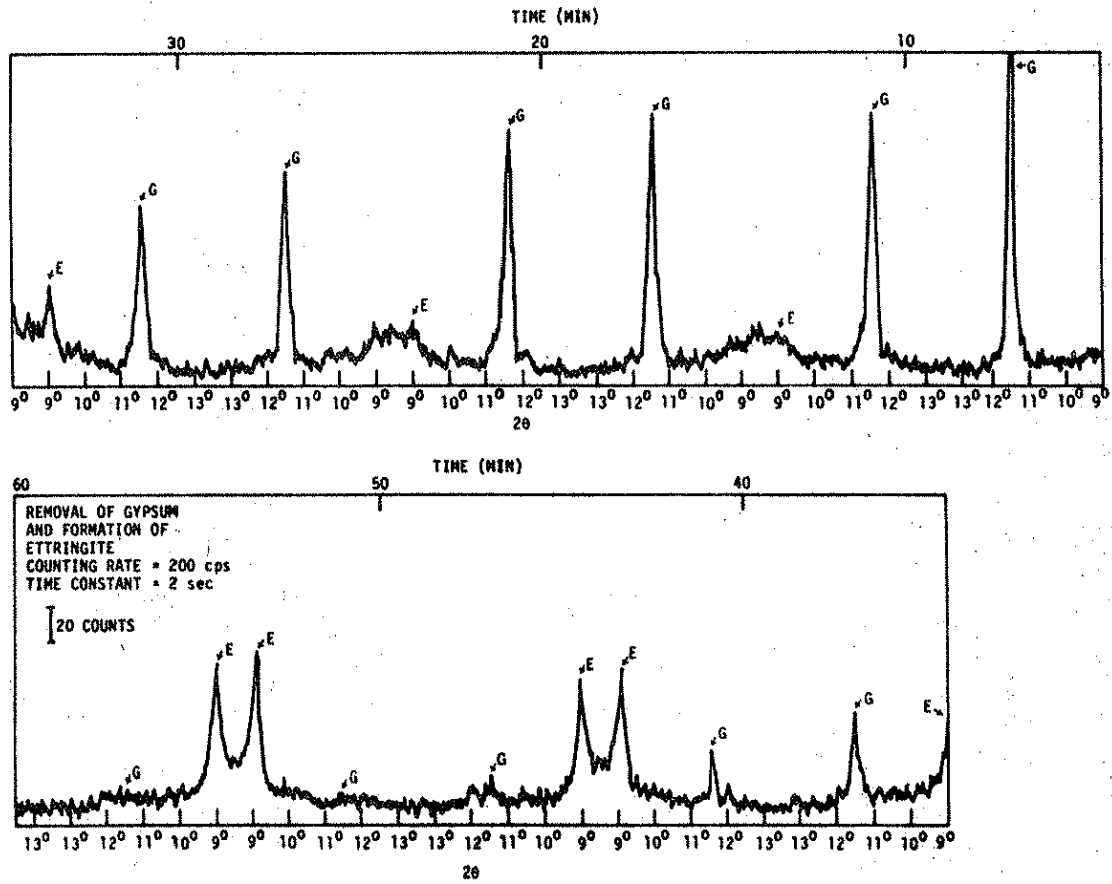


Figure 3. Example of Oscillation Diffraction Pattern

Table 7. Summary of Oscillating X-ray Diffraction Analysis of Lansing Fly Ash.

Reaction	Duration of reaction, min.				Relative amounts, %			
	Without added gypsum		With 3% gypsum added		Without added gypsum		With 3% gypsum added	
	Start	End	Start	End	Start	End	Start	End
Removal of calcium oxide	7	38	11	46	100	60 ^a	100	38
Removal of anhydrite	10	61	14	64	100	12	100	20
Removal of calcium aluminum sulfate	12	88	38	87	100	38	100	19
Formation or removal of gypsum	none	none	7	58	0	0	100	0
Formation of calcite	7	77	16	>90	0	100	0	100
Formation of Ettringite	4	22	13	55	0	100	0	100
Formation of mono sulfo-aluminate	12	58	none	none	0	100	0	0

^a With sample in CO₂ free atmosphere still 100%.

dioxide free environment showed no calcite formation and approximately 100% calcium oxide retention for up to 20 hours. These results also indicate that even after long curing periods a good deal of calcium oxide remains unreacted.

It appears that calcium oxide might react to form a thin shell of calcite on the outer surface of the diffraction sample in ambient conditions. In order to check this hypothesis several inner portions of hydrated fly ash samples were analyzed. These portions had not been directly exposed to the atmosphere and showed no calcite formation. An explanation derived from this data is that free, crystalline CaO exists in some fly ashes in a hard burned form. The exact reason for hard burned behavior is not thoroughly understood but some believe that it is due to glassy coatings formed on CaO particles. However, if this were so, carbonation should also be hindered. During this study some evidence has been obtained, which suggests that a thin carbonate coating on CaO particles may be the cause for the hindered hydration. Such a coating could form in the CO₂ rich atmosphere prevalent in combustion gases. Hard burned lime is known to be a critical component in performance of portland cement and may be equally detrimental for some fly ash applications. Under normal conditions the hydration of hard burned lime proceeds at a very slow rate due to a high diffusion energy barrier and may if present in sufficient quantity produce detrimental expansion in portland cement concrete.

During the oscillation analysis, it was observed that the magnesium oxide in the Lansing fly ash did not hydrate as is evidenced by the diffraction patterns in Fig. 1.

Aluminate hydrates appear to be the key reaction products in the

case of the Lansing fly ash. Oscillation diffraction analysis showed formation of ettringite in the period 4 to 22 minutes, monosulfoaluminate formation in the period of 12 to 58 minutes, and anhydrite removal in the period of 10 to 61 minutes. This seems to represent a good example of portland cement chemistry and can be rationalized as follows. Tricalcium aluminate is present in the fly ash (5.2% by weight) and is very reactive with water. Also present is an internal source of calcium sulfate in the form of anhydrite. When hydration begins the free calcium sulfate content of the paste is high and ettringite begins to form. As the sulfate content decreases, due to consumption by ettringite formation, monosulfoaluminate begins to form and continues to form, at the expense of ettringite formation, until the anhydrite is nearly exhausted. Ettringite formed from 4 to 22 minutes, monosulfoaluminate from 12 to 58 minutes and anhydrite consumption occurred from 10 to 61 minutes. This suggests that the hydration mechanism discussed above is possible. The consumption of tricalcium aluminate is quite important to this mechanism but has not yet been determined due to diffraction peak interference caused by formation of ettringite. The precise reaction mechanism might also be complicated due to the fact that the fly ash contained 2.3% calcium aluminum sulfate which might hydrate directly to ettringite.

Oscillation diffraction analysis was also performed during hydration on the fly ash mixed with 3% gypsum by weight as given in Table 7. The consumption trends of calcium oxide, anhydrite, and calcium aluminum sulfate were quite similar to those of the fly ash without gypsum. The major difference caused by the addition of gypsum was in the formation of the aluminate hydrates. Ettringite formed in

the period 13 to 55 minutes while no monosulfoaluminate was formed within the 90 minute analysis period. The added gypsum was completely consumed in the period 7 to 58 minutes. Relatively twice as much ettringite was formed in the gypsum treated ash compared to the ash without added gypsum. These findings appear to parallel tricalcium aluminate reactions observed in portland cement hydration and can be explained by the fact that gypsum greatly increased the calcium sulfate content of the paste which promoted ettringite formation.

Evaluation of Some Iowa Fly Ashes

Many Iowa fly ashes are produced from western subbituminous coals or lignites and if they are consistent with the observations of others could cover a broad spectrum of chemical composition. Thus the Class C family of fly ashes has prompted concern among concrete users. Seven fly ashes, representing significant sources for the Iowa construction industry, were provided by the Iowa Department of Transportation for this phase of the project. Table 8 is a list of the power plants along with the associated coal source. To allow for classification of the fly ashes, elemental oxide composition was determined by x-ray spectrometry according to the technique previously described and is presented in Table 9. With the exception of the Clinton power plant, all of the fly ashes used in this study were derived from Wyoming lignite/subbituminous coals and the ASTM C 618-80 classifications which are also given in Table 8 suggest that the coal type is not necessarily consistent with the existing classification scheme.

Table 8. Coal Sources and Fly Ash Classification

Power Plant (Fly Ash Source)	Coal Source ^a	ASTM C 618-80 Classification ^b
Neal #3	Hanna Soutn, Rosebud, and Medicine Bow Mine, Wyoming	F
Neal #4	Rawhide Ranch Mine, Wyoming	C
Lansing	Belle Ayr and Eagle Butte Mines, Wyoming	C
Council Bluffs	Belle Ayr and Eagle Butte Mines, Wyoming	C
Nebraska City	Caballo Mine, Wyoming	C
North Omaha	Rosebud Mine, Wyoming	F
Clinton	Illinois-Montana Blend	F

^aInformation from reference 4

^bReference 5

Table 9. Element Composition, % by Weight

Fly Ash	MgO	Na ₂ O	Fe ₂ O ₃	TiO ₂	SiO ₂	CaO	Al ₂ O ₃	K ₂ O	SiO ₂ + Al ₂ O ₃ + Fe ₂ O ₃
Clinton Class F*	1.3	0.6	18.1	0.8	55.8	4.3	19.2	2.14	93.1
North Omaha Class F*	1.4	0.5	14.6	0.6	50.0	1.5	27.7	0.2	92.3
Neal #3 Class F	3.1	0.5	7.9	0.7	50.5	13.6	18.1	1.2	76.5
Nebraska City Class C*	5.8	1.8	5.5	1.4	34.1	30.3	21.1	0.3	60.7
Neal #4 Class C*	7.7	2.2	5.8	1.2	32.1	29.5	19.7	0.3	57.6
Council Bluffs Class C*	5.8	1.8	5.1	1.4	29.7	31.5	20.3	0.3	55.1
Lansing Class C*	6.2	1.8	5.9	1.3	30.0	31.1	19.7	0.4	55.6

* ASTM Classification C 618-80

Variability in Elemental Composition

The rapid measurement capability of the x-ray spectrometer made it possible to monitor the elemental composition of fly ash samples over a period of several weeks. Approximately thirty samples were collected at weekly intervals from three of the seven power plants included in this study. The elemental oxide composition was determined, and sample means and standard deviations for each oxide were computed. To facilitate comparison among the different oxides, coefficients of variation, defined as the sample standard deviation divided by the mean, are presented along with the means in Table 10. Data for the statistical analysis are in Appendix A.

On the average, the ASTM C 618 classifications for the three fly ash sources used in the variability analysis are consistent with the single specimen analysis given in Table 9, and the variability assessment includes one Class F and two Class C fly ashes. When the product of these three plants is viewed in the context of variation for the major constituents by averaging coefficients of variation for SiO_2 , Al_2O_3 , Fe_2O_3 and CaO ; the Council Bluffs fly ash is the least variable, the Neal 3 product the most variable, and the Neal 4 fly ash is an intermediate. In terms of minor constituents (i.e., MgO , Na_2O , K_2O , and TiO_2), the Neal 3 and 4 fly ashes displayed about the same variability which was approximately three times that for the Council Bluffs plant and a similar pattern held when all elements were considered.

An obvious pattern illustrated in Table 10 is that elemental variability for these fly ash sources bears little or no relation to the class of fly ash being produced. The least variable source is a Class C fly ash while the most variable sources are both C and F materials.

Table 10. Summary of Fly Ash Chemical Variability

Oxide	Source					
	Neal #3 (26) ^a Class F		Neal #4 (34) ^a Class C		Council Bluffs (28) ^a Class C	
	Mean weight, percentage, %	CV ^b , %	Mean weight, percentage, %	CV ^b , %	Mean weight, percentage, %	CV ^b , %
SiO ₂	46.9	6.8	34.0	9.0	30.6	5.3
Al ₂ O ₃	17.4	9.4	19.8	1.8	20.8	2.3
Fe ₂ O ₃	9.0	10.3	6.6	7.9	5.3	5.2
CaO	16.0	18.4	26.0	14.6	31.1	4.5
CV, Major Constituents	---	11.2	---	8.3	---	4.3
MgO	3.7	21.0	6.8	18.5	6.0	10.7
Na ₂ O	0.4	37.9	0.9	23.9	1.8	6.5
K ₂ O	1.3	18.0	0.4	58.8	0.4	12.2
TiO ₂	0.7	23.8	1.2	10.1	1.5	7.3
CV, Minor Constituents	---	25.2	---	27.8	---	9.2
CV, All Constituents	---	18.2	---	18.1	---	6.8

^a Number of samples included in the analysis

^b Coefficient of variation

Additionally, Table 10 data shows that of the three fly ashes the greatest degree of variability occurs among the minor compounds.

Significance of the magnitude of the variability resulting from this study is difficult to assess because knowledge about the importance of individual compounds to various applications is not yet clearly established. However, to provide a comparison, elemental composition resulting from twelve Type I portland cements from different producers is presented in Table 11. For the major constituents the variability for the Council Bluffs fly ash is equivalent to that of the portland cements, and where minor constituents are involved, all of the fly ashes display significantly less variability than for the portland cements. It should be recognized that data in Table 11 represents a sample of the cement industry as it existed several years ago and advances in quality control may have reduced this variability. However, the data available thus far suggests that all three power plants operate within limits of overall elemental composition for Type I portland cement production as it once existed.

Since fly ash is a by-product, it has been conceived as being a highly variable or random material. However, when viewed in terms of objectives of power generation, it is not surprising that elemental variability in fly ashes from a single source can have variability similar to that of portland cement. Feed composition whether it be for manufacture of cement or efficient operation of a power generating unit should be the primary source of variability. In an attempt to realize maximum power output, power units are designed and operated for consistency and optimum utilization of combustible materials which unintentionally governs the composition of ash products under normal

Table 11. Variability in Portland Cements^a

Oxide	Mean	CV ^b , %
SiO ₂	21.31	2.6
Al ₂ O ₃	5.39	10.0
CaO	63.94	1.5
FeO	No Data	No Data
CV Major Constituents	---	4.7
MgO	2.18	45.5
Na ₂ O	0.16	54.7
K ₂ O	0.43	72.3
TiO ₂	0.25	11.7
CV Minor Constituents	---	46.0
CV All Constituents	---	28.3

^aFrom reference 6

^bCoefficient of variation

operation conditions. Major changes in feed, such as coal source and precipitation additives, could certainly result in short term variability differences. However, with constant monitoring of operational changes and rapid tests for composition, variations in elemental composition should not be a significant problem.

Crystalline Composition

Variability analysis of elemental composition in itself cannot totally address the potential for good or poor phenomena resulting from the use of fly ash because such factors as the amount of the elements present and the form that they take could easily be predominant factors to the behavior of fly ash in its various applications. For example, it has been shown that in the Lansing fly ash calcium and aluminum combine to form a cementitious phase, calcium exists in limited quantities as a crystalline oxide, and a portion of the magnesium also exists as periclase. Based on experience with portland cement, all of these compounds could easily be significant. To allow for evaluation of the crystalline composition, the seven fly ashes listed in Table 8 were evaluated by x-ray diffraction and the results are in Table 12. The amorphous fractions of the seven fly ashes were computed from the complete crystalline component analysis by subtracting the sum of the crystalline component percentages from one hundred.

These results appear to represent the first definitive measurement of the quantitative phase composition of fly ashes and also illustrates the potential for refining the existing ASTM classification scheme which is based largely on elemental composition. Neal 4, Lansing, and Council Bluffs fly ashes contain significant amounts of tricalcium aluminate and

Table 12. Crystalline Components in Fly Ashes.

Component	Source and weight percentage						
	Neal #3 * Class F	Neal #4 * Class C	Lansing * Class C	Council Bluffs * Class C	Nebraska City * Class C	North Omaha * Class F	Clinton * Class F
Tricalcium Aluminate	0.0	4.9	5.2	6.0	0.5	0.0	0.1
Tetracalcium Aluminate Sulfate (C_4A_3S)	0.1	1.1	2.3	0.2	0.0	0.0	0.1
Calcium Sulfate ($CaSO_4$), (Anhydrite)	0.3	1.3	1.7	0.9	0.1	.3	0.2
Calcium Oxide (CaO)	2.3	0.8	2.1	1.4	0.1	0.2	.2
Quartz (SiO_2)	7.0	8.0	10.1	5.3	7.1	9.9	8.2
Mullite ($Al_6Si_2O_{13}$)	0.0	2.3	0.9	0.0	2.9	3.6	3.0
Magnetite (Fe_3O_4)	0.7	0.0	1.0	0.2	0.0	10.0	7.4
Magnesium Oxide (MgO), (Periclase)	1.0	3.2	2.8	2.0	0.4	0.0	1.3
Amorphous Contribution (glass) By difference	88.6	78.4	73.9	84.0	88.9	76.0	79.6

* ASTM classification C 618-78

tetra-calcium trialuminate sulfate phases and are reactive with water in that they exhibit high heats of reaction and set within a few minutes. By ASTM standards these three fly ashes are categorized as Class C.

On-the-other-hand, the North Omaha and Clinton fly ashes are relatively inert because they contain small amounts of the cementitious compounds and rightfully fall into another category, which in this case is ASTM Class F. The problem is with the Nebraska City ash which also contains negligible amounts of the cement compounds and in terms of reaction with water is relatively inert. The Nebraska City fly ash is marginally designated as a Class C ash, yet its compound composition is more akin to that of the Class F ashes. Thus a logical scheme to guide future research and possibly field application would be classification according to reactivity with water which could then be used to make inferences about the presence, type and amount of cementitious compounds.

The data in Table 12 also serves to illustrate two additional points. The high heat of hydration of some fly ashes was thought to be due to hydration of lime. At least for the three reactive fly ashes used in this study, CaO is only a minor constituent and reaction heats should be largely due to hydration of the cementitious compounds. Also the ability to quantify amorphous contributions which contribute to pozzolanic reactions with lime, either added directly or derived from hydration of portland cement, suggests that for the seven fly ashes tested, the pozzolanic potential based on quantity alone should be about the same. Tests which are now used to assess pozzolanic activity should for three of the fly ashes investigated result in misleading information by incorporating the effects of strength due to cement hydration and the

pozzolanic reactions themselves. Lastly, these fly ashes display a considerable range of inert compounds such as quartz, mullite and magnetite which should contribute little, either positively or negatively, to performance. The lowest combination of relatively inert materials was 5.5 percent in the case of Council Bluffs ash while the highest was 23.5 percent for North Omaha. The reactive composition, whether it be cementitious compounds or amorphous materials, should have a significant influence on strength and possibly void structure through development of delayed pozzolanic reaction products.

Since the amorphous fraction is the most prominent portion of the fly ashes evaluated for this phase of the research, an estimate of the glass composition is also useful to characterization. Data in Tables 9 and 12 can be used to compute amorphous composition by subtracting from the total elemental composition, those elements identified in compounds. Results of these computations are in Table 13. With one exception, North Omaha, the glass phase of all of the fly ashes evaluated had alumina contents near twenty percent. A major difference was found in relative amounts of silica and calcium oxide with a pronounced tendency for high calcium glass corresponding to Class C fly ashes and high silica glasses for Class F fly ashes. The Neal 3 ash represents an intermediate.

Lime contents in the glass phase of the North Omaha and Clinton fly ashes are consistent with traditional concepts for pozzolanic reactions in that an external source of calcium is required to initiate reactions resulting in formation of cementitious calcium-silicate hydrates. Calcium hydroxide, a product of portland cement hydration, is the calcium source for normal pozzolanic reactions occurring in portland

Table 13. Composition of Amorphous Phase

Source	Weight Percentage Based on Amorphous Contribution					
	SiO ₂	Al ₂ O ₃	Fe ₂ O ₃	CaO	MgO	Others (K, Na, Ti, SO ₃)
Neal #3 Class F	49.1	20.4	8.4	12.6	2.4	7.1
Neal #4 Class C	29.9	20.0	7.4	28.1	5.7	8.9
Lansing Class C	26.6	21.6	7.1	32.8	4.6	7.3
Council Bluffs Class C	29.1	21.4	5.9	30.9	4.5	8.2
Nebraska City Class C	29.5	21.3	6.2	33.6	6.1	3.3
North Omaha Class F	51.5	33.1	10.4	1.6	1.8	1.6
Clinton Class F	55.0	21.3	16.5	4.9	0.0	2.3

cement-fly ash concrete. The manner in which high calcium glass can interact with hydrating or hydrated portland cement is not yet understood. However, high early strengths and optimum fly ash contents for maximum strengths, which will be discussed later, may be tied to high calcium amorphous fraction of some Iowa fly ashes.

Soundness of Fly Ash Concrete

Crystalline forms of calcium and magnesium oxide discovered in nearly all of the Iowa fly ashes (see Table 12) raised concerns about the potential for problems resulting in delayed hydration and the expansiveness of hydrates. In this phase of the investigation, three samples of Iowa fly ashes and one Type I portland cement were used. Substitution of fly ash for cement ranged from 20% (as required in ASTM C 311) to 50% by weight keeping the research construction oriented.

All test specimens were autoclaved in a Cenco autoclave which complied with all specifications listed in ASTM C 151. Length measurements were made with a Soil Test extensometer (model No. CT384) which complied with calibration requirements described in ASTM C 490. Elemental analysis of these materials is summarized in Tables 14 and 15.

Fly ashes were analyzed by QXRD and QXRF using the Siemens equipment described earlier. The details of the calibration, operation, and sample preparation were also described earlier.

The Type I portland cement was obtained from the IDOT and it consisted of a blend of cements from the various cement plants in Iowa. The IDOT also performed elemental analysis and some physical tests on the blended cement the results of which are listed in Table 14. The elemental analysis results are in good agreement with those obtained by QXRF.

Table 14. Type I portland cement.

Oxide	Wet chemistry analysis ^a wt. %	QXRF analysis (average of 2 samples) wt. %
CaO	66.97	63.68
Al ₂ O ₃	4.52	4.37
Fe ₂ O ₃	2.45	2.48
SiO ₂	-----	22.09
SO ₃	2.48	2.67
K ₂ O	0.61	0.64
TiO ₂	-----	0.24
MgO	3.12	3.62
Na ₂ O	0.19	0.23
P ₂ O ₅	-----	0.11
		Total = 100.13
Free CaO:		Physical properties: ^a
QXRD	0.2%	Specific surface: 3550 cm ² /g (Blaine)
wet chem.	0.8%	Insoluble residue: 0.35%
Free MgO:		Ignition loss: 1.16%
QXRD	2.0%	Autoclave expansion: 0.06%
C ₃ A: ^b	7.83%	

^aObtained from Iowa Department of Transportation Material Laboratory.

^bFrom Bogue's equations as listed in ASTM C 150.

Table 15. Characteristics of the three fly ashes used in this study.

Elements converted to oxides	Neal 3 ^a (F) ^b	Neal 4 ^a (C)	Omaha North (F)
<u>QXRF results</u>			
SiO ₂	50.54	32.09	49.95
Al ₂ O ₃	18.13	19.71	24.12
Fe ₂ O ₃	7.87	5.79	18.19
CaO	13.61	29.47	1.98
MgO	3.14	7.74	1.31
TiO ₂	0.66	1.17	0.65
Na ₂ O	0.51	2.23	0.56
K ₂ O	1.24	0.30	1.06
Total	95.70	98.51	97.82
Compound	Neal 3 ^a	Neal 4 ^a	Omaha North ^c
<u>QXRD results</u>			
CaO	2.3	1.1	0.2
MgO	1.0	3.0	0
3CaO·Al ₂ O ₃	0	3.9	0
SiO ₂	7.0	4.6	9.9
Fe ₃ O ₄	0.8	1.5	10.0
3Al ₂ O ₃ ·2SiO ₂	0	0.2	3.6
3(CaO·Al ₂ O ₃)CaSO ₄	0.2	0.5	0
CaSO ₄	0.3	1.8	0.3

^aDenotes the average of 3 tests, otherwise 2 tests were averaged.

^bLetters denote ASTM C 618 classification.

^cIndicates data taken from Progress Report #2 IDOT HR - 225.

Two methods were used to measure the free calcium oxide content of the cement while only one method was used to determine the free magnesium oxide content. The tricalcium aluminate content of the cement was calculated by using Bogue's equations as defined in ASTM C 150.

All autoclave samples were made, cured, and tested in accordance with ASTM C 151. Distilled water was used throughout the experiment.

To investigate the influence of chemical composition on autoclave expansion, the total composition of a given mixture can be computed as a weighted average using the results of the chemical analysis for the portland cement and fly ashes. For example, the percent of "A" in a given mixture can be expressed as:

$$\% A = \frac{W_T(FA)(\% A_{FA}) + W_T(PC)(\% A_{PC})}{W_T} \quad (2)$$

which reduces to

$$\% A = FA(\% A_{FA}) + PC(\% A_{PC})$$

where: A is the total amount of "A" in a mix

W_T is the total dry weight of a mix

FA is the weight fraction of fly ash in a mix

PC is the weight fraction of portland cement in a mix

$\% A_{FA}$ is the percent of "A" measured in the fly ash

$\% A_{PC}$ is the percent of "A" measured in the portland cement

Fifty-two specimens were molded and subjected to autoclaving. Included in the fifty-two samples were eight control samples composed

only of portland cement. Appendix B lists the autoclave expansion and chemical composition obtained for every cement-fly ash mixture investigated.

All of the expansion data for the cement-fly ash mixtures was divided by the average expansion observed for the control specimens, this normalization will be called the relative expansion (RE) which is simply the expansion observed for a given cement-fly ash mixture relative to the average expansion of portland cement. The Statistical Analysis System (SAS) was used for investigating possible relationships between the relative expansion and the chemical composition of the cement-fly ash mixtures (5).

Regression analysis indicates that free calcium oxide has by far the most significant influence on the relative expansion of the cement-fly ash pastes. In fact, it was the only single variable that correlated well with relative expansion, all the other variables listed in Appendix B did poorly. Figure 4 shows a plot of the expansion data versus the free calcium oxide of a given mixture.

For practical purposes the data in Figure 4 can be split into two distinct parts. One part would consist of the nearly linear, lower portion while the other part would consist of the steeply inclined portion of the curve. Engineers who wish to design on the conservative side would always desire to be on the lower portion of the curve where expansion is fairly predictable. Regression of the data from the lower portion of the curve indicates that two variables (free calcium oxide and calcium aluminate) play a role in the autoclave expansion of the different mixtures. The resulting model generated with the help of statistics is as follows:

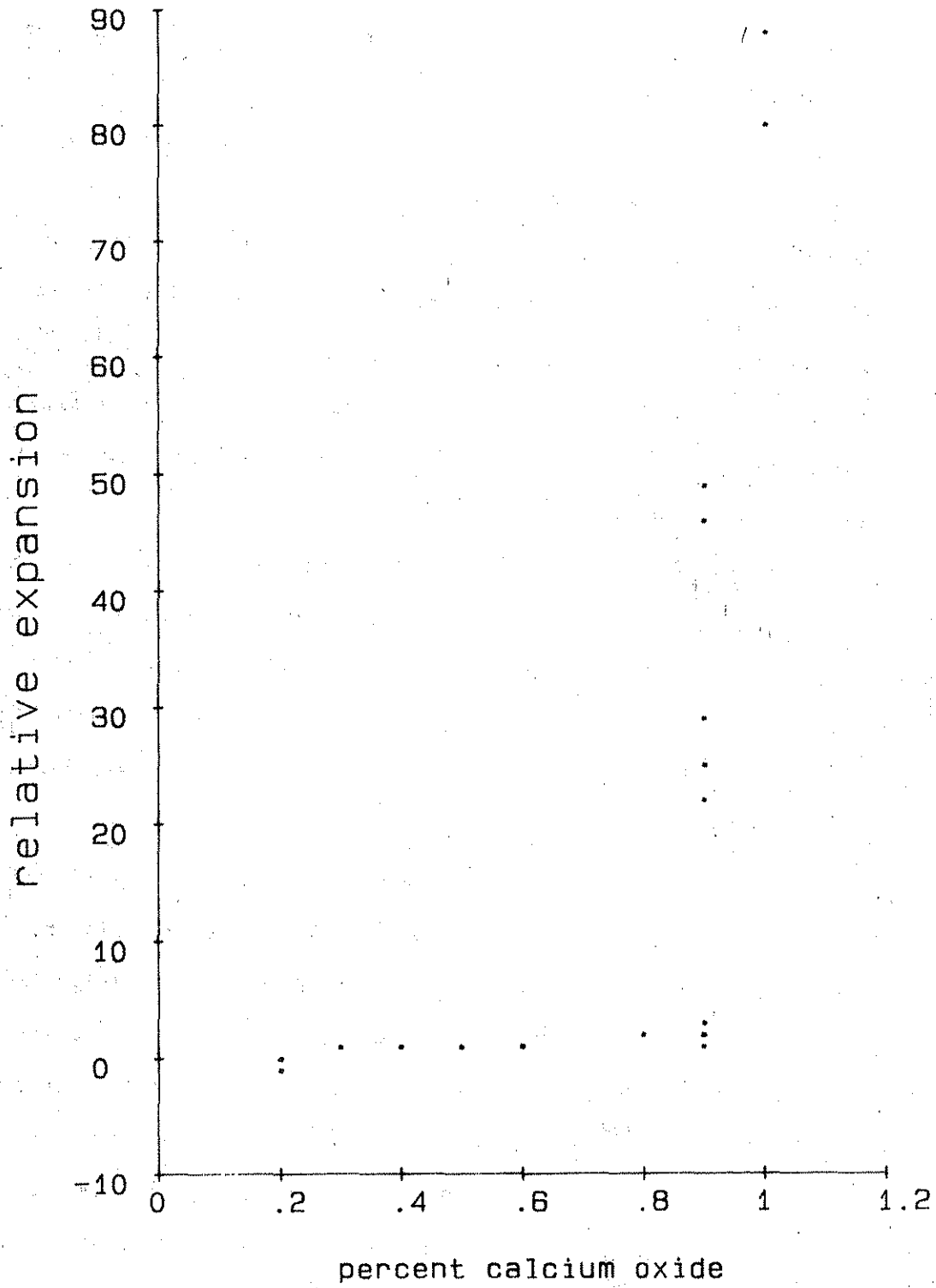


Figure 4. Effect of calcium oxide content on relative expansion.

$$RE = 3.46 (\% \text{ CaO}) + 0.38 (\% \text{ C}_3\text{A}) - 2.66, \quad R^2 = 0.90 \quad (3)$$

On the other hand the upper right hand portion of the figure is dominated entirely by the free calcium oxide content of the mixture, for which a relationship can be expressed as follows:

$$RE = 722.05 (\% \text{ CaO}) - 665.08 \text{ for CaO } 70.85\%, \quad R^2 = 0.96 \quad (4)$$

In summary the significance of this evaluation is that the detrimental expansions caused by the compounds in fly ash are due to free CaO alone as indicated by equation 4.

Lime Pozzolanic Activity

During the conduct of this research, a question arose about the validity of the pozzolanic activity test specified by ASTM C-618 and described in ASTM C-311. The intent of this test is to provide a rapid (seven-day) assessment of the pozzolanic character of fly ash through accelerated, high temperature curing of fly ash-lime mixtures with success being expressed as a minimum 800 psi compressive strength, regardless of fly ash class. It was found that most high-lime fly ashes which produced superior results with portland cement consistently failed lime-pozzolan tests while low-lime fly ashes passed the ASTM standard. Also, it was found that results for ISU tests on high-lime fly ashes were not consistent with those from another laboratory outside the state. ISU lime-pozzolan results were negative and the other laboratory's results always exceeded the standard.

Figure 5 summarizes the results of experiments dealing with the pozzolanic activity test as defined in ASTM C-311. Three types of hydrated lime were used in the experiment. Reagent grade indicated lime

S
T
R
E
N
G
T
H

I
N

P
S
I

LIME POZZOLAN TEST

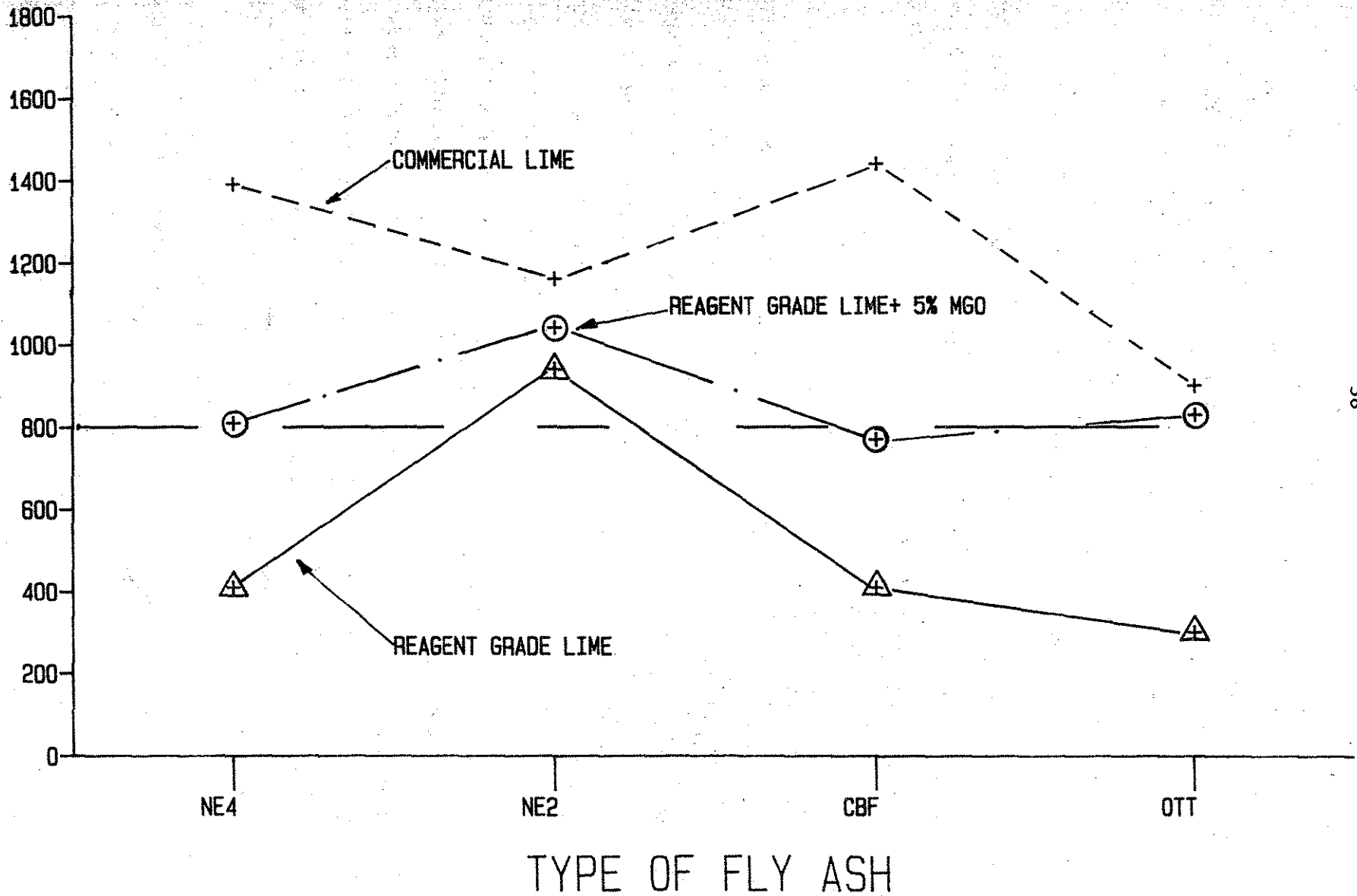


Figure 5. Lime Pozzolan Test Results

or pure calcium hydroxide as specified in ASTM C-311 was obtained from Fisher Scientific Co. Commercial lime was obtained from Snowflake and a third lime was prepared by mixing 95% (by weight) of reagent grade lime with 5% of reagent grade magnesium oxide. Four different fly ashes were used in this study, three were classified as ASTM Class C (Neal 4, Council Bluffs, and Ottumwa) while one (Neal 2) was designated as Class F. Compressive strength cylinders were prepared and cured in accordance with ASTM C-311. After seven days of curing at 55 °C the samples were cooled to room temperature and tested in unconfined compression.

The differences between the three types of lime are quite dramatic. If ASTM C-311 is followed to the letter and reagent grade lime is used to mold the test specimens then all three Class C fly ashes fail the test. The Class F fly ash passes the test by exceeding the 800 psi minimum.

When commercial lime is used all of the fly ashes easily pass the test. Strength is enhanced by about a factor of three for all of the specimens containing the Class C fly ashes. The strength of the specimens containing the Class F fly ash increased only 23%, an increase that may not have statistical significance. The reason for the drastic increase in strength is not fully understood at this time but small amounts of impurities in the commercial lime appear to play an important role.

One of the common impurities in lime is magnesium oxide and that was the rationale behind preparing the third type of lime which contained 95% calcium hydroxide and 5% magnesium oxide. The addition of magnesium oxide to the mixes enhances the strength of the specimens containing the Class C fly ashes by a factor of two; the strength gain

of the specimens containing a Class F fly ash is negligible.

It was found that several laboratories routinely run lime-pozzolan tests with commercial grade lime because it produces better results. The primary issues are, however, whether the lime-pozzolan test has meaning with regard to determining suitability of fly ashes for use with portland cement and why minor additives such as magnesium oxide and others probably present in commercial lime can have little or no influence on the Class F fly ash and pronounced strength enhancement with the Class C fly ashes. To address the first question, it is necessary to reconsider the view that pozzolanic reactions are entirely associated with calcium hydroxide as simplistic chemical models indicate. In reality, portland cement contains numerous trace elements (i.e. as crystalline substitutions, in an amorphous phase, and as distinct compounds) along with as much as 5% magnesia (6). If fly ashes perform well with portland cement, it is suspected that such behavior is due at least in part to impurities in a commercial product. If such impurities are nonexistent in reagent grade lime, a test involving such a material is of little practical value. A lime-pozzolan test using an impure commercial lime may also be of little value, mostly because there is at present no means for insuring that impurities are representative of those from portland cement. Due to trace variations in raw cement feed, it seems possible that different sources of portland cement could behave differently with a given fly ash and the best recourse is to evaluate fly ashes with the cement proposed for use, that is until the problem is better defined. Also, it seems entirely possible that an accelerated version of the normal 28-day cement pozzolan test is possible for the high-lime fly ashes.

The second aspect of the lime-pozzolan study involves differences in behavior of fly ashes in conjunction with impurities in hydrated lime. The Class F fly ash, one typically noncementitious and containing low calcium glass, showed little difference in response regardless of impurities. On the other hand, impurities from commercial lime or reagent grade calcium hydroxide with magnesium oxide improved strengths for the three cementitious, high calcium glass fly ashes. At this point, an analysis must remain speculative because of the complexities of the system. Although present knowledge of portland cement chemistry (7) does not suggest that impurities should have an influence on tricalcium aluminate reactions, such a possibility cannot be eliminated. Even less is known about reactions associated with the high-calcium amorphous phase; however, Iowa DOT research being conducted under project HR 260 shows the presence of trace compounds can cause the dissociation of such amorphous materials and the formation of calcium-aluminate-silicate hydrates in the absence of calcium hydroxide.

Definition of impurities and the resultant reaction products could lead to more efficient use of fly ash not only with portland cement but as a cement itself. However, a hypothesis can be proposed to explain the influence of MgO on pozzolanic activity of Type C fly ashes. The glassy phase of a Type C fly ash rich in CaO resists the attack by $\text{Ca}(\text{OH})_2$ because of saturation with Ca ions. MgO which forms $\text{Mg}(\text{OH})_2$, brucite, upon hydration, is isomorphous with octahedrally coordinated $\text{Al}(\text{OH})_3$ (gibbsite structure) present in the glassy phase. Therefore the hydration product $\text{Mg}(\text{OH})_2$ can penetrate the glass in the form of solid solution replacing $\text{Al}(\text{OH})_3$ octahedra and breaking the glass structure rich in CaO. The result then would be crystallization of cementitious

products consisted of silicates and aluminates of calcium. Type F fly ashes lean in CaO contents are vulnerable to the attack by Ca(OH)_2 and therefore less prone to the manifestation of the action of Mg(OH)_2 .

Heat Evolution Test

Knowledge that some Iowa fly ashes contain aluminous compounds leads to the notion that a practical method for diagnosing the presence and possibly the quantity of these compounds could involve evaluation of the heat generated during hydration or more simply correlation to temperature change in an inexpensive calorimeter. Knowing the quantity of cementitious compounds in fly ashes could have particular significance when these materials are used as soil stabilizers thus a test involving a dewar vacuum flask, a chromel-alumel thermocouple and an electronic chart recorder was devised. The procedure involves placing twenty milliliters of tap water in a styrofoam cup, placing the cup inside the dewar flask, and positioning the thermocouple junction in the water. Thirty grams of fly ash are then sprinkled into the water and a cork is used to seal the dewar. The recorder and thermocouple system then produce a curve which shows temperature increase versus reaction time during hydration. The heat evolution test was performed on six Iowa fly ashes and to evaluate the potential for retarding C_3A hydration the Lansing ash was mixed with different percentages of gypsum. It should be noted that a similar test was developed at the Texas Transportation Institute in an attempt to find a quick method of correlating elemental calcium content expressed as oxide to temperature rise which occurs when fly ash reacts with hydrochloric acid (8).

The results obtained from the heat evolution tests are presented in

Figures 6 and 7 and are summarized in Table 16. Peak temperature increases for fly ashes containing aluminous cements fell in the range of 10-20°C. These fly ashes definitely belong to Class C. Non-reactive ashes showed a temperature increase of 1°C over a period ranging from 30 to 60 minutes. Two of these fly ashes, namely Clinton and North Omaha, are definitely Type F ashes. However, the Nebraska City fly ash behaves similar to Type F ash in all aspects except for sesquioxides plus silica content which place it in the Class C category.

The data obtained from the heat evolution test on Lansing fly ash are of interest because they show the influence of gypsum in delaying the time to peak temperature. The test run on the Lansing ash without gypsum showed a temperature increase over a period of 22.5 minutes with the peak temperature increase at 22.5 minutes being 20°C. The analysis of the ash with 3% gypsum showed a 19 °C temperature increase over an extended period of 66.0 minutes. When the oscillation diffraction data in Table 7 are compared to these results, an interesting trend can be seen. The periods of ettringite formation or consumption of tricalcium aluminate correspond to that of time to peak temperature as shown in Figure 8.

Although the data available thus far are not adequate to support a predictive correlation, the trends show that there is potential for developing a correlation between temperature rise and the amount of aluminous compounds if such phases are present alone in fly ash. Such a test would involve nothing more than a styrofoam container and thermometer.

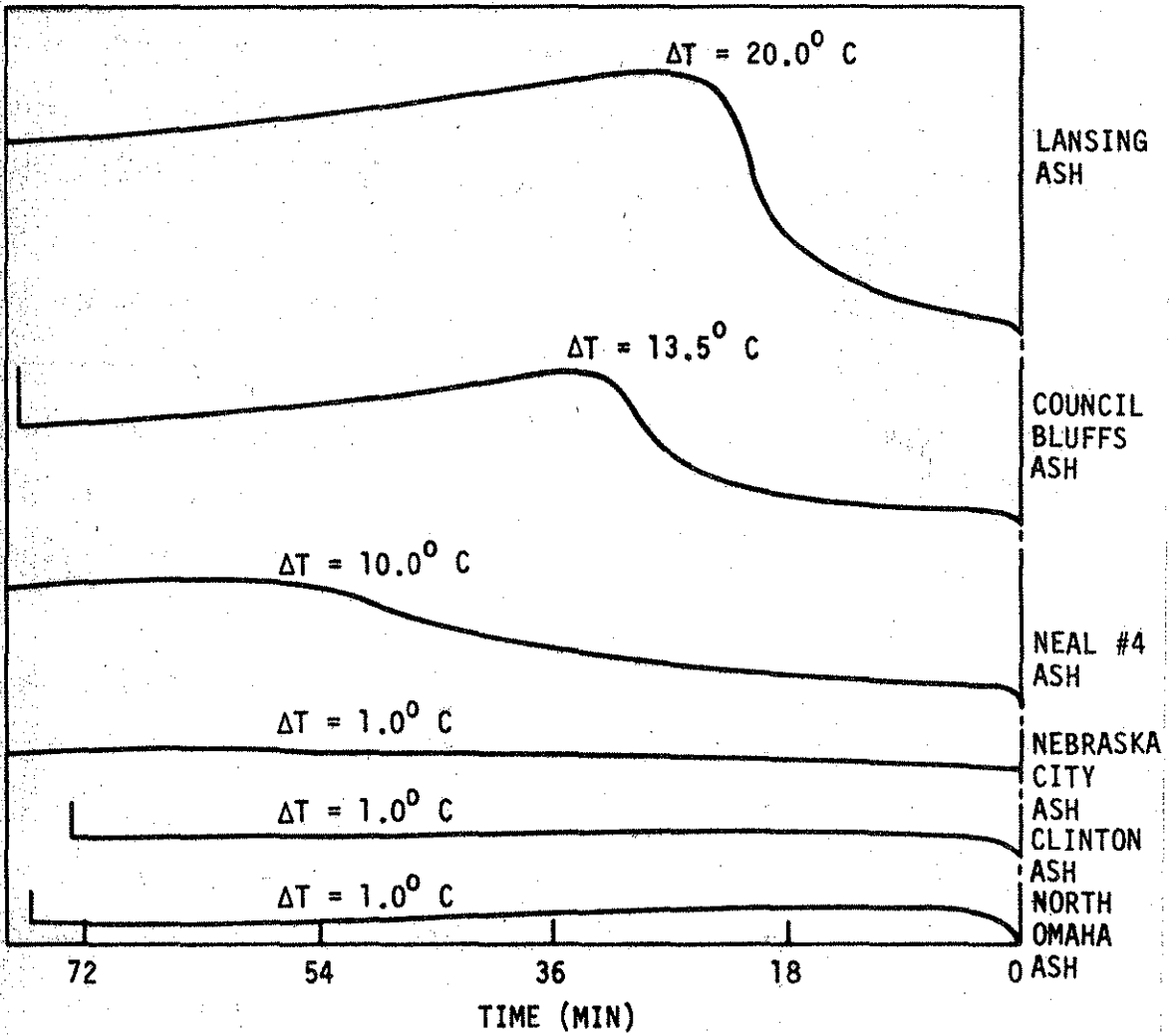


Figure 6. Heat evolution results for six fly ashes.

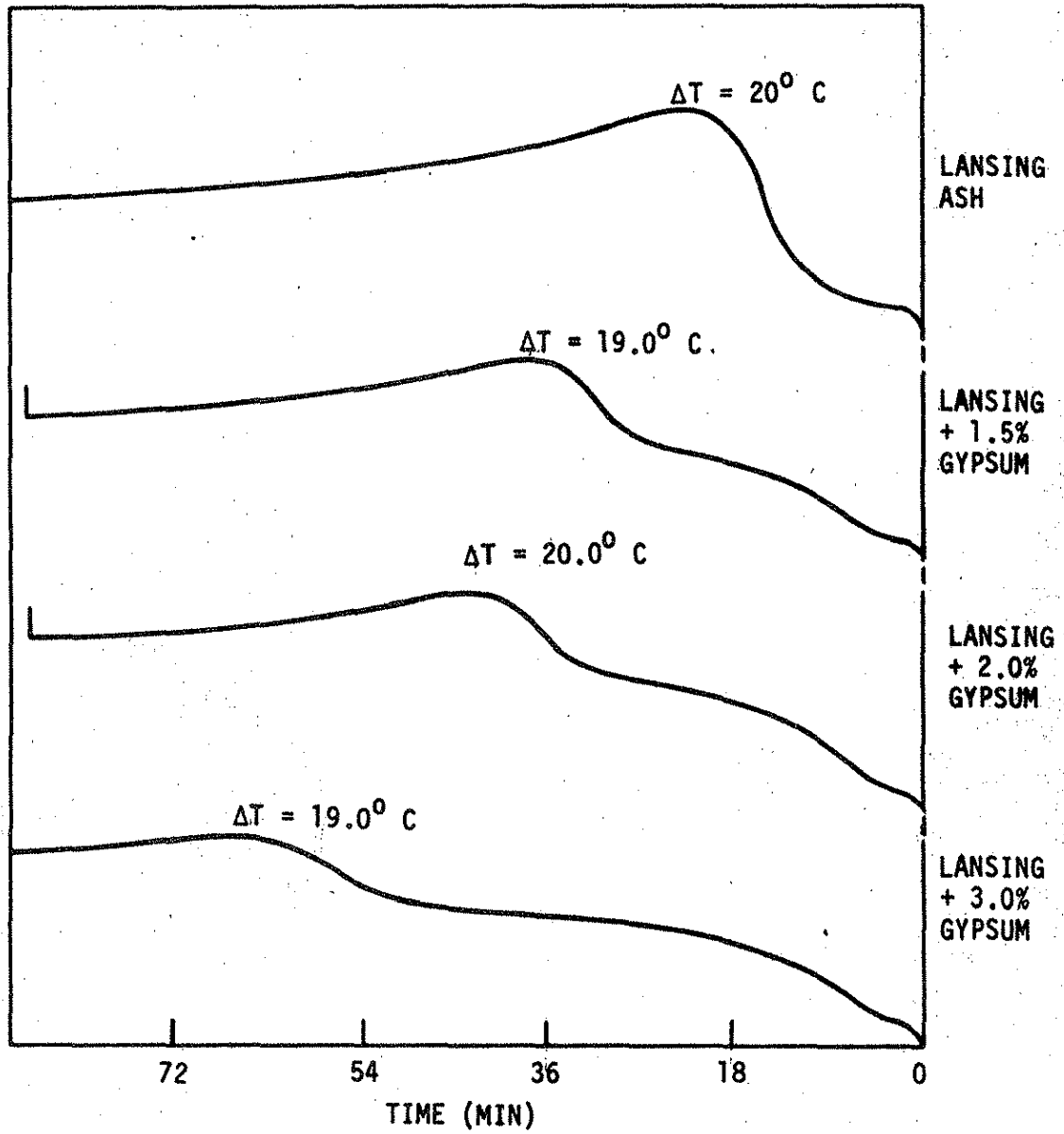


Figure 7. Heat evolution with gypsum.

Table 16. Summary of Heat Evolution Tests

Fly ash	Maximum temperature rise, ΔT , °C	Elapsed time, t, min. for attainment of maximum temperatures
Council Bluffs	13.5	38.3
Neal #4	10.0	70.0
Lansing	20.0	22.5
Lansing + 1.0% gypsum	18.0	32.5
Lansing + 1.5% gypsum	19.0	36.0
Lansing + 2% gypsum	20.0	43.5
Lansing + 3% gypsum	19.0	66.0
Nebraska City	1.0	60.0
Clinton	1.0	30.0
North Omaha	1.0	30.0

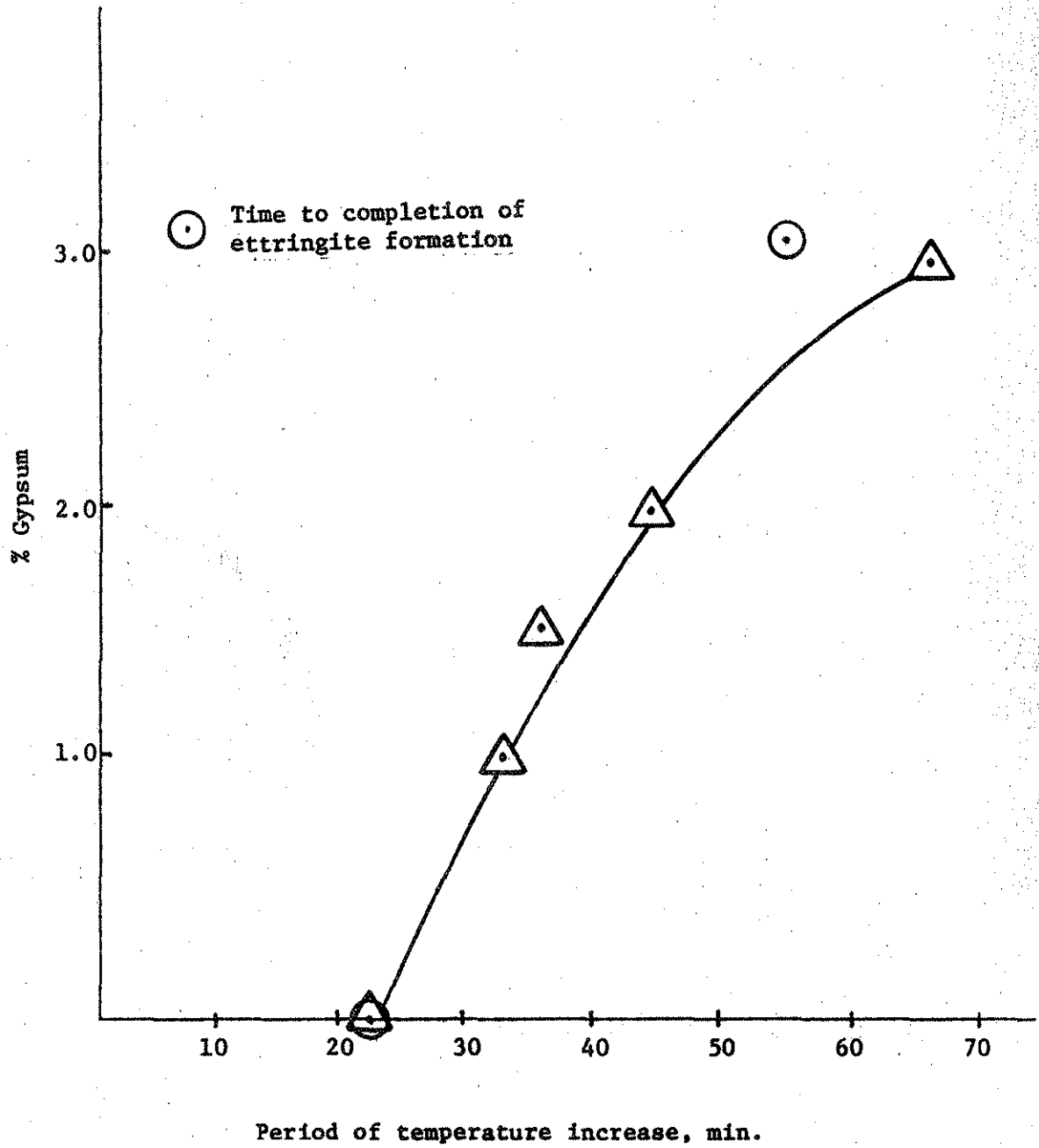


Figure 8. Effect of Gypsum on the Rate of Hydration of Lansing Fly Ash.

Freeze-thaw Durability

In Figure 9b durability factor, a relative measure of sonic modulus before and after a specimen has undergone freeze-thaw action, is plotted against percent fly ash for all the mixes listed in Appendix C. Obviously, an extreme range in performance is possible for fly ash replacements up to 75 percent while at 100 percent fly ash, durability factor plummeted to zero. To comfortably use fly ash as a replacement for portland cement, it is essential that causative factors be established. With guidance from knowledge of what factors can influence freeze-thaw durability, it is possible to use a computerbased sorting routine to make sense of the available data. Iowa DOT research has previously established the importance of aggregate type on resistance to cyclic freezing (9) while the concrete literature indicates that void composition and water cement ratio are significant factors (10).

One aspect of concrete void composition, entrained air, will be used as a starting point for an evaluation of variables. Figures 10 and 11 illustrate the influence of air entrainment on concretes made with Neal 4 fly ash. These data are for concrete batches with 0, 25, and 50 percent fly ash, and two aggregate types - Montour and Alden. Neutralized Vinsol resin was used to entrain air at contents ranging from 2.6 to 12 percent. Air contents were measured by the pressure method in accordance with ASTM C 231-82. For the Alden aggregate, durability factors exceeding 90 percent can be achieved for fly ash replacements up to 50 percent, that is if air content exceeds a critical value on the order of 5 percent. Critical air contents also exist for the Montour aggregate, but ultimate durability is also controlled by fly ash content. At 0 and 25 percent fly ash an ultimate durability factor

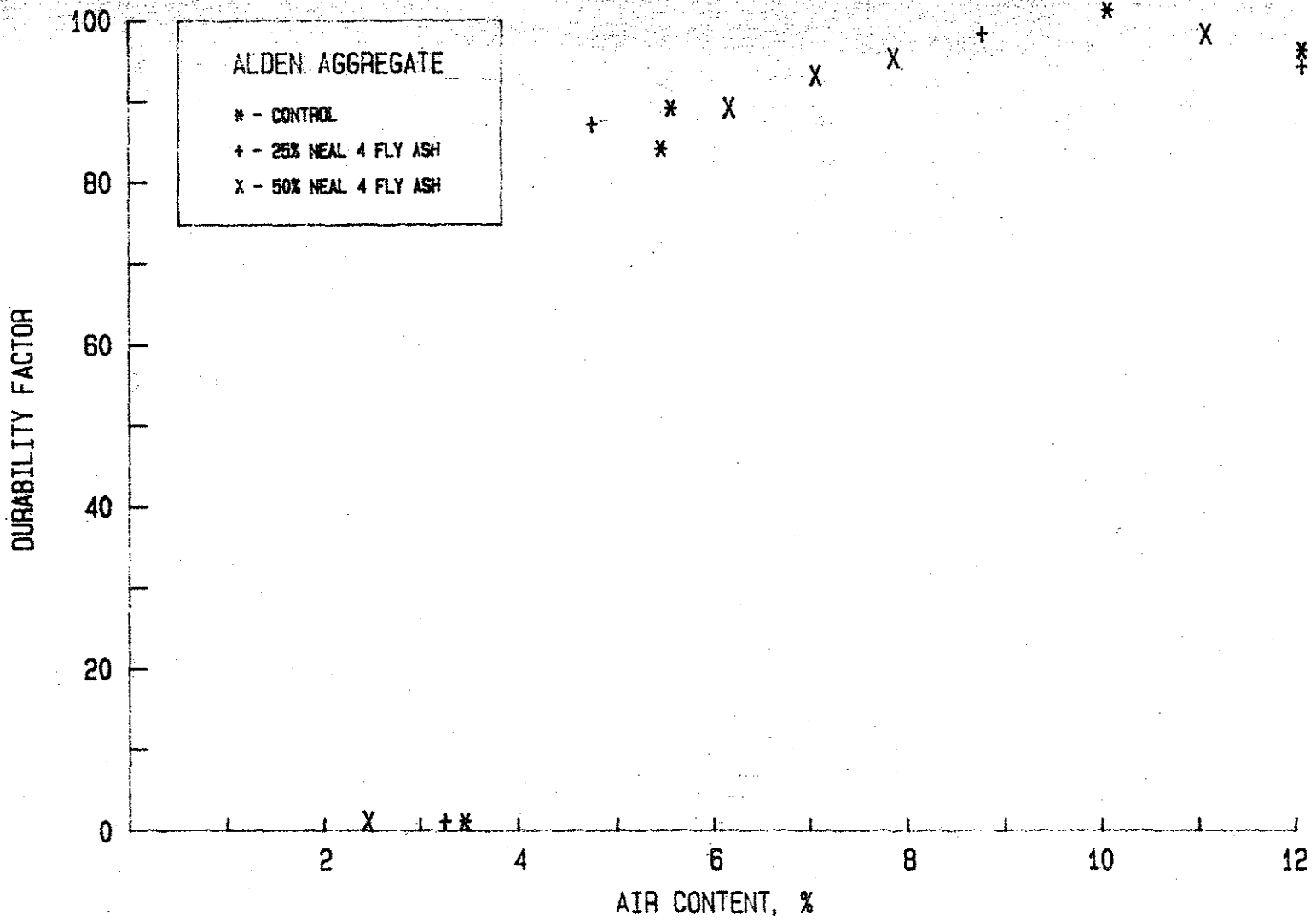


Figure 10. Durability and air content - Alden aggregate.

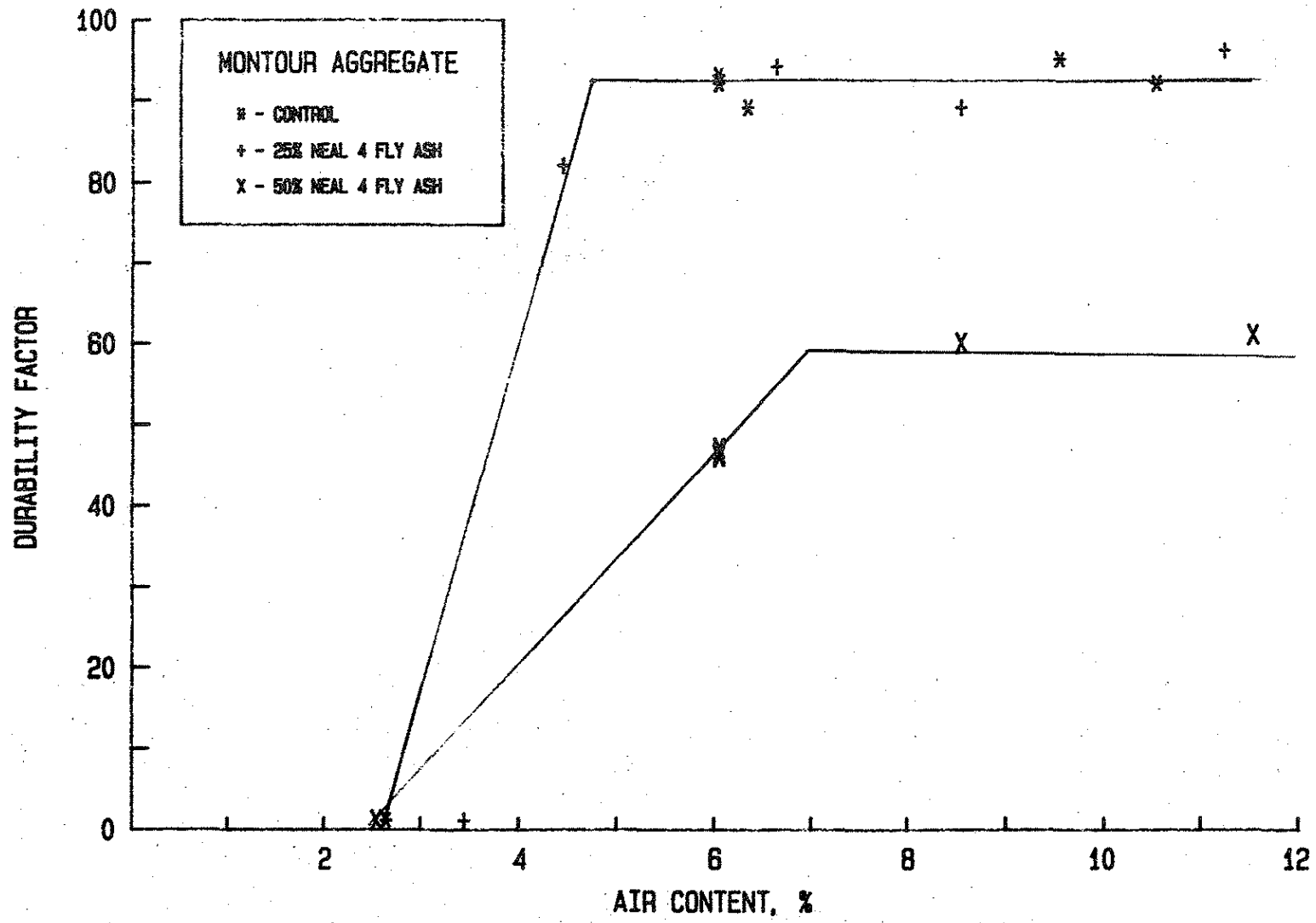


Figure 11. Durability and air content - Montour aggregate.

of 90 percent was realized while at 50 percent fly ash a durability factor of 60 percent was the upper limit.

If data for air contents exceeding that required for ultimate durability are considered, behavior relative to aggregate type can be evaluated. Figures 12 and 13 are results for durability tests on concretes made from Alden and Montour aggregates and Neal 4 fly ash replacements up to 100 percent. Water/cement ratio, based on cement and fly ash, was reduced with added fly ash content such that slump was maintained at less than six and more than two inches. Without fly ash, a five batch average durability factor was 92 percent. At 25 percent fly ash, average durability for both aggregates remained at the untreated level, but at 50 percent replacement a significant difference was observed. Durability factor for the Montour aggregate held constant to 75 percent replacement, and dropped to zero somewhere between 75 and 100 percent fly ash replacement. The Montour aggregate however, showed a significant loss in durability beginning at 50 percent replacement.

A second series of data sufficient to support general observations on the influence of fly ash on durability factor was developed with Gilmore City aggregate and fly ashes from five different Iowa sources. The same sorting criteria were used for the data in Figure 14 which in this case shows a slight decrease in durability factor at replacements from 35 to 50 percent.

In a general sense, results presented in this section serve to confirm those previously discovered in Iowa DOT research (9), namely, that coarse aggregate type can have an influence on durability of concrete made with fly ash. Differences between this and previous work are that the aggregate-fly ash interaction phenomenon has been explored

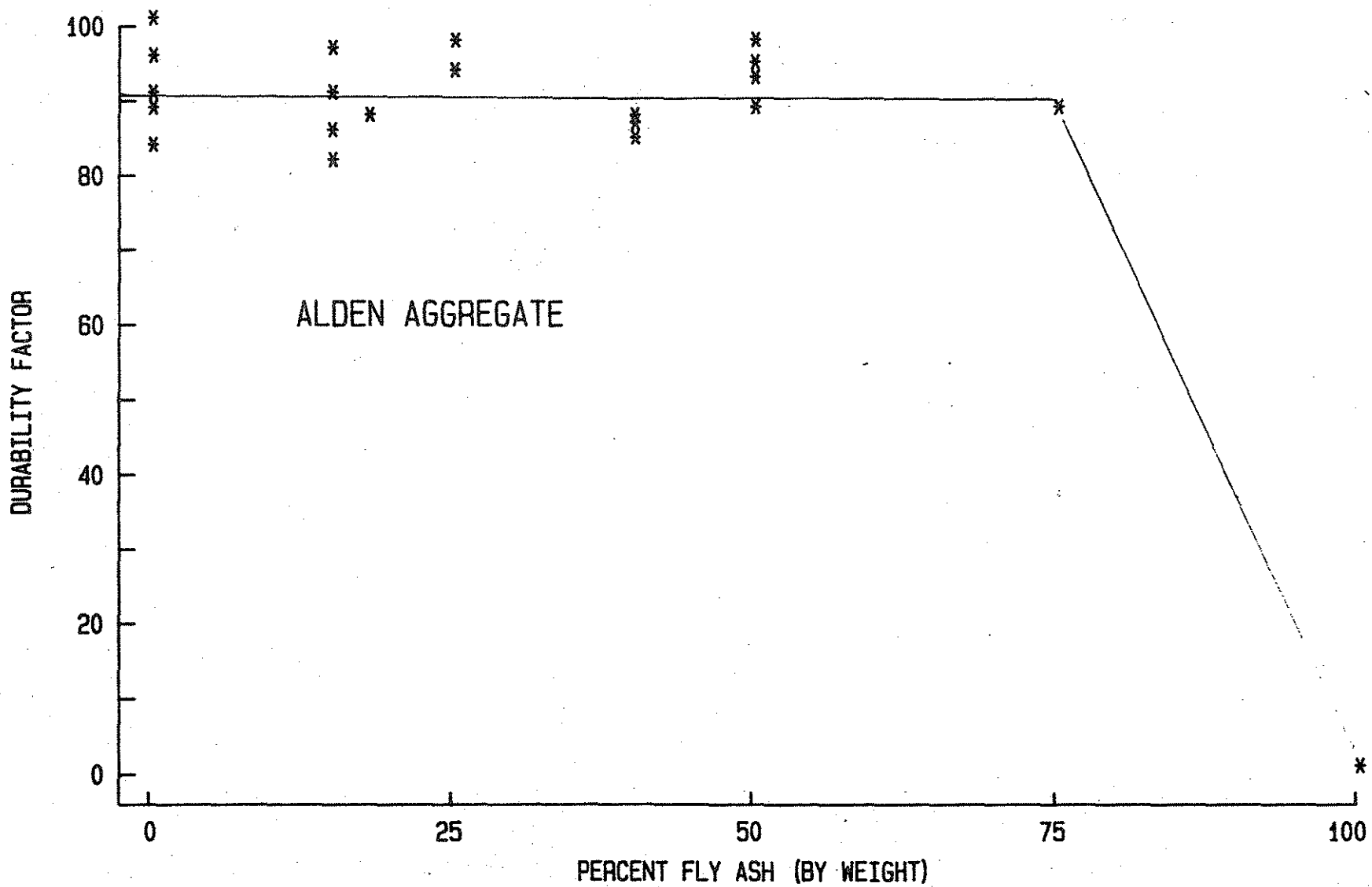


Figure 12. Durability - Alden aggregate and Neal 4 fly ash.

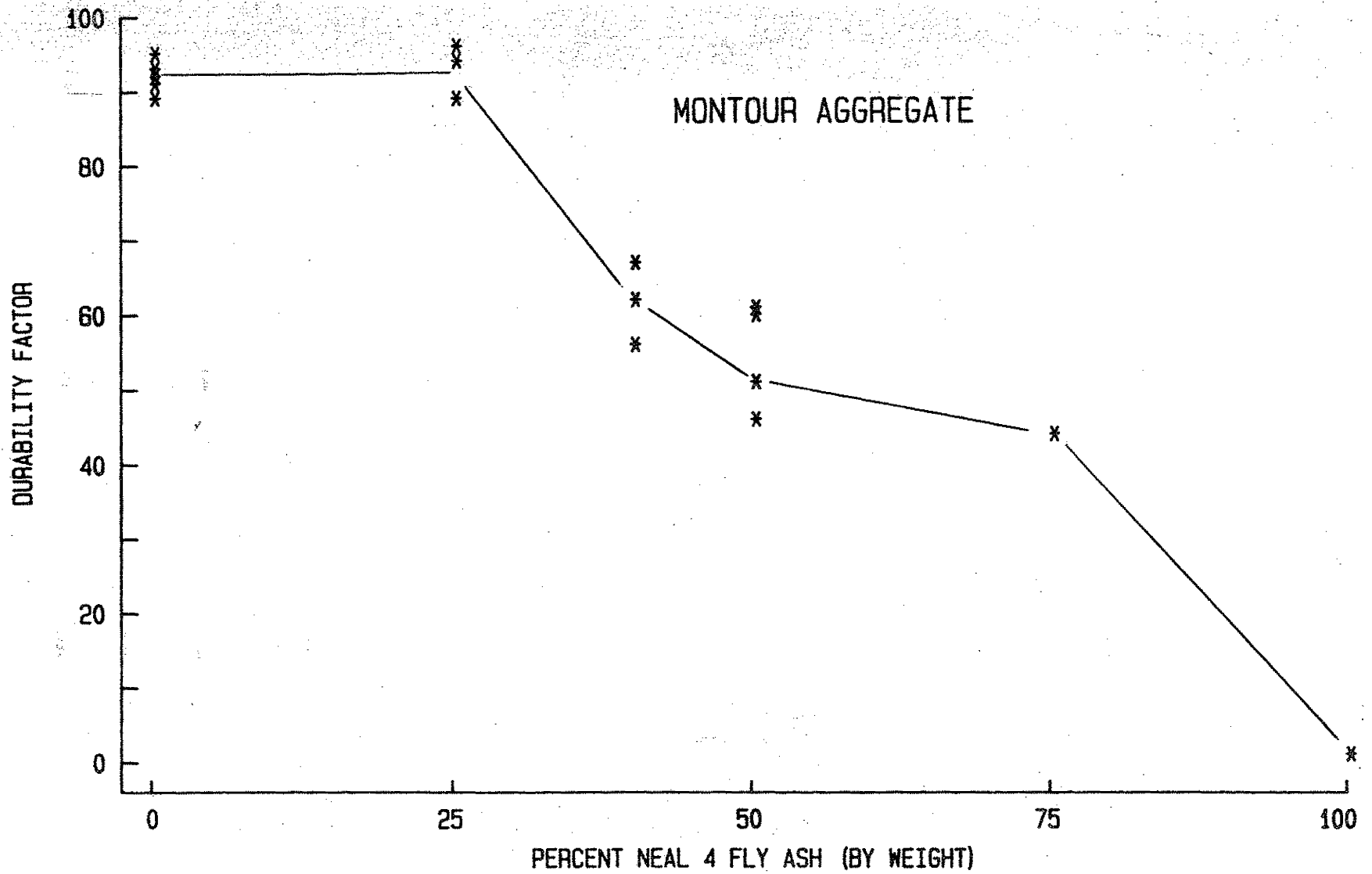


Figure 13. Durability - Montour aggregate and Neal 4 fly ash.

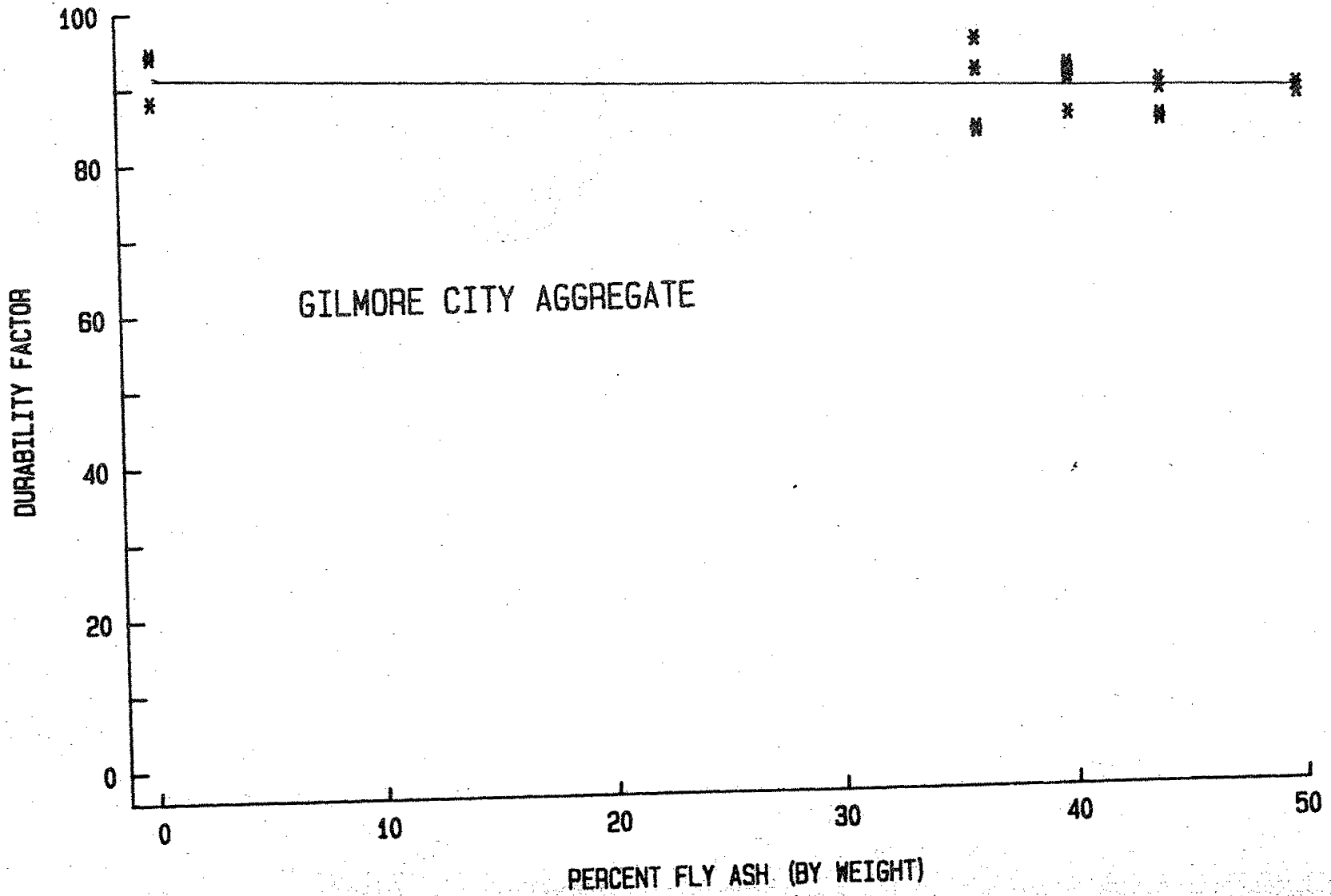


Figure 14. Durability - Gilmore City aggregate and several fly ashes.

for higher fly ash substitutions and that loss in durability for Alden aggregate is somewhere beyond the 75 percent replacement level. Durability reduction for the Montour aggregate occurs at much lower fly ash replacements (i.e. between 25 and 50 percent). The Gilmore City aggregate appears to be an intermediate material where a slight degeneration in durability with fly ash can be observed, at least up to the 50 percent fly ash replacement level.

In as much that the ASTM C 666-80 durability tests are capable of predicting field performance of portland cement concrete, these results suggest that for at least one aggregate (Alden) the introduction of fly ash has little influence on resistance to frost action, even at fly ash replacements up to 75 percent. For a second aggregate (Montour), these results indicate a 25 percent fly ash replacement limitation. Although traditionally, the Alden and Montour aggregates occupy different positions in the Iowa DOT durability classification scheme (11), samples used in these tests show very little difference in non-fly ash concretes. A significant question leading from these results is how might differences in behavior of these and other aggregates be predicted short of the lengthy, time consuming ASTM C 666 durability test. A necessary element to prediction is understanding the mechanism.

Durability and Pore Structure

For a given aggregate, pore structure of the mortar phase of hardened concrete is widely accepted as a major contributor to the freeze-thaw durability of concrete (10,12,13). The pore structure exclusive of entrained air is comprised of two distinct groups of pores, capillary pores and gel pores. Capillary pores are voids that were

originally water in the fresh paste, and as the water was consumed during hydration of the cement compounds, these voids remained. In immature pastes, these voids are interconnected, but as hydration proceeds, hydration products may block or at least reduce the size of these pores (13). It has also been shown that introduction of fly ash can further reduce capillary size through production of solid pozzolanic products (10). Capillary pores determine porosity of concrete, can act as a reservoir of unfrozen water, and can thus play an important role in determining the concrete's durability against frost action (10).

A second somewhat arbitrarily defined group of pores are called gel pores. These are the very small interconnected, interstitial spaces between the gel particles with an average diameter of 15-10 Å (10,12). Both groups of these pores are important to freeze-thaw durability, but it is not just the total number of each group, or their combined volume, but rather the overall pore system distribution that determines durability.

An important aspect of evaluating the influence of capillary and gel pores on freeze-thaw durability is the phenomenon of freezing point depression in capillaries. Pore water freezes in capillaries at different temperatures based on the equation 5:

$$r = \frac{2\gamma T_0}{\rho \lambda \Delta T} \quad (5)$$

where

r = radius of capillary

γ = 29 ergs/cm² (surface energy)

λ = 80 calories/gram (heat of fusion of ice)

T_0 = 273°C (absolute zero)

$\rho = 1 \text{ gram/cm}^3$ (density of water)

$\Delta T =$ temperature ($^{\circ}\text{C}$) at which freezing occurs,

which reduces to

$$r = \frac{473}{\Delta T}$$

where r is in Angstroms (\AA). (It must be remembered that this equation is based on ideal properties and is therefore an approximation.)

If the standard freeze-thaw durability test (ASTM C-666) is followed and the temperature is reduced to 0°F (-18°C), then freezing would be initiated in all capillaries larger than 26\AA radius. Thus, the water will not freeze in pores smaller than 26\AA but they are still important to the durability by being a source capable of feeding water to larger pores, where water can be frozen.

A third factor in concrete durability is entrained air. Entrained air is voids that are intentionally incorporated into the paste by means of a suitable agent. These voids have average diameters of 10-50 μm . The main function of entrained air voids is believed to relieve the osmotic pressures caused when water starts freezing in the larger capillary pores and the freezing water moves toward bulk ice in the freezing front to reach thermodynamic equilibrium (12). Thus, the actual controlling factor in determining the effectiveness of air entrained voids is the distance between adjacent entrained air voids interconnected by capillary pores or the spacing factor. The shorter the spacing factor, the easier and more quickly osmotic pressures can be relieved. It is generally accepted that for the voids to provide adequate protection, a spacing factor as measured by microscopical determination (ASTM C 457-71) of approximately 0.20 mm or less is required (14).

Previous research has shown that air bubble stability is influenced by water-soluble alkali present in portland cement (16) while more recent work suggests that alkalis in fly ash can have a similar influence (17). It was hypothesized that bubbles in a plastic fly ash-concrete mortar were less stable and coalesced, thus diminishing the abundance of small bubbles and increasing the spacing factor. Neutralized Vinsol resin (the standard for laboratory testing) was found to be less stable in the presence of fly ash than neutralized salts of sulfonated hydrocarbons. These observations were further supported by observing air content retained in plastic fly ash concretes with time. ASTM C 618 Class C fly ashes appeared to be more stable than Class F ashes (17).

Pore Structure Evaluation

In an attempt to explain the fly ash-concrete durability phenomenon for Montour and Alden aggregates, three techniques were used to evaluate pore composition of hardened concrete. Three groups of specimens were made from selected concrete batches for ranges in fly ash replacement and frost durability performance. These specimen groups are defined in Table 17. It should be emphasized that what is termed constant water-cement ratio is in terms of water-portland cement ratio a variable. As fly ash content increases, so does water-portland cement ratio.

Table 17. Pore structure evaluation groups

Group	Description	Appendix C Batch Number
I	Constant water-cementitious materials (cement plus fly ash) = 0.43 Slump = 2 1/2" to 8" Fly ash content = 0, 25, 50, 75 & 100% Air content = 5.4 to 7% Aggregate = Montour and Alden	32, 34, 36, 41.1, 41.2 42 to 46
II	Constant slump = 2" + 1/2" Water-cement ratio = 0.42 to 0.30 Fly ash content = 0, 25, 50, 75 & 100% Air content = 4.7 to 6.0% Aggregate = Montour and Alden	37 through 41 47 through 51
III	Variable air = 2.6 to 12.5% Slump = 2 1/2" to 6" Water-cement ratio = 0.43 to 0.38 Fly ash replacement = 0, 25 & 50% Aggregate = Montour and Alden	52 through 67

Mercury Porosimetry

Mercury porosimetry (MP) is a fairly simple and versatile method of investigating the pore size distribution of porous materials. The basic principle is that mercury, a non-wetting liquid, is forced into pores by a gradually increasing pressure. The pressure applied can be converted into the pore radius using the equation:

$$r = \frac{-2\gamma \cos\theta}{P} \quad (6)$$

where

r = radius of the pore

γ = surface tension of mercury (484 dynes/cm)

θ = contact angle (117° for concrete paste)

P = pressure.

The mercury porosimeter (Quantachrome SP-200) used in this investigation is equipped with a microprocessor. It measures the volume of mercury intruded, and plots the cumulative volume of mercury versus the pressure or radius and the first derivative of the volume-pressure function (dV/dp). This function, when converted to change in volume with respect to radius (dV/dr) and plotted versus r , represents the size distribution of pore volume. That is, the area under the dV/dr versus r curve for a particular range of radii represents that radii range of total pore volume. For example, if the total area under the curve was 100 units and the area under the curve from 20 \AA to 30 \AA was 2, then 2% of the total pore volume would be comprised of pores with radii from 20 \AA to 30 \AA . Thus, the plot of dV/dr versus r is a form of pore size distribution.

As porosimeter pressure is increased, mercury is intruded into

smaller and smaller pores. When the pressure is high enough to force mercury into a small pore that is connected to a larger air void, the air void is also filled with mercury. The porosimeter reads this volume as if it belongs to the smaller pore radius whereas in reality much of that volume is air voids. This limitation is partially overcome by gradually reducing the pressure after the application of the maximum pressure. This depressurization results in the extrusion of mercury from the uniform pores intruded up to constrictions which connect uniform capillary pores to large voids. Therefore by gradually reducing the pressure an extrusion curve, showing the size distribution of constricting capillary pores is obtained. A second intrusion may also be used to obtain the size distribution of the constricting capillary pores. But in mercury porosimetry the sizes of constricted larger voids remain unknown. The ratio of the volume intruded to the volume extruded within a pressure range (which corresponds to a capillary size range) reflects the volume of large voids with constrictions of this size range.

The evaluation of concrete mortar pore structure by mercury porosimetry was accomplished using two sets of graphs. The volume versus radius (V/r) plot primarily illustrates total pore volume, and the dV/dr versus r ($dV(r)$) plot illustrates pore size distribution.

The V/r curves for constant w/c , Group I, concrete and constant slump, Group II, concrete are shown in Figures 15 and 16, respectively. Total pores occupy twice as much volume in the constant w/c mixes as they do in the constant slump mixes, except at 100% fly ash replacement. This dramatically illustrates how w/c effects pore structure of hardened concrete mortar. Comparing Montour aggregate and Alden aggregate from

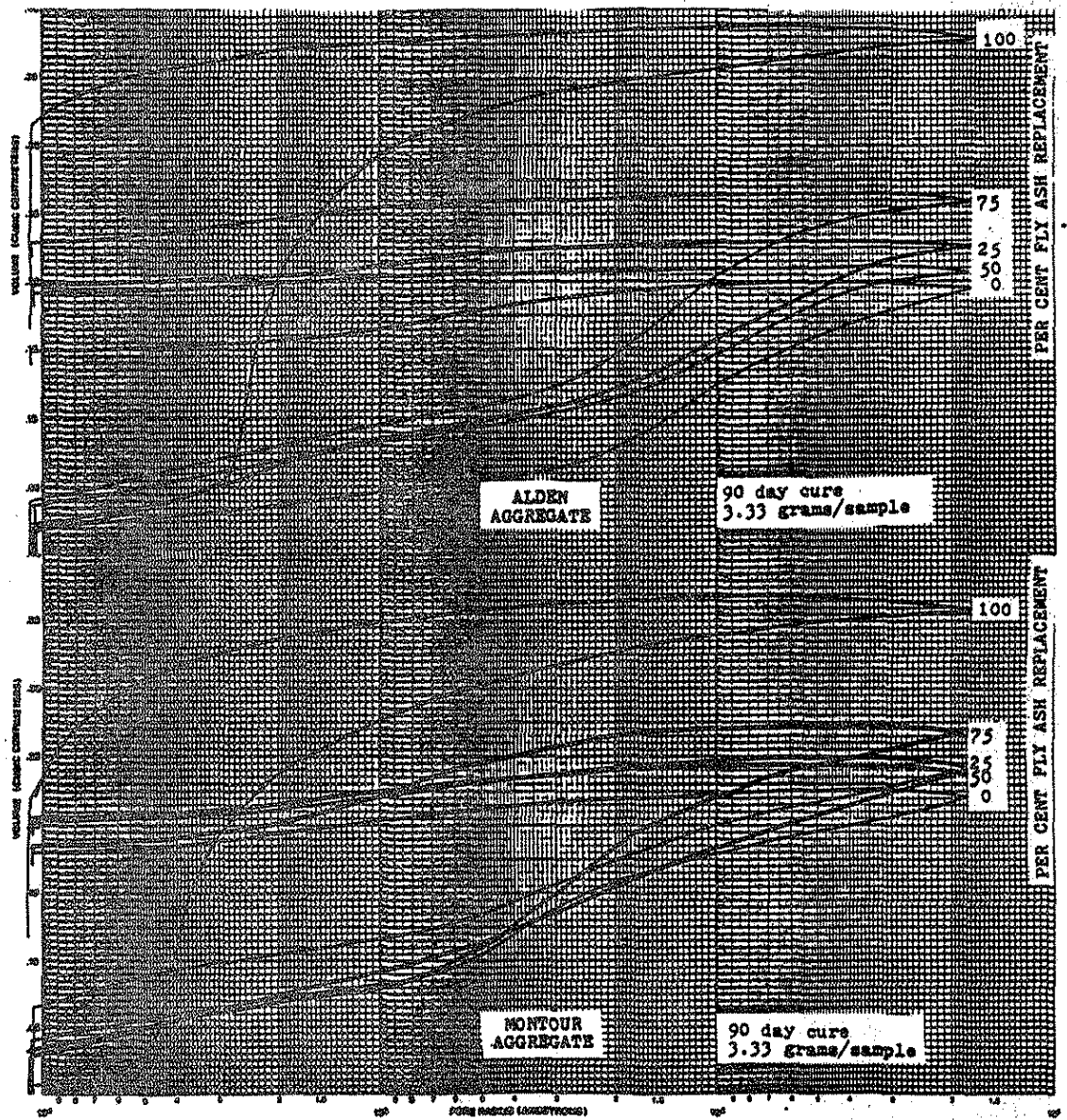


Figure 15. V/r curves for constant w/c mortar, Group I.

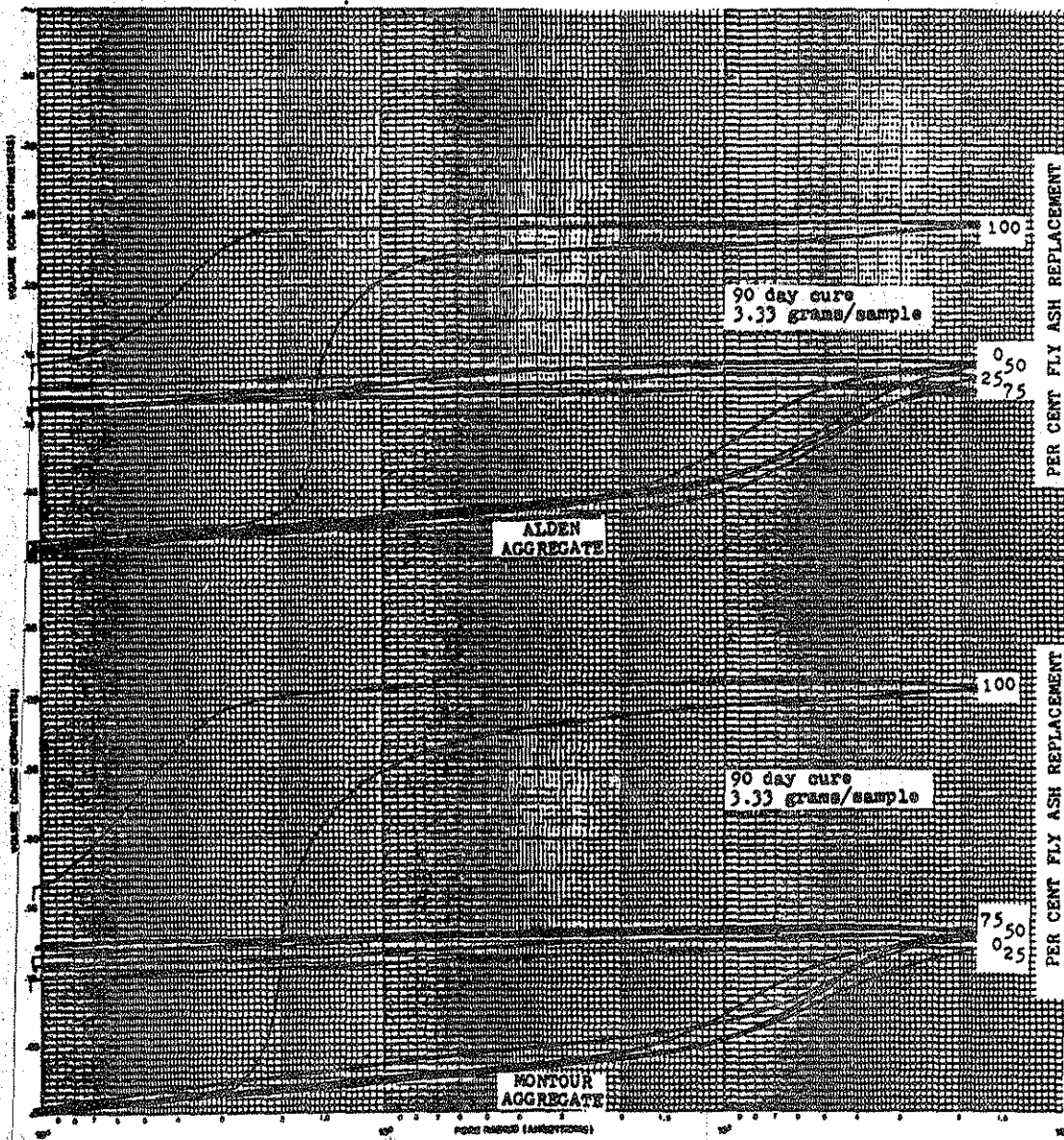


Figure 16. V/r curves for constant slump mortar, Group II.

the same figure, it does not appear that total pore volume is significantly changed by coarse aggregate, in either constant w/c or constant slump mortars.

The $dV(r)$ curves illustrate pore size distribution from approximately 200 Å to 18 Å. By comparing the general shape of these plots, it is possible to determine how different factors such as fly ash, aggregate, and w/c, influence the pore size distribution.

The first comparison is the constant w/c (Group I) mixes. The Montour aggregate (Figure 17) control mortar shows an increasing percentage of pores, as pore radius decreases. In contrast, the Alden aggregate (Figure 18) control mortar has a much more uniform pore size distribution. This difference is significant because it implies a novel concept: the pore constriction distribution of concrete mortar may be altered by coarse aggregate. Comparing the 25%, 50%, and 75% fly ash replacements in Figure 17, to those same replacements in Figure 18, also illustrates what appears to be an alteration of pore distribution.

When fly ash replacement percentage is increased beyond 75%, the pores smaller than 26 Å decrease in percentage, while the larger pores increase in percentage of total pore volume. This trend is more evident in concrete made with Alden aggregate, but is also true in Montour aggregate concrete as well.

The second comparison is with the constant slump mixes (Figures 19 and 20). Here, durability factors (DF) should be kept in mind because the strength through 75% fly ash replacements for both aggregates were stronger than the controls (See Appendix C). The concrete made with Montour aggregate was only durable through 25% replacement, while Alden aggregate concrete was durable through 75% fly ash replacement. Yet,

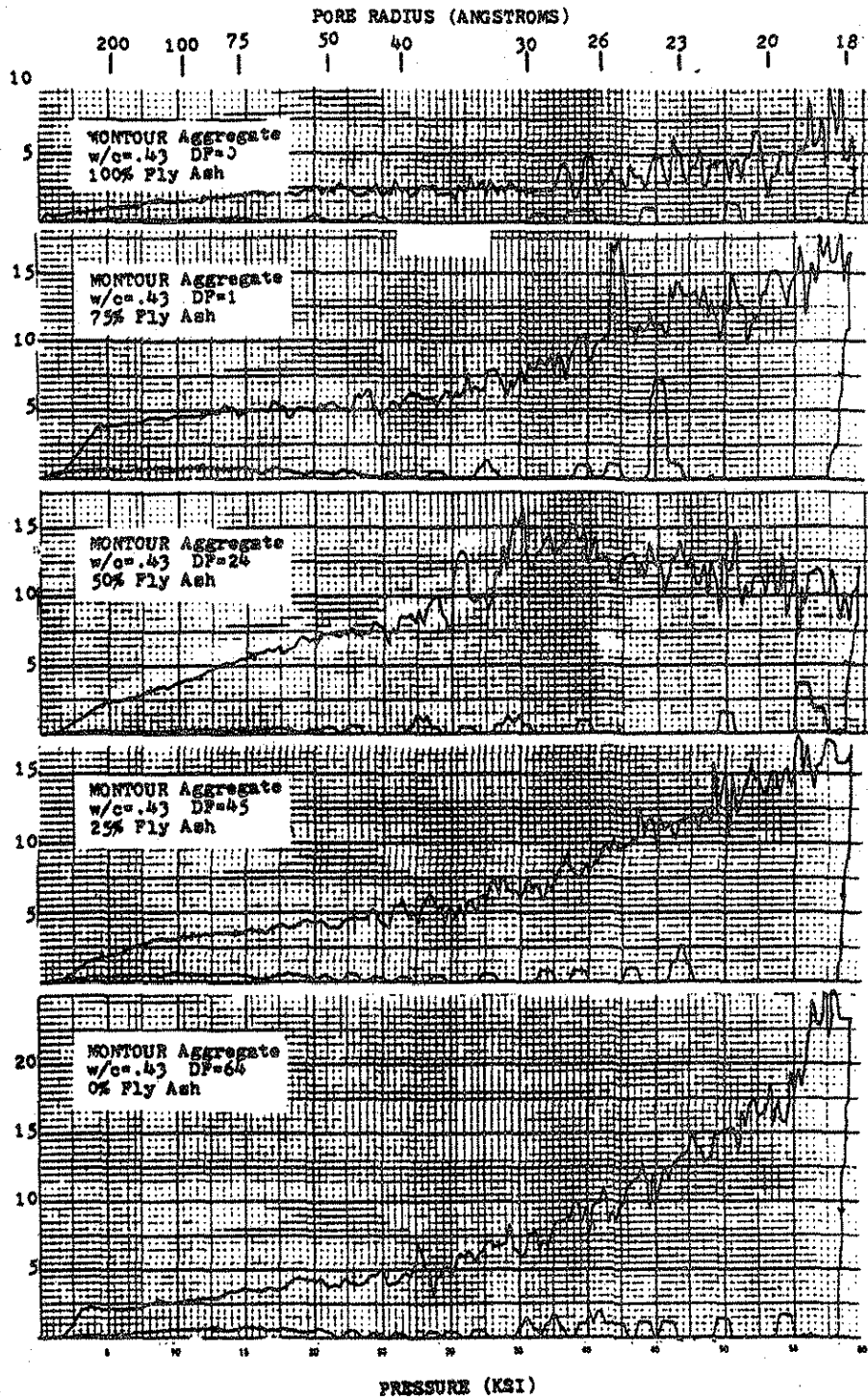


Figure 17. $dV(r)$ curves for constant w/c concrete made with Montour aggregate.

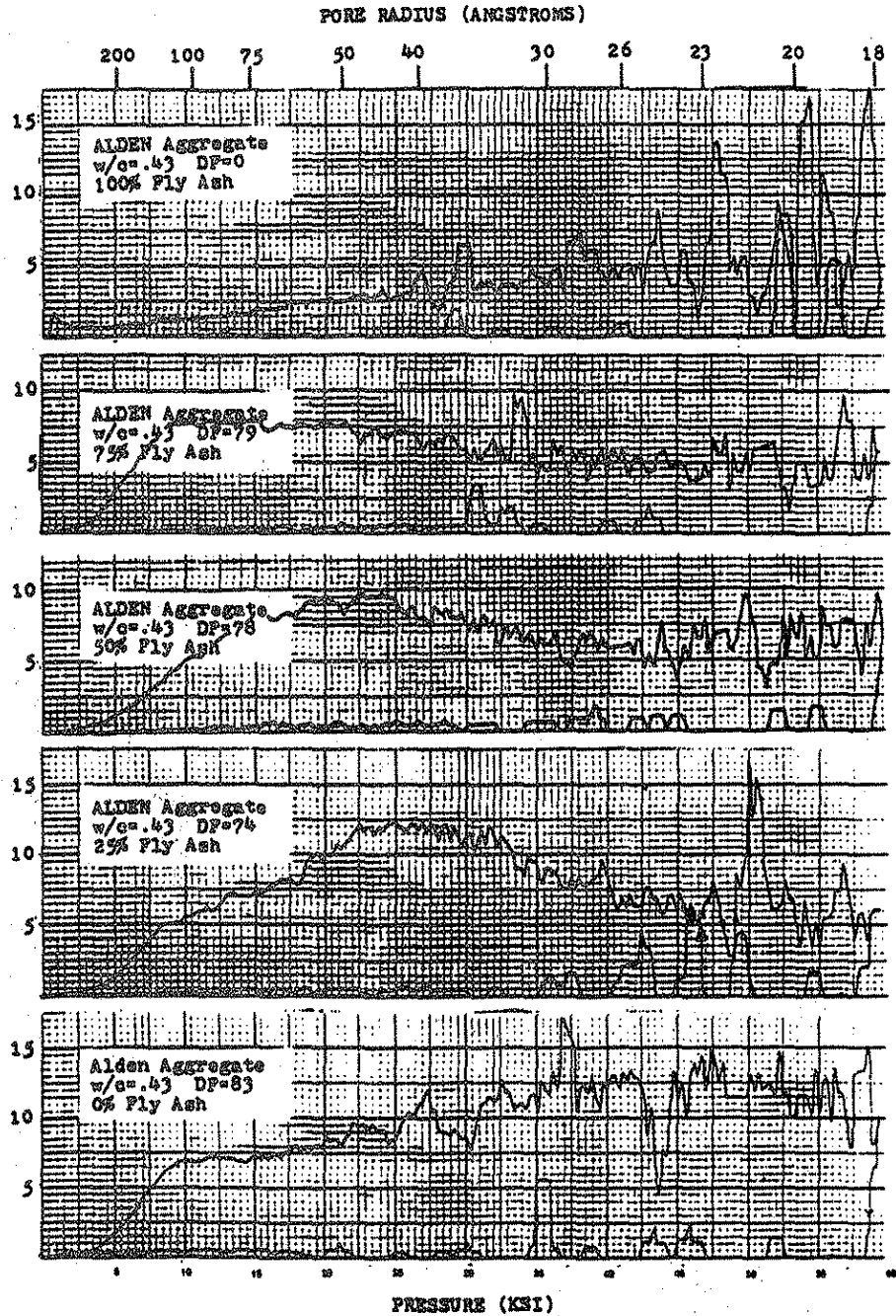


Figure 18. $dV(r)$ curves for constant w/c concrete made with Alden aggregate.

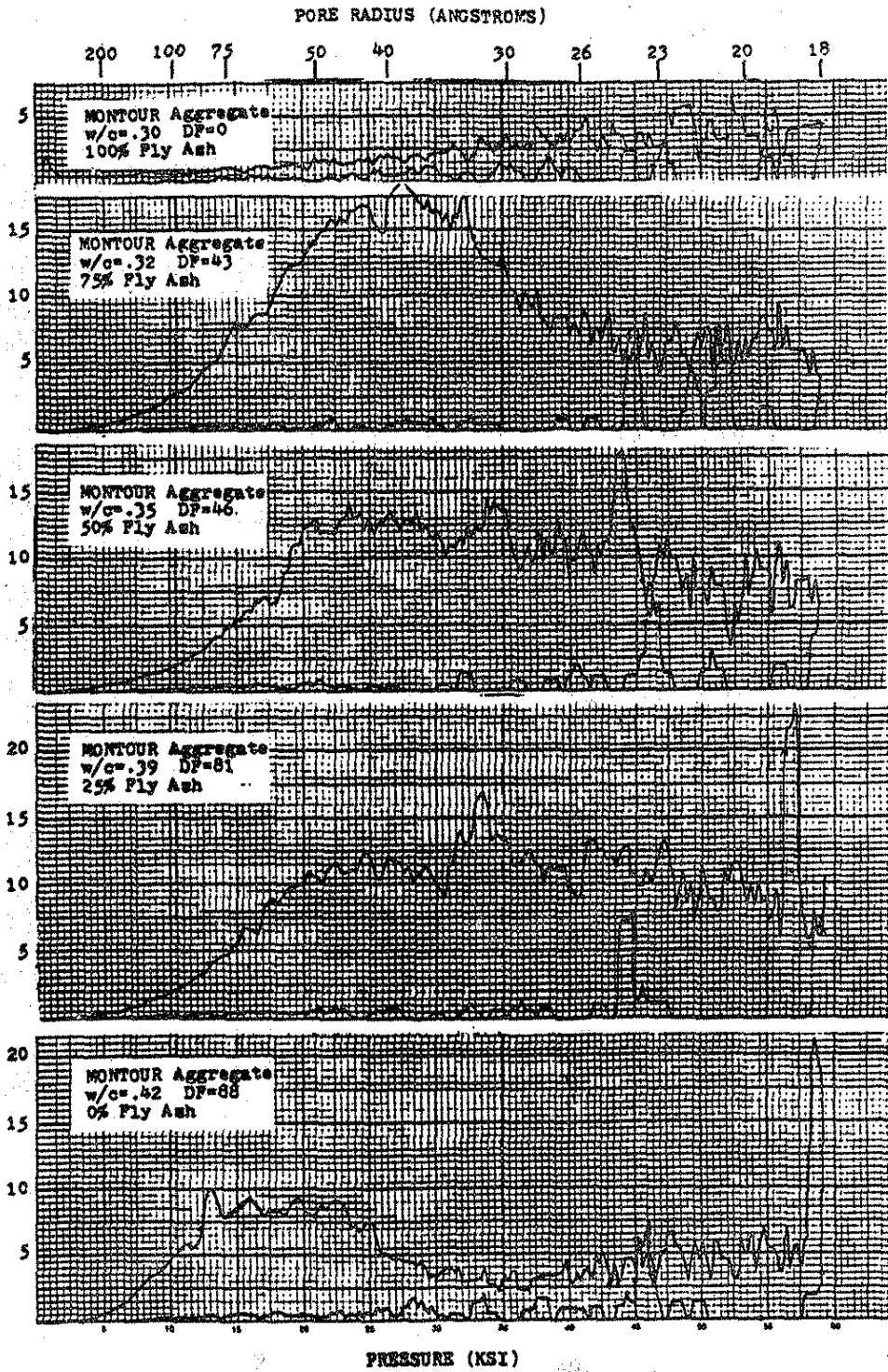


Figure 19. $dV(r)$ curves for constant slump concrete made with Montour aggregate.

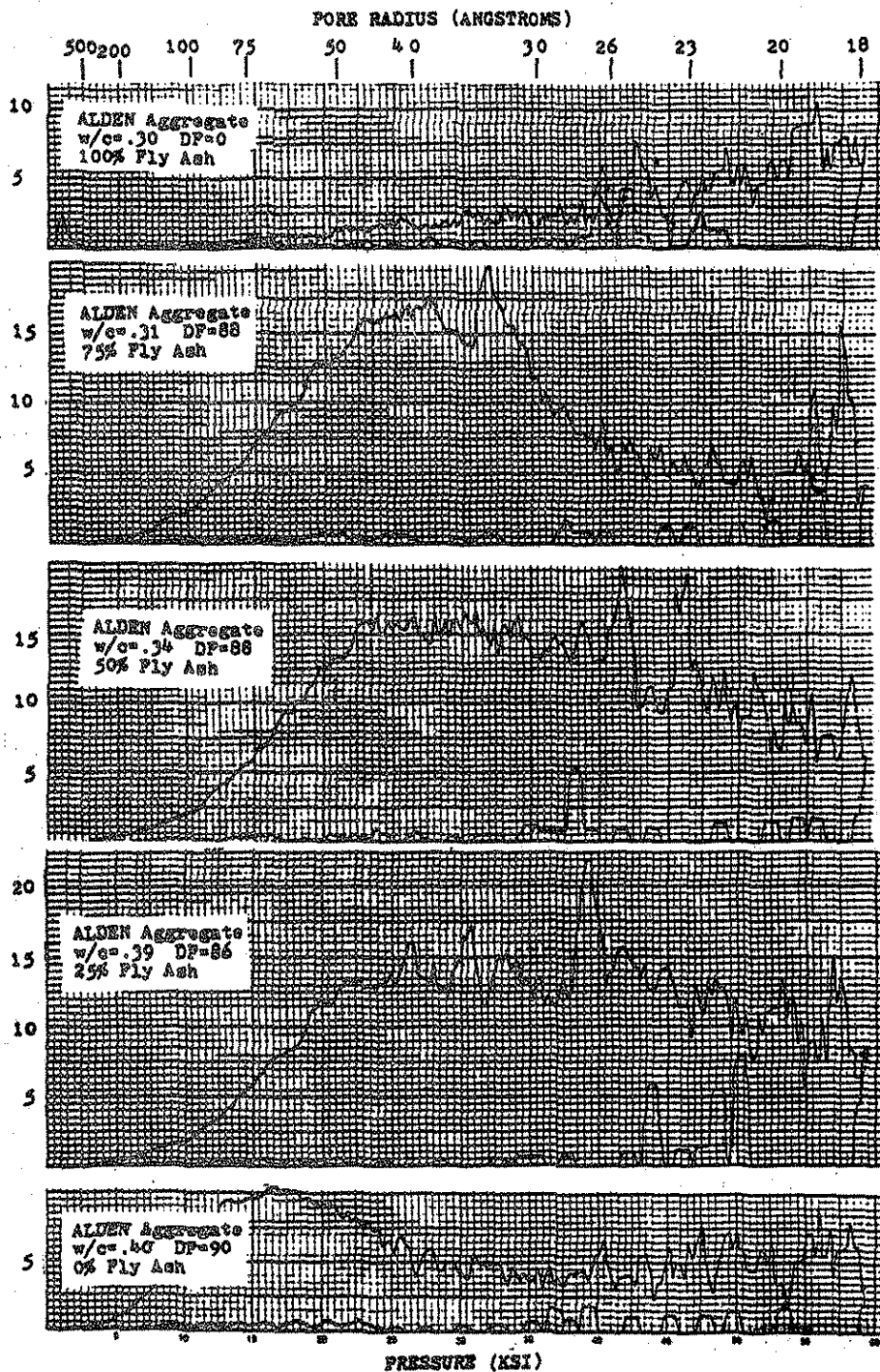


Figure 20. $dV(r)$ curves for constant slump concrete made with Alden aggregate.

there is no substantial difference in pore size distribution of 50% and 75% replacements made with Montour aggregate (Figure 19), and the same fly ash replacements made with Alden aggregate (Figure 20). This suggests that as measured by mercury intrusion, pore size distribution is influenced by variation in water-portland cement ratio but there does not appear to be a correlation to durability factor. This is particularly true where water-cement (portland cement plus fly ash) ratios were reduced to maintain constant slump.

In an attempt to clarify this obscurity the third group of experiments were initiated during the latter part of the project. The summary of results obtained during this period are tabulated in Tables 18 and 19. More detailed pore size distribution bar graphs are given in Appendix D. The data in Tables 18 and 19 and Appendix D were obtained by graphical integration of mercury porosimetry results. The difference between the total volumes intruded during the first and second intrusion cycles indicate the volume of large pores (which include the air voids) interconnected by capillary pores. The data reported in these tables and Appendix D indicate a pore volume and structure change with age and the volume of pores with openings larger than 500 \AA along with the amount of entrained air appear to play a decisive role in concrete durability. Only those concrete mixes with very low entrained air contents failed in durability. All other mixes tested thus far showed satisfactory durability. It is possible that mixes made with higher fly ash contents (especially those prepared with Montour aggregate) will show larger variability in durability making correlation of durability with pore structure possible. Results of tests with higher fly ash contents which should offer more decisive differences in durability will

Table 18. Summary of mercury porosimetry results for mortar phase of concrete prepared with Montour aggregate and durability results.

Fly ash, %	W/C	Entrained air, %	Cure, days	% Total vol. intruded		$\left(\frac{\Delta V_1}{\Delta V_2}\right)^*$ 500	Strength, psi	Durability factor
				ΔV_1 1st Intr.	ΔV_2 2nd Intr.			
0	.43	2.6	3	14.2	5.9	2.1		
			7	7.9	2.3	1.9	5250	
			28	9.0	2.9		6500	0
			90				7300	0
0	.41	6.0	3	17.4				
			7	15.9	4.9	2.4		
			28	10.7	1.9	5.4	4750	93
			90				5650	89
0	.41	9.5	3	24.7	9.2	7.0		
			7	19.4	3.7	5.5	3600	
			28	20.7	7.1	6.4	4450	94
			90				4950	93
0	.41	10.5	3	21.9	6.2	3.8		
			7	21.2	3.3	4.4	3400	
			28	21.6	4.2	12.8	4200	91
			90				4700	81
25	.40	3.2	3	12.9	6.5	1.1		
			7	14.1	8.1	2.0	5250	
			28	9.9	3.5	1.3	6650	0
			90				7600	0
25	.38	6.6	3	17.4	8.1	3.5		
			7	29.2	8.9	4.3	4450	
			28	14.1	2.7	2.4	5750	94
			90				6550	84
25	.38	8.5	3	20.1	8.3	4.2		
			7	21.4	7.0	20.8	4100	
			28	15.6	5.5	2.0	5150	89
			90				5600	85
25	.38	11.2	3	21.6	5.6	7.4		
			7	25.9	9.5	2.7	3100	
			28				4050	96
			90				4450	79

* Ratio of first and second intrusion volume of pores larger than 500 Å.

Table 19. Summary of mercury porosimetry results for mortar phase of concrete prepared with Alden aggregate and durability results.

Fly ash, %	W/C	Entrained air, %	Cure, days	% Total vol. intruded			Strength, psi	Durability factor
				ΔV_1 1st Intr.	ΔV_2 2nd Intr.	$\left(\frac{\Delta V_1}{\Delta V_2}\right)_{500}$		
0	.43	3.4	3	13.9	5.5	1.6		
			7				5550	
			11	15.8	9.8	2.7		
			28	12.3	6.6	2.6	6300	0
			90				7600	0
0	.42	10.5	3	21.5	5.4	4.3		
			7	21.2	11.2	2.0	3250	
			28	19.9	6.2	9.8	4150	100
			90				4850	88
0	.42	12.0	3	26.9	7.7	4.7		
			7				2950	
			11	27.71	9.5	6.9		
			28				3600	95
			90				4250	93
25	.39	3.2	3	12.8	5.3	1.4		
			7				6050	
			11	14.9	9.0	2.8		
			28				7150	0
			90			1.0	8100	0
25	.39	8.7	3	20.4	9.0	3.8		
			7	18.5	7.5	10.1	4550	
			28	14.9	4.0	6.2	5150	98
			90				6100	89
25	.39	12.5	3	25.7	9.2	7.0		
			7	22.7	7.9	7.8	3250	
			28				4000	93
			90				4600	88

be available in the near future and should prove useful; these results and an analysis will be submitted as a special report.

Entrained Air in Hardened Mortar

Although mercury porosimetry is a useful means of measuring pore structure, its inability for providing a direct measure of entrained void distribution could lead to an improper diagnosis of aggregate fly ash durability. Thus, two methods for directly measuring entrained void composition were used. The first involved development of a computerized image analysis technique using a Lamont image analyzer and a scanning electron microscope. Figure 21 shows the image resulting from a concrete specimen where pores have been impregnated with epoxy resin. When viewed with the image analyzer, electron emissions from low atomic weight materials (epoxy filled voids) show as dark spots which can be measured by electronically superimposing a grid over the image and allowing the computer to count squares. Figure 22 is a typical result for the void area distribution of the image in Figure 21. A total of 28 voids were detected and their frequency by area measured in square micrometers is presented as a histogram. Alternate forms of output include histograms for edge-to-edge free path (twice the spacing factor) and percentage voids on the surface area.

Table 20 summarizes the results of image analysis data on specimens cut from concrete mixes 32, 34, 41.1, 41.2 and 42 through 45 listed in Appendix C. For comparison, ASTM C 457-82 linear traverse measurements made on the same specimens are also reported in Table 20. Spacing factor is the only result of the two methods which is readily comparable. With one exception, Alden aggregate concrete without fly

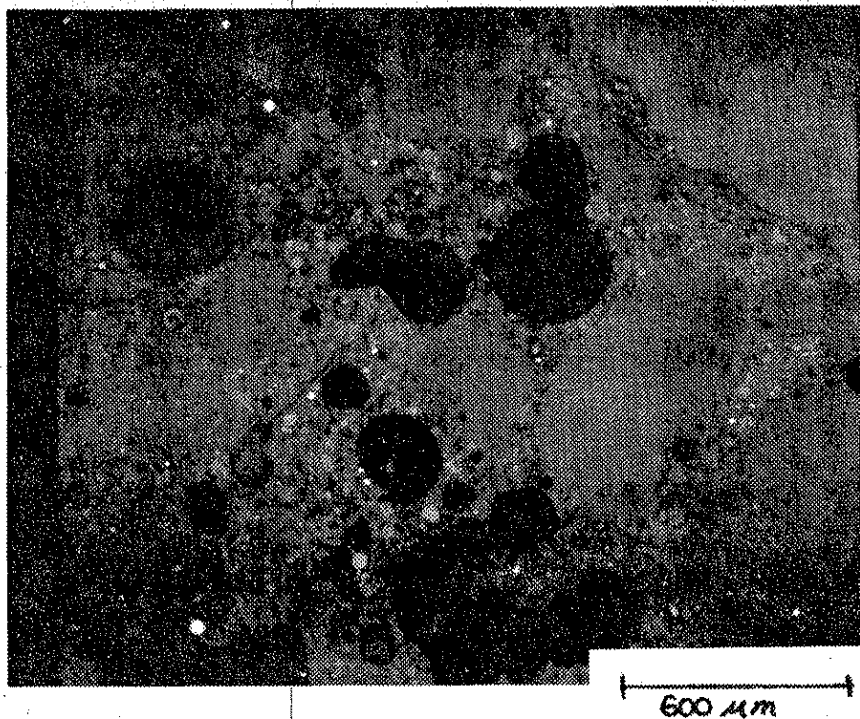


Figure 21. Typical image analysis of fly ash concrete.

SAMPLE ID: 50X FLYASH 2

PARTICLE AREA (SQ UM.) DISTRIBUTION FOR LL TYPES MACR = 0

MOST PROBABLE= 7.30E 03 MEDIAN= 3.40E 03 AVG= 2.39E 04 SIGMA= 5.46E 04

CLASS	LIMIT	COUNT	%	0	1	2
1.20E 02	0	0	0.00	[
2.40E 02	2	7.14	7.14	*****		
4.80E 02	4	14.29	14.29	*****		
1.00E 03	4	14.29	14.29	*****		
2.40E 03	3	10.71	10.71	*****		
4.80E 03	2	7.14	7.14	*****		
1.20E 04	5	17.86	17.86	*****		
2.40E 04	2	7.14	7.14	*****		
4.80E 04	0	0.00	0.00			
1.20E 05	5	17.86	17.86	*****		
2.40E 05	0	0.00	0.00			
4.80E 05	1	3.57	3.57	*****		

Figure 22. Void area distribution for fly ash concrete.

Table 20. Evaluation of hardened mortar.

Fly ash replacement, %	Montour								Alden							
	0		25		50		75		0		25		50		75	
Evaluation method	IA	LT	IA	LT	IA	LT	IA	LT	IA	LT	IA	LT	IA	LT	IA	LT
Spacing factor (micrometers)	619	432	559	416	588	404	465	517	1034	577	465	315	417	419	332	513
Average void diameter (micrometers)	61	--	75	--	80	--	122	--	110	--	129	--	126	--	142	--
Void area in mortar fraction, %	5.4	--	7.8	--	8.8	--	12.6	--	8.3	--	14.5	--	11.5	--	16.2	--
Durability factor	64		45		24		1		63		74		76		79	

IA = Image analysis

LT = Linear traverse ASTM C 457-82

ash, linear traverse and image analysis produced similar results, particularly when viewed in light of the fact that it has been demonstrated that the linear traverse can be an imprecise technique (18). Also, a comparison is not totally valid because the linear traverse produces a computed spacing factor, based on chord length measurements as the traverse happens to intersect the voids. A major presumption of the linear traverse is a uniform distribution of voids. On the other hand, image analysis makes no such presumption about void distribution and can resolve a feature to 0.4 micrometers. Thus spacing factor is based on a precise measurement of distances between nearest neighbor voids.

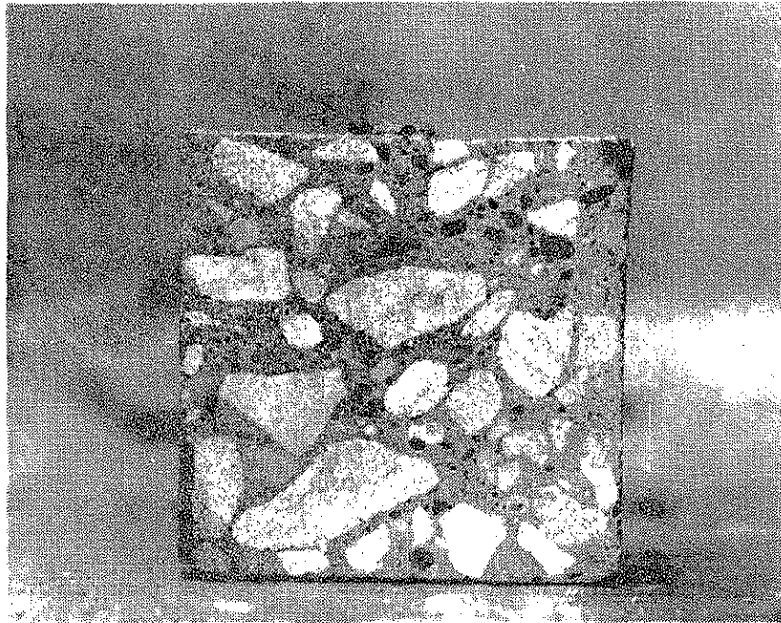
Table 20 also shows some interesting results with regard to durability. For all cases, spacing factors are more than twice the 200 micrometer upper limit considered necessary for durable concrete (14). Spacing factor for these specimens appears to be relatively independent of fly ash content and also durability. There is, however, a relation between average void diameter, fly ash content and durability factor for Montour aggregate. Void diameter increases with fly ash content and durability decreases. For Alden aggregate, void diameter remains relatively constant for different fly ashes and so does durability. These results are inconsistent with traditional concepts of air entrainment and its role in reducing frost action. Durability should correlate to spacing factor, not void diameter. One possible explanation is that air entrainment void structure in these concretes may not be uniformly distributed throughout the mass and the averaging process used for both linear traverse and image analysis may not offer an adequate definition.

Microscopic observations of sections sawed from specimens subjected to 300 freeze-thaw cycles showed a significant part of the deterioration was associated with the aggregate-mortar interface. Comparative photographs of Montour aggregate concrete specimens after being subjected to 300 freeze-thaw cycles are shown in Figure 22a. Neal 4 fly ash at 25 and 50 percent replacement was used to make these specimens and frost deterioration is evident at the upper surface of the lower photograph. Photographs in Figure 23 are close-ups of the deteriorated zone of the 50 percent fly ash specimen where it can be seen that a significant factor to the deterioration is cracks around aggregate perimeters. This tendency for aggregate to peel away from the mortar suggests the region of interest should be aggregate boundaries.

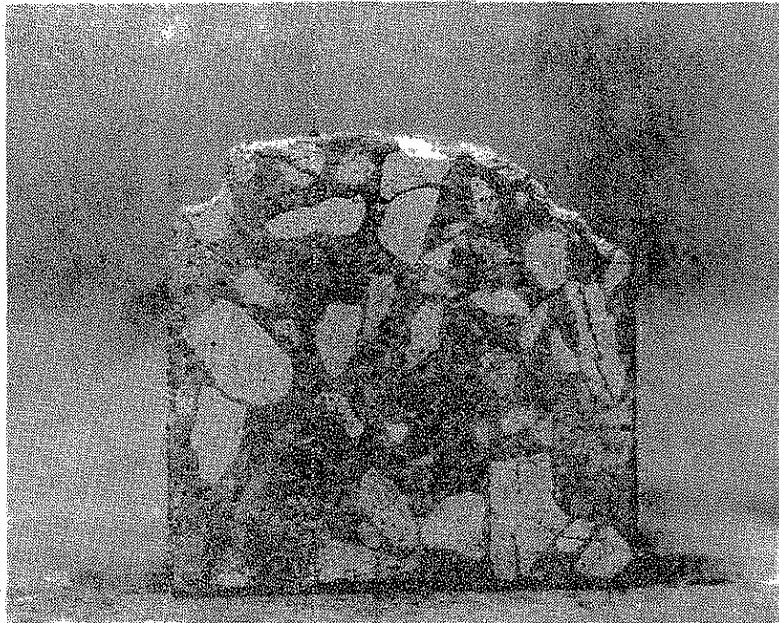
Light microscope (5x magnification) photographs for a sequence of specimens not subjected to frost action are in Figure 24. Numbers in the lower right hand corner are fly ash replacements and each unit on the scale at the bottom represents 1 mm. The interesting feature here is a concentration of air bubbles (noted by arrows) at several aggregate-mortar boundaries. This air bubble concentration is a prominent, consistent feature with Montour aggregate concretes at fly ash concentrations of 50 percent or more. Bubble rings have not been observed with the Alden aggregate at any fly ash concentration.

Pore Distribution Along Aggregate Edge

To quantify the bubble ring phenomenon, a simple adaptation of the linear traverse was developed. Specimens were sliced from representative concrete cylinders with a diamond saw and then ground and polished to an essentially planar surface in which the edges of air



a) Montour aggregate - 25% Neal 4 fly ash.



b) Montour aggregate - 50% Neal 4 fly ash.

Figure 22a. Durability beams after 300 freeze-thaw cycles.

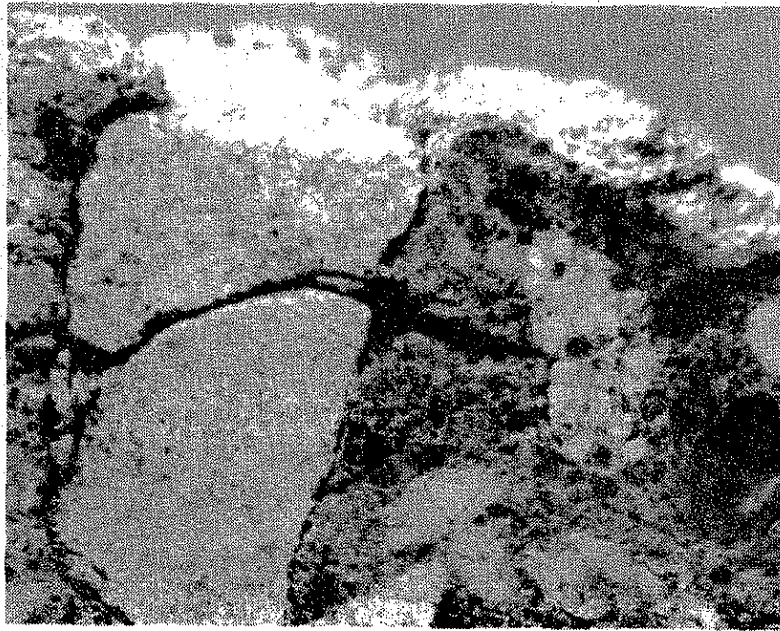
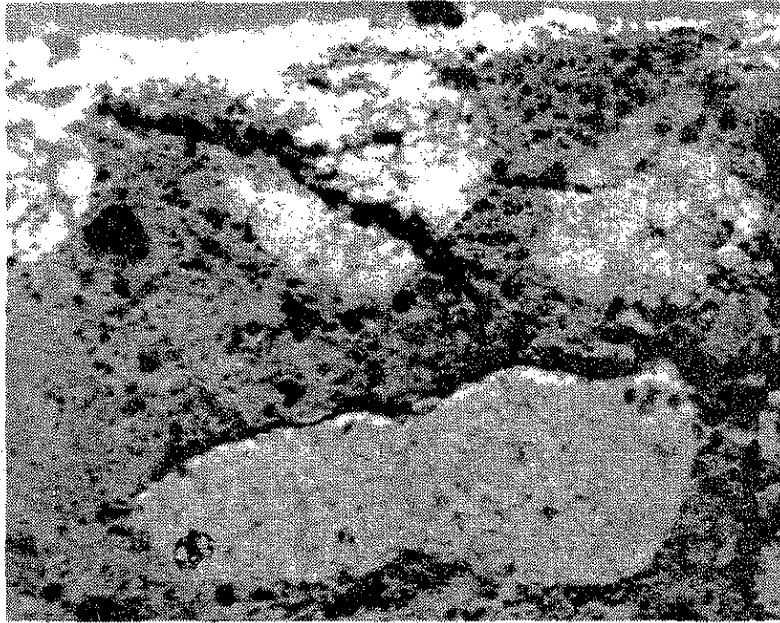


Figure 23. 5X magnification of 50% fly ash specimen - Montour aggregate.

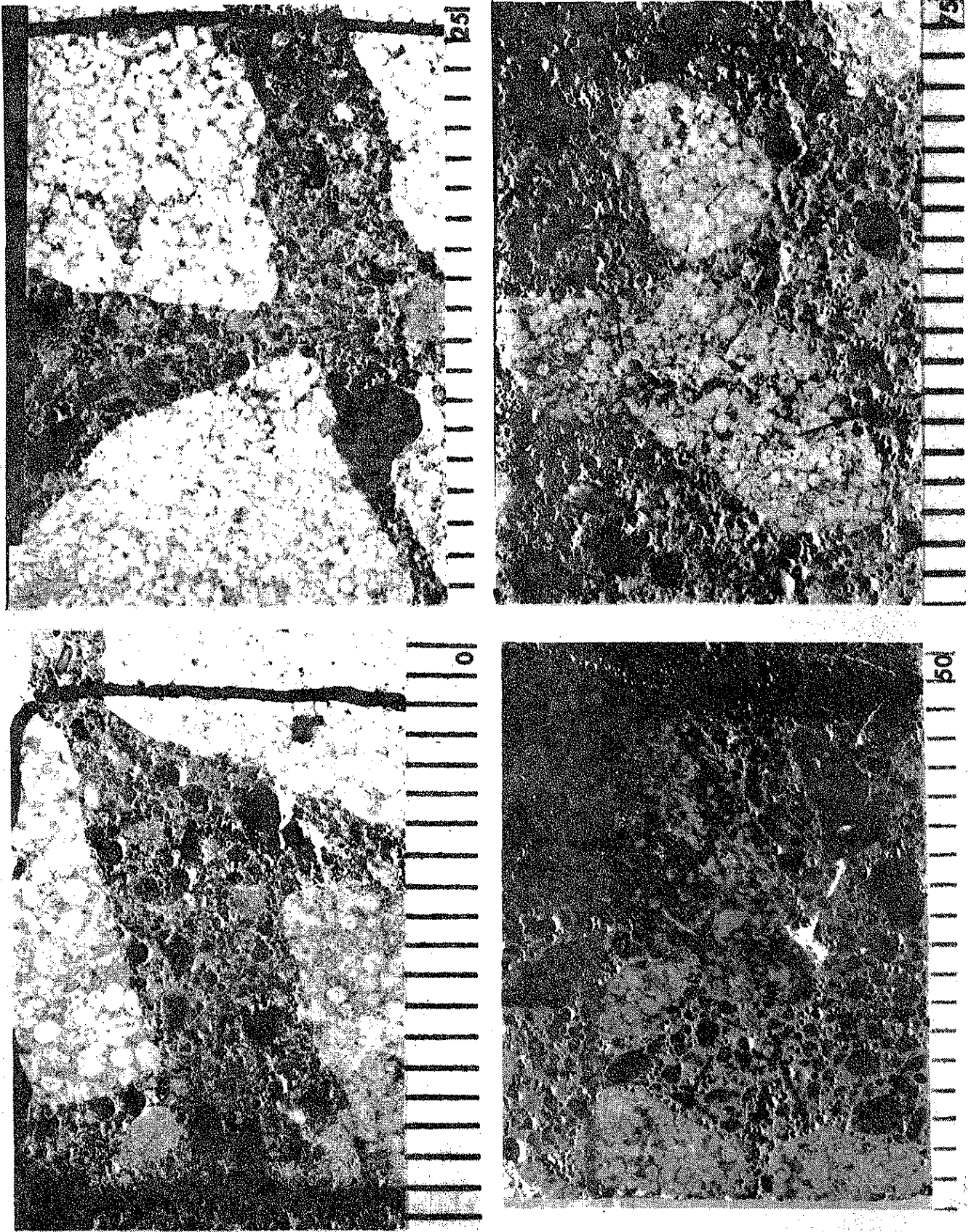


Figure 24. Montour aggregate-fly ash concrete microphotographs.

voids appeared sharp and defined when viewed under the light microscope. The test procedure consisted of locating straight planar edges on the large aggregates and performing a series of parallel, equally spaced traverses progressing away from the aggregate into the mortar. A series of traverses were performed on several aggregate particles of each specimen and analyzed for air content at the various distances from the aggregate surfaces as shown in Figure 25. The result of the modified linear traverse is a percentage of air in the traverse at different distances from the aggregate-mortar boundary. In addition to tests on Montour aggregate, tests were performed on concrete containing Alden aggregate and fly ash contents equal to those used with the Montour specimens to determine whether the phenomena is measurable with this type of aggregate.

Figure 26 presents results of the linear traverse performed on the Montour aggregates illustrating a definite concentration of entrained air bubbles along the periphery of the large aggregates when fly ash is introduced into the concrete. At 0% fly ash an essentially uniform and equal pore distribution occurs throughout the paste, but with an increase in fly ash content the air content increases along the edge of the aggregate. Figure 27 graphically reflects the results of a similar series of linear traverses performed on fly ash concrete containing Alden coarse aggregate. As with the 0% fly ash concrete containing Montour aggregate, the 0% fly ash-Alden aggregate specimen shows essentially a uniform distribution of entrained air voids throughout the paste. However, when fly ash was introduced, slightly higher air contents were observed along the periphery of the aggregate particles, though not nearly as substantial as with the Montour aggregate.

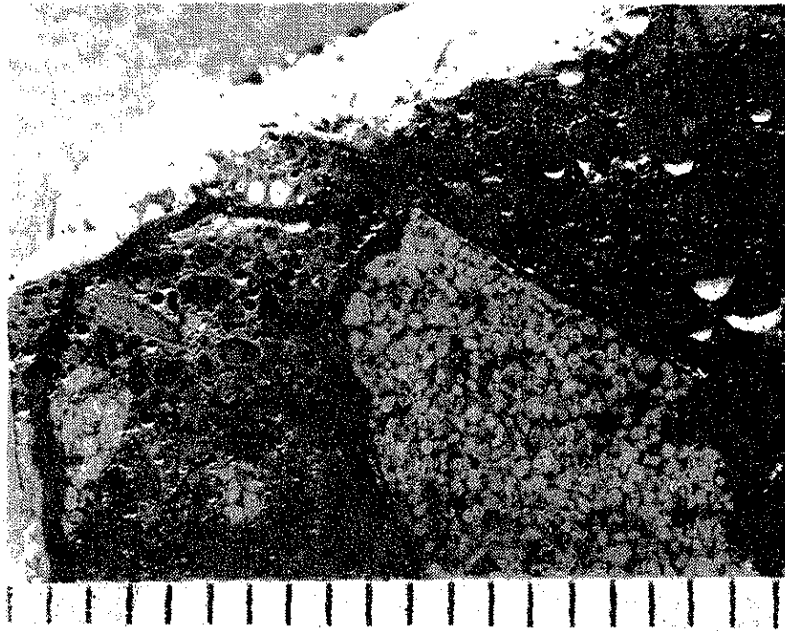


Figure 25. Modified linear traverse paths.

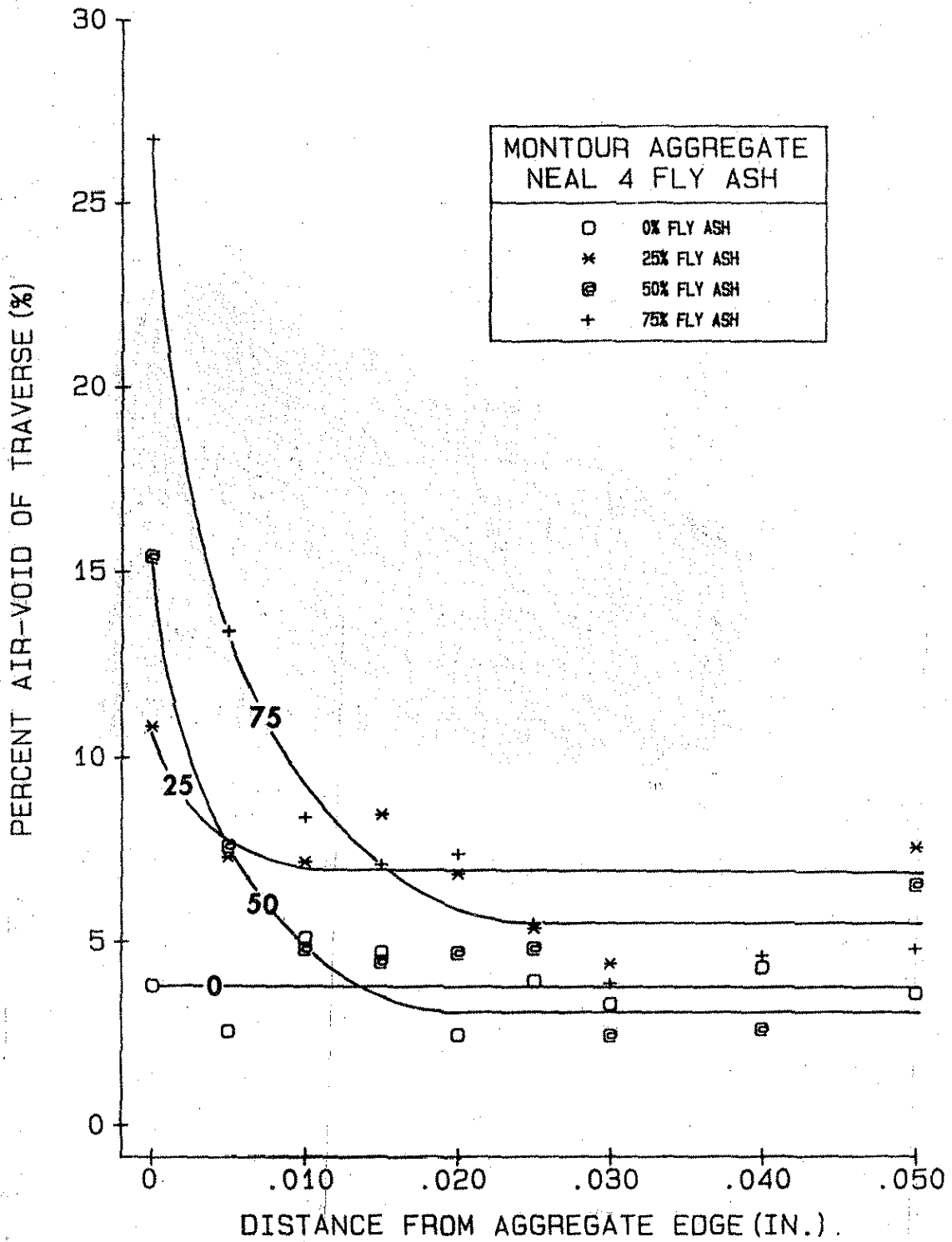


Figure 26. Modified linear traverse - Montour aggregate.

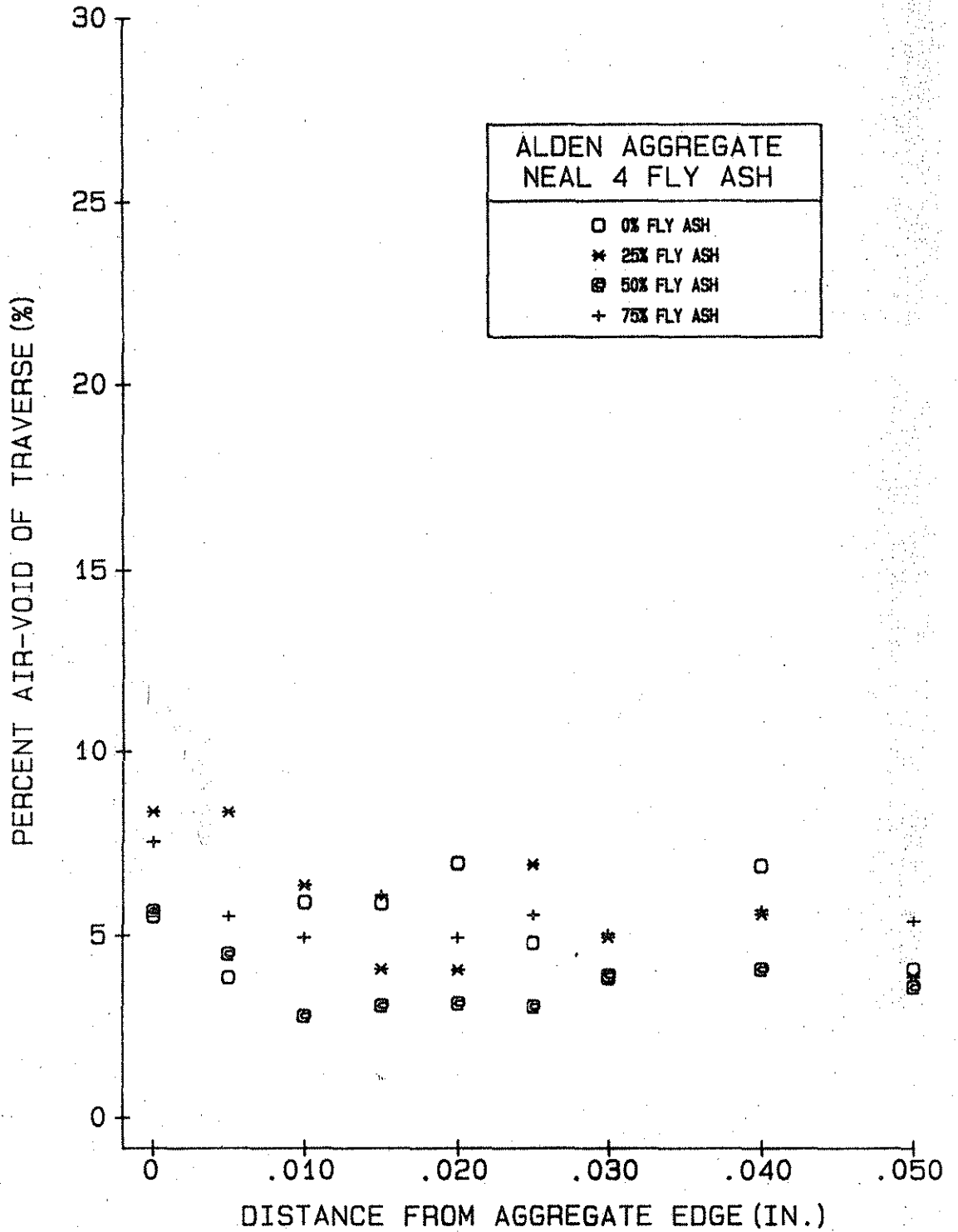


Figure 27. Modified linear traverse - Alden aggregate.

At a minimum, bubble rings mean a weak zone at aggregate boundaries which could influence mechanical resistance to frost action. In terms of mechanisms of frost action, the fact that there is an air entrained starved region away from the aggregate boundary could mean, under normal freezing temperatures, there is a source of unfrozen capillary water sufficient to allow ice growth and filling of boundary bubbles. An alternative mechanism may be that the bubble rings themselves are interconnected and can act as channels for inflow of exterior water. However, visual observation indicates that freeze-thaw deterioration is associated with aggregate-mortar boundaries.

Surface Activity

Although a bubble ring failure mechanism has not yet been established, the fact remains that the phenomena exists and presents a striking correlation to durability of fly ash concrete. Another question is why does a bubble ring develop and how might it be prevented? Previous work (16,17) suggests that air entrainment can be influenced by components found in fly ash (i.e. alkalis and sulfur trioxide) but does not explain interactions with aggregate. It is common to view concrete aggregate as being physicochemically inert. This may not be accurate and it is possible that the Montour and Alden limestones may possess different activities which could depend on crystalline structure, ionic substitution and presence of trace compounds. Both Montour and Alden aggregates are predominately calcium carbonate but the Montour has a more complex oolitic structure.

To determine whether there is a difference in surface activity of Montour and Alden aggregates in conjunction with fly ash and portland

cement, a simple flotation test where aggregate particles were floated in a foam generated by neutralized Vinsol resin air entraining agent was performed.

Flotation Test

Samples of both Montour and Alden aggregates were crushed and ground in a shatterbox and then sieved in a sonic sieve for three minutes. The aggregate passing a 45 micron sieve, but retained on a 20 micron sieve, was collected and placed in an oven to dry over a period of 24 hours. After the drying time had elapsed, 1000 milliliters of distilled water were mixed with two milliliters of air entraining agent. This ratio is comparable to a concrete mix design for 6 + .5% air. 5.00 grams of aggregate were placed in a separatory funnel along with 125 milliliters of the water-air entraining solution. The mixture was shaken for 30 seconds and then allowed to stabilize for 15 seconds. All of the mixture except for the foam was drained and discarded. The foam was washed into a clean glass dish and placed into the oven to dry over a period of 24 hours. The aggregate which clung to the foam bubbles was then weighed and recorded. This procedure was repeated with 5.00 grams of aggregate blended with 2.50 grams Neal 4 fly ash and 2.50 grams Type I portland cement. Results of this test are tabulated in Table 21. The fact that significantly different percentages of material were suspended in the Montour foams and similar quantities were retained for the Alden aggregate suggests an increase in surface activity in the fly ash, cement, and Montour aggregate system. Surface activity was not altered by fly ash and portland cement in the Alden aggregate system. This surface activity, possibly induced by fly ash, explains why air voids

Table 21. Flotation test.

Aggregate	Wt. of aggregate (gm)	Wt. of fly ash (gm)	Wt. of portland cement (gm)	Wt. of material which clung to foam (gm)	Solids in foam, %
Montour	5.00	----	----	0.09	1.80%
Montour	5.00	2.50	2.50	0.95	9.50%
Alden	5.00	----	----	0.26	5.20%
Alden	5.00	2.50	2.50	0.54	5.40%

have a tendency for attraction to Montour aggregate surfaces. This suggests that a simple flotation test can be developed for evaluation of aggregates in respect to concrete durability. Such a test may also be used to find remedial measures such as the selection of an appropriate air entraining agent.

Summary and Conclusions

An x-ray fluorescence technique was developed such that elemental composition of fly ashes can be accurately and rapidly determined at a fraction of the cost of methods specified in ASTM C 618-80. The x-ray fluorescence technique is routinely being used to monitor quality of most Iowa fly ashes being marketed for use in portland cement concrete. The cost effectiveness of x-ray fluorescence also provided sufficient data to support a statistical evaluation of fly ash composition for three power plants. Difference in elemental character existed for each source, but variability for a given plant was on the same order as that for Type I portland cement production.

X-ray diffraction techniques were developed to determine compound composition of fly ash. An evaluation of fly ashes from seven sources indicates a more pronounced difference in fly ash character than can be seen from elemental analysis, and thus classification by ASTM C 618-80. Composition and quantity of the crystalline phase of the seven fly ashes differed significantly. In some fly ashes, a part of the crystalline phase was alumina cements while to some degree all fly ashes contained relatively inert compounds such as quartz, mullite, and magnetite. All fly ashes were found to contain significant amounts of crystalline

magnesium and/or calcium oxide - compounds known to cause soundness problems in portland cement. By considering balances between total elemental composition and those elements in compounds, elemental composition of the amorphous phase was determined. The differentiating factor noted in amorphous composition of the seven fly ashes was the amount of calcium in the glass. Calcium in glass should have an influence on pozzolanic reactivity.

Based on the compound evaluation of the seven fly ash samples used in this study, it appears that a more definitive characterization than that offered by ASTM C 618-80 is possible. Such a classification scheme involves categorization according to elemental calcium composition and cementitious character. From the existing ASTM Class C and borderline C and F fly ashes would come the more definitive high calcium cementitious and high calcium noncementitious varieties. This reflects the cementitious and pozzolanic properties of these fly ashes. The remaining part of the existing ASTM Class F spectrum is low-calcium, noncementitious fly ash. At present, a precise demarcation for calcium content cannot be defined, because of limited compound composition data.

Knowledge of compound and amorphous composition leads to a detailed evaluation of soundness of portland cement-fly ash mortar. It was found that crystalline calcium oxide, not magnesium oxide, was responsible for soundness problems and that high levels of crystalline calcium oxide can be acceptable if aluminous cements are present in fly ash. A heat evolution test was demonstrated as having potential for a quick, inexpensive method for determining the presence and amount of alumina cements, supporting the suggested classification scheme. However, free CaO contents of noncementitious C and F fly ashes exceeding about two

percent should limit the fly ash replacements because of soundness problems.

An evaluation of the current ASTM C 618-80 lime pozzolan test suggests the role of trace elements and amorphous composition of fly ash are significant factors to fly ash performance. To provide a timely, yet definitive assessment of fly ash, a reasonable replacement to the lime-pozzolan test appears to be development of an accelerated portland cement-fly ash reactivity test.

Work done in the area of fly ash concrete and its resistance to cyclic freezing and thawing involved development of an air void evaluation method with computerized image analysis and use of established mercury porosimetry and linear traverse techniques. A series of tests on two aggregate types indicates that fly ash can have a pronounced influence on freeze-thaw durability but is dependent on the type of coarse aggregate. Evaluation of pore structure by mercury porosimetry and conventional microscopic linear traverse produced inconclusive results. However, adaptations to linear traverse method revealed that poor performance of fly ash-portland cement concrete is related to a nonhomogeneous distribution of entrained air voids. Air voids were concentrated near aggregate-mortar boundaries where deterioration appeared to initiate. It was suspected that surface activity of the poor performing aggregate was the cause of the problem and an air entrainment flotation test was devised to evaluate the phenomena. The results indicate that aggregate surface activity is enhanced by the presence of fly ash. Also, the flotation test may be a means of diagnosing the problem.

Recommendations

The fundamental approach used in this research has broadened our knowledge about Iowa fly ashes but has undoubtedly raised more questions than existed at the onset of the project. Because of time limitations, techniques for rapid characterization of fly ash were only briefly explored and their utilitarian application will require concentrated and systematic development. It seems, however, a well developed heat evolution test and accelerated cement-fly ash reactivity test represent significant contributions supporting rational use of fly ash as a portland cement replacement.

Verification and explanation of the fly ash-coarse aggregate interaction phenomenon was based only on two aggregate types. This leads to the question of how widespread is this phenomena and more importantly, how might air void accumulation or bubble ringing be stopped for surface active aggregates. If the current Iowa DOT aggregate classification scheme involved representation of this phenomena, all Class II aggregates could be involved. This represents a significant source portion of aggregate available in Iowa. This means definition of those components in fly ash which initiate and support the physicochemical reactivity and screening several aggregates to find predictive factors. The result could be rational support for development of a simple foam flotation test of air entraining agents not sensitive to the mechanism.

This research demonstrated a very frustrating aspect of the existing method cyclic freeze-thaw testing. The time it takes to get a durability result is on the order of 135 days and means support for a

decision comes infrequently and progress is delayed. The authors perceive a need for a technique which can reduce the time for test results and/or provide increased capacity for the existing methodology. Work under Iowa DOT reseearch project HR 258 indicates that conductance measurements made in conjunction with existing freeze-thaw apparatus can provide a working tool useful to assessment of the fly ash-aggregate interaction problem.

Acknowledgements

This investigation was sponsored by the Iowa Highway Research Board, Iowa Department of Transportation. Special appreciation and sincere thanks are extended to Vernon Marks, Ken Isenberger, Bernard Brown, Wendell Dubberke and Sam Moussalli, all of the Iowa Department of Transportation, for their assistance in providing guidance, materials, and laboratory support during the conduct of this research. Appreciation is extended to Lon Zimmerman, Midwest Fly Ash, for supplying and in many cases delivering much of the fly ash used in this evaluation.

References

1. Chung, F. H., "A New X-ray Diffraction Method for Quantitative Multicomponent Analysis," *Advances in X-ray Analysis*, Vol. 17, pp. 106-115, Plenum Press, 1974.
- 1a. Demirel, O. S., "Detection and Quantitative Analysis of Sodium Aluminosilicates Suspended in Water," Unpublished M.S. Thesis, ISU Library, 1978.
2. Sariahmed, M., "The Siemens Software System for the D-550," Siemens Corporation, Cherry Hill, N.J., 1978.
3. Beard, D. W. and Harkins, C. R., "Siemens Floppy Disk Software System for Diffrac V," *Operator's Manual*, Siemens Corporation, Cherry Hill, N.J., 1981.
4. Plesch, R. and Thiele, G., "Fundamentals of the Siemens Computer Programs for X-ray Spectrometry," *Siemens X-ray Analytical Application Note*, No. 33, Sept. 1977.
5. SAS User's Guide, SAS Institute, Inc., Raleigh, N.C., 1979 Edition.
6. Mindess, S and Young, J. F., *Concrete*, Prentice-Hall, N.J., 1981.
7. Lea, F. M., *The Chemistry of Cement and Concrete*, Third Edition, Chemical Publishing Co., N.Y., 1971.
8. McKerall, W. C., Ledbetter, W. B. and Teague, D. J., "Analysis of Fly Ashes Produced in Texas," *Research Report 240-1*, Texas Transportation Institute, January 1980.
9. Isenberger, K., *Fly Ash Concrete Compressive Strength and Freeze-Thaw Durability*, Iowa Department of Transportation, June 1981.
10. Neville, A. M., *Properties of Concrete*, Pitman International, 1981.

11. General Aggregate Source Information, Iowa Department of Transportation, Division of Highways, Office of Materials, Ames, IA, 1983.
12. Powers, T. C., "Freezing Effects in Concrete," American Concrete Institute, SP 47-1, 1975.
13. Verbeck, G. J., "Hardened Concrete Pore Structure," ASTM STP 169, 1956.
14. ACI Committee 201, "Guide to Durable Concrete," (ACI 201.2R-77) (Reaffirmed 1982), ACI Manual of Concrete Practice, Part I, 1977.
15. Enustun, B. V., Senturk, H. S. and Yurdakul, "Capillary Freezing and Melting," Jour. of Colloid Interface Science, No. 65, pp. 509-516, 1978.
16. Mulenz, R. C. Vladimir, W. E., Backstron, J. E. and Flack, H. L., "Origin, Evaluation, and Effects of the Air Void System in Concrete. Part 1 - Entrained Air in Unhardened Concrete," Jour. of the American Concrete Institute, No. 1, Vol. 30, pp. 95-121, July 1958.
17. Pistilli, M. F., "Air-Void Parameters Developed by Air-Entraining Admixtures, as Influenced by Soluble Alkalies from Fly Ash and Portland Cement," Jour. of the American Concrete Institute, No. 3, Vol. 80, pp. 217-222, 1983.
18. Sommer, H., "The Precision of the Microscopical Deterioration of the Air-Void System in Hardened Concrete," Cement, Concrete, and Aggregate, ASTM, Vol. 1, No. 2, pp. 49-55, 1979.

APPENDIX A. Elemental Composition of Fly Ash

Sample Identifi- cation	Mg	Na	Fe	Ti	Si	Ca	Al	K
CB D	2.67	0.44	3.07	0.83	14.52	13.51	12.80	0.49
CB V1	3.55	1.15	3.38	0.97	11.67	26.13	10.91	0.26
CB V2	3.47	1.33	3.55	0.82	13.88	22.48	10.74	0.28
CB V3	3.90	1.43	3.73	0.85	14.49	22.68	10.71	0.30
CB V4	3.72	1.27	3.56	0.86	13.71	22.38	10.82	0.34
CB V5	3.35	1.27	3.72	0.86	13.86	22.13	10.83	0.31
CB V6	3.32	1.25	3.45	0.89	13.47	23.36	10.82	0.29
CB V7	3.62	1.35	3.74	0.75	13.71	22.52	10.46	0.28
CB V8	3.04	1.06	3.56	0.87	15.22	21.57	10.92	0.35
CB V9	3.25	1.23	3.60	0.97	14.51	22.80	11.21	0.29
CB V10	3.08	1.25	3.61	0.87	14.24	21.60	11.07	0.30
CB V11	3.18	1.29	3.61	0.91	14.62	21.82	11.13	0.30
CB V12	3.20	1.33	3.79	0.94	14.60	22.16	11.14	0.28
CB V13	3.35	1.30	3.61	0.88	15.41	21.25	10.93	0.34
CB V14	2.88	1.11	3.51	0.74	15.28	19.88	10.55	0.44
CB V15	4.08	1.38	3.96	0.74	14.98	21.83	10.30	0.35
CB V16	3.93	1.34	3.89	0.96	15.18	22.21	11.06	0.35
CB V17	3.33	1.23	3.84	0.96	14.77	21.93	11.21	0.29
CB V18	3.87	1.30	3.90	0.93	14.28	22.57	10.98	0.29
CB V19	3.60	1.25	3.89	0.94	15.26	22.02	11.08	0.30
CB V20	3.54	1.25	3.86	0.92	14.93	21.84	10.98	0.30
CB V21	3.86	1.21	3.42	0.95	14.07	23.23	11.08	0.29
CB V22	3.60	1.18	3.58	0.92	14.26	21.86	11.19	0.30

APPENDIX A. Elemental Composition of Fly Ash (Cont'd.)

Sample Identifi- cation	Mg	Na	Fe	Ti	Si	Ca	Al	K
CB V23	3.52	1.27	3.66	0.91	14.69	21.96	11.13	0.30
CB V24	3.40	1.11	3.19	0.95	14.42	21.96	11.44	0.29
CB V25	3.63	1.26	3.52	0.88	14.00	22.57	11.03	0.27
CB V26	4.17	1.26	3.69	0.93	14.53	21.46	11.30	0.27
CB V27	4.48	1.26	3.74	0.89	13.78	21.83	11.05	0.26
CB V28	4.21	1.25	4.01	0.90	13.71	22.12	11.04	0.27
N3 V1	2.14	0.30	6.06	0.39	21.68	12.61	8.75	1.09
N3 V2	1.88	0.38	5.77	0.36	21.38	12.10	8.54	1.22
N3 V3	2.09	0.35	6.70	0.02	22.27	12.75	6.92	1.17
N3 V4	2.28	0.28	6.35	0.42	21.43	11.94	9.10	1.08
N3 V5	2.10	0.25	6.18	0.40	22.05	11.02	9.19	1.10
N3 V6	2.60	0.43	5.59	0.47	20.11	12.90	9.83	0.79
N3 V7	2.06	0.25	6.24	0.41	21.92	11.00	9.23	1.11
N3 V8	2.09	0.24	6.27	0.42	22.06	10.57	9.33	1.13
N3 V9	2.05	0.23	6.15	0.41	21.33	11.47	9.22	1.09
N3 V10	2.05	0.20	6.23	0.41	22.12	10.64	9.27	1.14
N3 V11	2.18	0.21	6.62	0.41	23.23	8.66	9.44	1.27
N3 V12	2.10	0.22	7.22	0.42	23.72	9.27	8.46	1.57
N3 V13	2.30	0.22	7.40	0.45	22.46	10.60	8.46	1.50
N3 V14	2.38	0.22	7.80	0.48	22.20	11.03	8.58	1.44
N3 V15	2.27	0.23	7.34	0.46	22.36	11.84	8.38	1.38
N3 V16	2.38	0.23	5.66	0.49	22.46	10.10	11.90	0.27
N3 V17	2.31	0.21	6.73	0.44	22.35	9.87	9.44	1.20
N3 V18	1.95	0.25	6.38	0.41	21.47	11.18	9.21	1.11
N3 V19	2.02	0.27	6.49	0.43	23.55	10.57	9.20	1.12

APPENDIX A. Elemental Composition of Fly Ash (Cont'd.)

Sample Identifi- cation	Mg	Na	Fe	Ti	Si	Ca	Al	K
N3 V20	1.90	0.30	5.90	0.39	22.14	10.44	9.38	1.09
N3 V21	1.81	0.33	6.07	0.40	22.56	9.50	9.63	1.10
N3 V22	1.99	0.31	5.90	0.40	22.47	10.16	9.45	1.10
N3 V23	1.83	0.29	5.52	0.48	22.20	9.67	10.15	1.07
N3 V24	4.28	0.75	4.75	0.69	15.48	19.63	10.50	0.27
N3 V25	2.07	0.28	6.23	0.42	22.46	10.21	9.54	1.08
N3 V26	2.01	0.26	6.42	0.36	22.68	9.83	8.95	1.25
N4 V1	4.28	0.52	4.70	0.63	16.39	17.91	10.58	0.22
N4 V2	4.23	0.54	4.69	0.62	16.72	17.72	10.52	0.23
N4 V3	4.08	0.57	4.49	0.63	16.72	17.87	10.56	0.22
N4 V4	4.31	0.51	4.70	0.63	16.11	18.54	10.47	0.25
N4 V5	3.97	0.58	5.03	0.62	16.31	17.62	10.56	0.22
N4 V6	3.62	0.59	4.85	0.57	17.28	15.91	10.60	0.22
N4 V7	1.20	0.62	5.56	0.70	14.83	19.53	10.54	0.22
N4 V8	4.00	0.56	4.93	0.65	16.07	18.35	10.54	0.22
N4 V9	4.26	1.18	4.29	0.81	12.78	24.36	10.33	0.27
N4 V10	4.28	0.71	4.94	0.70	15.76	19.39	10.55	0.24
N4 V11	4.50	0.87	4.70	0.66	15.23	19.98	10.35	0.26
N4 V12	4.54	0.85	4.94	0.68	15.31	19.97	10.38	0.26
N4 V13	4.45	0.78	4.74	0.66	15.30	19.71	10.40	0.26
N4 V14	3.07	1.16	3.75	0.88	14.35	20.88	11.13	0.30
N4 V15	1.55	0.29	5.83	0.48	22.13	8.71	9.82	1.16
N4 V16	4.10	0.77	4.74	0.68	15.17	19.77	10.44	0.27
N4 V17	4.14	0.84	4.55	0.67	15.59	19.35	10.46	0.27
N4 V18	4.44	0.94	4.33	0.72	14.57	20.56	10.51	0.29

APPENDIX A. Elemental Composition of Fly Ash (Cont'd.)

Sample Identifi- cation	Mg	Na	Fe	Ti	Si	Ca	Al	K
N4 V19	4.12	0.61	4.57	0.63	15.60	10.52	10.52	0.21
N4 V20	3.98	0.80	4.51	0.64	15.60	18.80	10.43	0.27
N4 V21	4.20	0.72	4.60	0.65	16.00	18.52	10.53	0.23
N4 V22	4.31	0.72	4.55	0.69	15.76	19.16	10.60	0.22
N4 V23	4.28	0.55	4.66	0.66	15.83	19.92	10.36	0.24
N4 V24	4.94	0.78	4.32	0.79	13.88	21.98	10.61	0.26
N4 V25	4.47	0.66	4.65	0.70	15.19	19.72	10.60	0.22
N4 V26	4.59	0.70	4.53	0.71	15.46	20.14	10.56	0.24
N4 V27	4.41	0.72	4.31	0.68	15.99	19.22	10.59	0.24
N4 V28	4.59	0.72	4.50	0.71	16.68	19.21	10.68	0.24
N4 V29	4.49	0.68	4.43	0.70	16.66	18.99	10.69	0.23
N4 V30	4.29	0.78	4.36	0.70	15.74	19.57	10.61	0.22
N4 V31	3.89	0.77	4.33	0.64	17.12	17.56	10.67	0.26
N4 V32	4.12	0.73	4.70	0.64	16.71	18.05	10.57	0.25
N4 V33	4.19	0.79	4.50	0.67	16.39	18.70	10.59	0.24
N4 V34	4.06	0.74	4.36	0.63	16.74	17.66	10.63	0.24

Note: CB = Council Bluffs

N3 = Port Neal # 3

N4 = Port Neal # 4

	EXP	WT% FA	CAO	MGO	C3A	CA ^a	MG ^a	SI ^a	FE ^a	AL ^a	TYPE ^b
1	0.094	20.00	0.62	1.80	6.30	52.84	3.12	27.18	3.53	7.24	1
2	0.092	20.00	0.62	1.80	6.30	52.84	3.12	27.18	3.53	7.24	1
3	0.150	30.00	0.83	1.70	5.50	47.94	3.13	30.10	4.08	8.60	1
4	0.144	30.00	0.83	1.70	5.50	47.94	3.13	30.10	4.08	8.60	1
5	0.138	32.00	0.87	1.70	5.30	46.96	3.13	30.68	4.18	8.88	1
6	0.140 ^c	32.00	0.87	1.70	5.30	46.96	3.13	30.68	4.18	8.88	1
7	0.216 ^c	34.00	0.91	1.70	5.20	45.98	3.13	31.27	4.29	9.15	1
8	0.255 ^c	34.00	0.91	1.70	5.20	45.98	3.13	31.27	4.29	9.15	1
9	0.138	34.00	0.91	1.70	5.20	45.98	3.13	31.27	4.29	9.15	1
10	0.132	34.00	0.91	1.70	5.20	45.98	3.13	31.27	4.29	9.15	1
11	0.173	34.00	0.91	1.70	5.20	45.98	3.13	31.27	4.29	9.15	1
12	0.168	34.00	0.91	1.70	5.20	45.98	3.13	31.27	4.29	9.15	1
13	0.160	34.25	0.92	1.70	5.10	45.85	3.13	31.34	4.31	9.18	1
14	0.166	34.25	0.92	1.70	5.10	45.85	3.13	31.34	4.31	9.18	1
15	0.157	34.50	0.92	1.70	5.10	45.73	3.13	31.41	4.32	9.22	1
16	0.147	34.50	0.92	1.70	5.10	45.73	3.13	31.41	4.32	9.22	1
17	0.176	35.00	0.94	1.65	5.10	45.49	3.13	31.56	4.35	9.28	1
18	0.161	35.00	0.94	1.65	5.10	45.49	3.13	31.56	4.35	9.28	1
19	1.737	36.00	0.96	1.64	5.00	45.00	3.13	31.85	4.40	9.42	1
20	1.730	36.00	0.96	1.64	5.00	45.00	3.13	31.85	4.40	9.42	1
21	1.530	36.00	0.96	1.64	5.00	45.00	3.13	31.85	4.40	9.42	1
22	2.017	36.00	0.96	1.64	5.00	45.00	3.13	31.85	4.40	9.42	1
23	3.360	37.00	0.98	1.63	4.90	44.51	3.13	32.14	4.46	9.56	1
24	3.140	37.00	0.98	1.63	4.90	44.51	3.13	32.14	4.46	9.56	1
25	5.400	40.00	1.04	1.60	4.70	43.03	3.13	33.02	4.62	9.96	1
26	6.000 ^d	40.00	1.04	1.60	4.70	43.03	3.13	33.02	4.62	9.96	1
27	8.300 ^d	50.00	1.25	1.50	3.90	38.13	3.13	35.94	5.16	11.33	1
28	0.095	20.00	0.38	2.20	7.04	56.02	4.04	23.49	3.12	7.56	2
29	0.091	20.00	0.38	2.20	7.04	56.02	4.04	23.49	3.12	7.56	2
30	0.115	30.00	0.47	2.30	6.65	52.70	4.51	24.57	3.45	9.08	2
31	0.115	30.00	0.47	2.30	6.65	52.70	4.51	24.57	3.45	9.08	2
32	0.126	40.00	0.56	2.40	6.26	49.38	4.97	25.64	3.79	10.60	2

33	0.124	40.00	0.56	2.40	6.26	49.38	4.97	25.64	3.79	10.60	2
34	0.132	50.00	0.65	2.50	5.87	46.07	5.43	26.72	4.12	12.12	2
35	0.123	50.00	0.65	2.50	5.87	46.07	5.43	26.72	4.12	12.12	2
36	0.010	20.00	0.20	1.60	6.26	50.52	2.76	27.06	5.60	8.44	3
37	0.020	20.00	0.20	1.60	6.26	50.52	2.76	27.06	5.60	8.44	3
38	0.001	30.00	0.20	1.40	5.48	44.45	2.58	29.91	7.17	10.40	3
39	0.002	30.00	0.20	1.40	5.48	44.45	2.58	29.91	7.17	10.40	3
40	-0.011	40.00	0.20	1.20	4.70	38.38	2.40	32.77	8.75	12.36	3
41	-0.007	40.00	0.20	1.20	4.70	38.38	2.40	32.77	8.75	12.36	3
42	-0.027	50.00	0.20	1.00	3.92	32.32	2.22	35.62	10.32	14.33	3
43	-0.033	50.00	0.20	1.00	3.92	32.32	2.22	35.62	10.32	14.33	3
44	0.072	0.00	0.20	2.00	7.83	62.65	3.12	21.34	2.45	4.52	0
45	0.066	0.00	0.20	2.00	7.83	62.65	3.12	21.34	2.45	4.52	0
46	0.082	0.00	0.20	2.00	7.83	62.65	3.12	21.34	2.45	4.52	0
47	0.070	0.00	0.20	2.00	7.83	62.65	3.12	21.34	2.45	4.52	0
48	0.070	0.00	0.20	2.00	7.83	62.65	3.12	21.34	2.45	4.52	0
49	0.060	0.00	0.20	2.00	7.83	62.65	3.12	21.34	2.45	4.52	0
50	0.060	0.00	0.20	2.00	7.83	62.65	3.12	21.34	2.45	4.52	0
51	0.060	0.00	0.20	2.00	7.83	62.65	3.12	21.34	2.45	4.52	0

^aExpressed as oxides.

^bType 0 = portland cement only
 Type 1 = portland cement + Neal 3 fly ash
 Type 2 = portland cement + Neal 4 fly ash
 Type 3 = portland cement + North Omaha fly ash.

^cPossible outlier.

^dIndicates that this single value was not used in regression analysis.

DBS	NO	CEM	ASH	CL	PA	AIR	WC	AGG	SLP	DF3	07	228	290
1	1.0	648	CO	N	0	6.3	0.43	MON	3.00	88	.	.	.
2	2.0	648	N41	N	17	4.0	0.43	MON	1.50	52	.	5550	.
3	3.0	670	NO1	F	18	4.5	0.41	MON	2.30	57	.	4150	.
4	4.0	648	NC1	F	15	6.2	0.43	MON	3.00	78	.	3550	.
5	5.0	670	CL1	F	18	4.5	0.41	MON	2.00	70	.	3500	.
6	6.0	645	CB1	C	15	5.5	0.43	MON	1.50	83	.	4050	.
7	7.0	648	LA1	C	15	6.5	0.49	MON	5.30	91	.	3300	.
8	8.0	648	CO	N	0	5.8	0.43	MAL	2.00	91	.	.	.
9	9.0	645	N41	N	15	6.8	0.43	MAL	3.00	94	.	.	.
10	10.0	670	NO1	F	18	4.0	0.41	MAL	1.50	73	.	4950	.
11	11.0	645	NC	F	15	6.3	0.43	MAL	1.80	95	.	.	.
12	12.0	670	CL1	F	18	5.0	0.41	MAL	1.50	86	.	4950	.
13	13.0	645	CB1	C	15	5.8	0.43	MAL	3.50	90	.	4600	.
14	14.0	670	LA1	C	15	5.3	0.43	MAL	1.50	79	.	4450	.
15	15.0	648	CO	N	0	5.5	0.43	ALD	3.00	88	.	.	.
16	16.0	645	N41	N	15	6.3	0.43	ALD	2.50	90	.	4250	.
17	17.0	670	NO1	F	18	5.6	0.41	ALD	1.75	87	.	4200	.
18	18.0	645	NC1	F	15	6.3	0.43	ALD	2.50	96	.	.	.
19	19.0	670	CL1	F	18	4.5	0.41	ALD	2.00	88	.	4550	.
20	20.0	645	CB1	C	15	5.5	0.43	ALD	2.00	85	.	4750	.
21	21.0	645	LA1	C	15	6.3	0.43	ALD	2.80	81	.	3450	.
22	22.0	648	CO	N	0	6.5	0.43	CLA	3.00	92	.	.	.
23	23.0	645	N41	N	15	6.3	0.43	CLA	2.50	60	.	3650	.
24	24.0	670	NO1	F	18	4.3	0.41	CLA	1.80	37	.	3850	.
25	25.0	645	NC1	F	15	5.3	0.43	CLA	2.00	88	.	.	.
26	26.0	670	CL1	F	18	5.3	0.49	CLA	4.50	56	.	3550	.
27	27.0	645	CB1	C	15	5.5	0.49	CLA	4.00	63	.	4150	.
28	28.0	645	LA1	C	15	5.5	0.43	CLA	2.80	26	.	2450	.
29	29.0	655	CO	N	0	7.3	0.43	HAY	4.80	24	.	3400	.
30	30.0	655	N41	N	15	6.3	0.43	HAY	6.30	35	.	3950	.
31	31.0	680	N31	F	18	5.5	0.41	HAY	5.80	40	.	4200	.
32	32.0	600	CO	N	0	6.4	0.43	MON	4.30	64	4200	5200	5400
33	33.0	600	N42	C	25	8.5	0.43	MON	8.00	72	3100	4500	4750
34	34.0	600	N42	C	50	6.0	0.43	MON	7.00	45	3100	4400	5050
35	35.0	600	N42	C	75	8.5	0.43	MON	8.00	26	1400	2650	4250
36	36.0	600	N42	C	100	7.0	0.43	MON	8.00	0	.	650	800
37	37.0	600	CO	N	0	6.0	0.42	MON	2.30	91	4600	5500	6950
38	38.0	600	N42	C	25	4.4	0.39	MON	2.30	81	4800	6850	7400
39	39.0	600	N42	C	50	6.0	0.35	MON	2.50	46	4600	6250	7600
40	40.0	600	N42	C	75	5.8	0.32	MON	2.00	43	3150	5850	7050
41	41.0	600	N42	C	100	6.0	0.30	MON	2.50	0	1000	1150	1350
42	41.1	600	N42	C	25	7.0	0.43	MON	8.00	52	3700	4500	5000
43	41.2	600	N42	C	75	6.5	0.43	MON	8.00	21	1300	2550	3900
44	41.3	600	CO	N	0	4.5	0.43	MON	6.50	59	4400	6000	6400
45	42.0	600	CO	N	0	5.4	0.43	ALD	3.00	83	3550	4700	5300
46	43.0	600	N42	C	25	6.9	0.43	ALD	7.00	74	3050	4200	4700
47	44.0	600	N42	C	50	6.5	0.43	ALD	7.00	78	2450	3800	4500
48	45.0	600	N42	C	75	5.9	0.43	ALD	8.00	79	1100	2600	3550
49	46.0	600	N42	C	100	6.3	0.43	ALD	8.00	0	500	550	700
50	47.0	600	CO	N	0	5.5	0.40	ALD	2.50	30	4700	5700	5550
51	48.0	600	N42	C	25	4.7	0.39	ALD	2.50	86	5600	6350	7550
52	49.0	600	N42	C	50	5.1	0.34	ALD	2.30	88	5550	6400	7150
53	50.0	600	N42	C	75	5.6	0.31	ALD	1.50	84	4950	6350	6800
54	51.0	600	N42	C	100	6.2	0.30	ALD	2.50	0	1000	1150	1350
55	52.0	600	CO	N	0	2.5	0.43	MON	4.00	8	5250	6000	7500
56	53.0	600	CO	N	0	5.8	0.41	MON	3.00	7	4750	5500	6450

185	190	CE	ASH	CL	PA	AIR	WC	AGG	SLP	DF	Q7	Q20	230
57	54	500	CO	N	0	9.5	0.41	MON	5.8	74	3400	4450	4950
58	55	500	CO	N	0	10.5	0.41	MON	6.0	71	3400	4250	4700
59	56	500	N43	C	25	3.4	0.40	MON	2.3	70	5250	6550	7500
60	57	500	N43	C	25	6.6	0.39	MON	3.0	73	4450	5750	6500
61	54	500	N43	C	25	4.5	0.38	MON	4.5	82	4100	5150	5700
62	59	500	N43	C	25	11.2	0.38	MON	5.5	95	3100	4050	4450
63	60	600	CO	N	0	3.4	0.43	ALD	2.2	0	5550	6300	7600
64	61	600	CO	N	0	.	0.42	ALD
65	62	600	CO	N	0	10.0	0.42	ALD	5.0	100	3250	4150	4950
66	63	600	CO	N	0	12.0	0.42	ALD	6.0	93	2950	3600	4250
67	64	600	N43	C	25	3.2	0.39	ALD	2.5	0	6050	7150	8100
68	65	600	N43	C	25	.	0.39	ALD
69	65	600	N43	C	25	8.7	0.39	ALD	4.0	97	4550	5150	5100
70	67	600	N43	C	25	12.5	0.39	ALD	5.3	93	3250	4000	4600
71	68	434	CO	N	0	6.5	0.46	GC	2.8	93	3300	3900	4300
72	69	483	CO	N	0	6.4	0.43	GC	2.8	87	4050	4900	5050
73	70	544	CO	N	0	5.4	0.41	GC	2.8	93	4700	5450	5700
74	71	439	N43	C	44	6.7	0.42	GC	3.5	82	4000	5100	5450
75	72	489	N43	C	40	6.2	0.40	GC	4.0	88	4500	5100	6300
76	73	450	N43	C	36	5.2	0.36	GC	2.8	75	5250	6550	7250
77	74	438	N21	F	44	6.6	0.43	GC	3.5	82	2850	4600	5750
78	75	495	N21	F	40	5.2	0.40	GC	4.0	83	3450	5300	6300
79	75	455	N21	F	36	5.5	0.37	GC	3.3	89	4200	6150	6900
80	77	445	OT1	C	44	6.4	0.39	GC	3.0	85	4100	5850	6950
81	78	500	OT1	C	40	5.3	0.37	GC	2.8	88	4950	6700	7050
82	79	550	OT1	C	36	5.6	0.35	GC	2.8	81	5750	7200	7450
83	80	443	CB2	C	44	5.8	0.42	GC	3.3	76	4250	5000	6200
84	81	491	CB2	C	40	6.4	0.38	GC	3.5	88	4750	5900	6350
85	82	546	CB2	C	36	5.7	0.46	GC	3.5	81	5700	6400	7200
86	83	436	LA2	C	44	6.7	0.46	GC	4.0	87	3450	4350	5300
87	84	490	LA2	C	40	6.9	0.37	GC	3.3	89	4450	5250	6350
88	85	544	LA2	C	36	6.4	0.35	GC	3.8	93	5100	6300	7200
89	86	500	N2N4	B	40	6.9	0.39	GC	3.8	88	4400	6000	6950
90	87	500	N2N4	B	50	6.5	0.38	GC	3.5	86	4300	5950	6200
91	88	500	N2N4	B	60	5.9	0.39	GC	3.5	88	4050	5950	6200
92	89	500	N2LA	B	40	6.8	0.36	GC	2.5	89	4600	6050	7100
93	90	500	N2LA	B	50	7.2	0.39	GC	3.5	85	4050	5550	6550
94	91	500	N2LA	B	60	6.5	0.37	GC	3.0	86	4000	5650	6500
95	92	410	CO	N	0	4.5	0.59	FA	0.3	80	3200	3650	4100
96	93	410	CO	N	0	5.8	0.56	FA	2.0	92	3000	3650	4350
97	94	410	SH	C	13	4.2	0.61	FA	1.0	97	3000	3500	4050
98	95	410	SH	C	13	5.9	0.55	FA	2.5	89	2950	4100	4750
99	96	410	SH	C	25	4.2	0.61	FA	2.0	49	2750	3750	4350
100	97	410	SH	C	25	6.1	0.52	FA	2.5	83	2850	3800	5050
101	99	410	SH	C	40	4.0	0.61	FA	2.5	82	2700	3700	3850
102	99	410	SH	C	40	5.2	0.51	FA	3.0	83	2500	3900	5000
103	100	410	CO	N	0	7.0	0.51	AL	2.5	76	3000	3750	4250
104	101	410	AL	C	13	8.0	0.51	AL	4.5	87	2600	3350	4450
105	102	410	AL	C	25	5.5	0.51	AL	0.5	87	3350	4400	5150
106	103	410	AL	C	40	8.0	0.49	AL	7.0	82	1500	2650	3100
107	104	423	CO	N	0	12.0	0.53	MO	5.8	84	1350	2400	2350
108	105	423	CO	N	0	6.0	0.64	MO	2.0	76	2500	3300	3550
109	106	423	SH	C	13	9.0	0.53	MO	7.3	84	2150	2950	2100
110	107	423	SH	C	13	6.4	0.62	MO	3.5	86	2350	3350	4450
111	108	423	SH	C	25	5.0	0.51	MO	2.0	84	2400	4250	4200
112	109	423	SH	C	25	6.5	0.57	MO	3.5	84	2350	4550	4750

APPENDIX C. Summary of Physical Tests (Cont'd.)

QBS	VO	CEM	ASH	CL	PA	AIR	WC	AGG	SLP	DF3	Q7	Q23	Q90
113	110	423	SH	C	40	8.0	0.53	MO	7.3	38	1750	3150	3350
114	111	423	SH	C	40	6.7	0.55	MO	3.0	72	2300	3450	3950
115	112	423	CO	N	0	6.0	0.59	ORT	3.0	94	2500	2950	3050
116	113	423	CO	N	0	4.4	0.62	ORT	2.3	54	2750	3303	3600
117	114	423	SH	C	13	10.2	0.59	ORT	7.3	67	1350	2000	2000
118	115	423	SH	C	13	4.0	0.64	ORT	2.5	19	2550	3603	3600
119	116	423	SH	C	25	10.0	0.56	ORT	7.0	74	1500	2300	2150
120	117	423	SH	C	25	5.2	0.57	ORT	3.5	64	2350	3350	3550
121	115	423	SH	C	40	7.3	0.52	ORT	6.0	47	1550	2800	2750
122	119	423	SH	C	40	4.9	0.53	ORT	3.0	50	2400	3350	4150

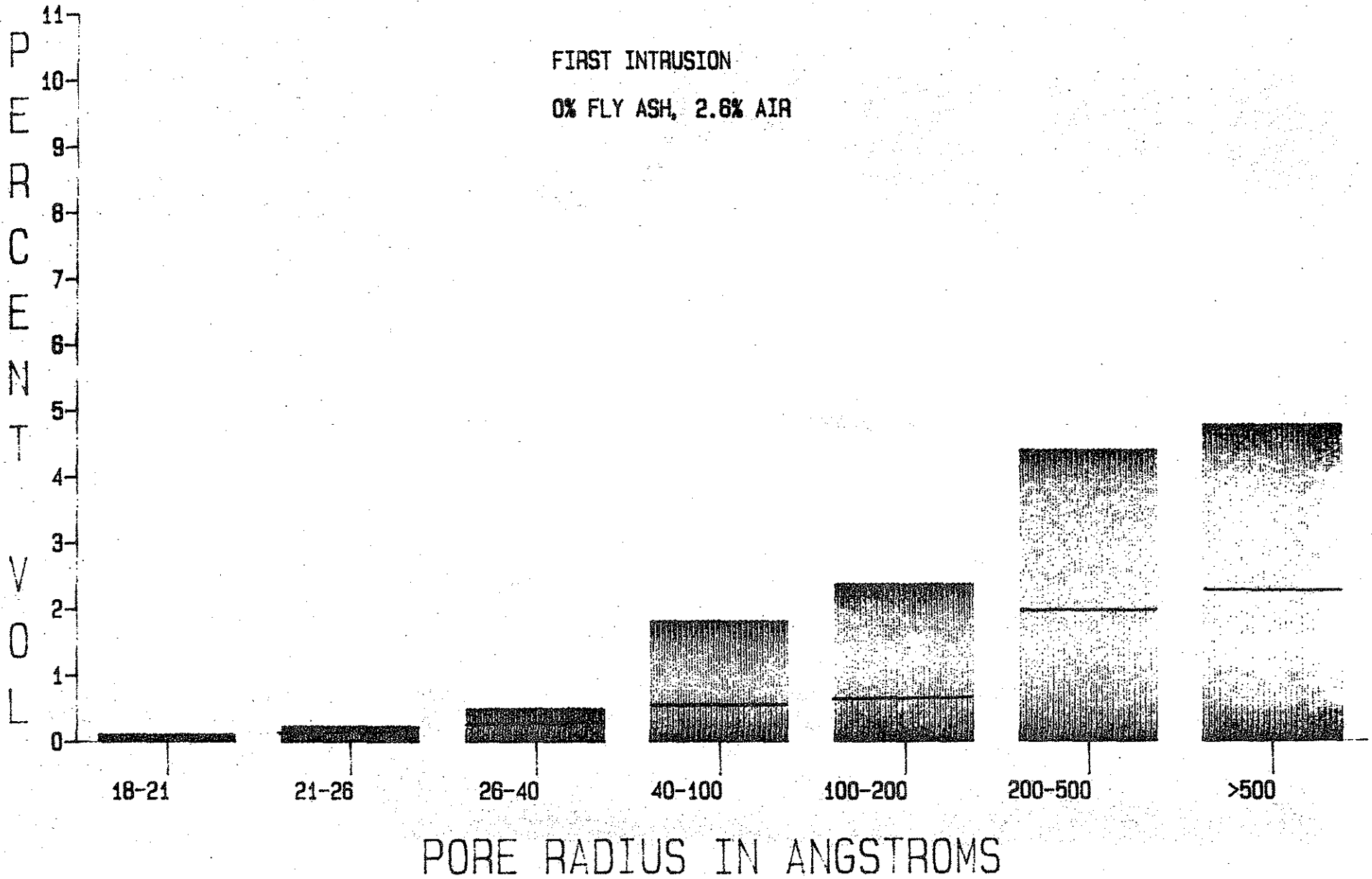
APPENDIX D

Pore size distribution of the mortar phase of concrete mixes studied by mercury porosimetry. (Total height of the bars indicates percent volume intruded during the first intrusion; levels of the second intrusion are indicated by the lines across the bars.)

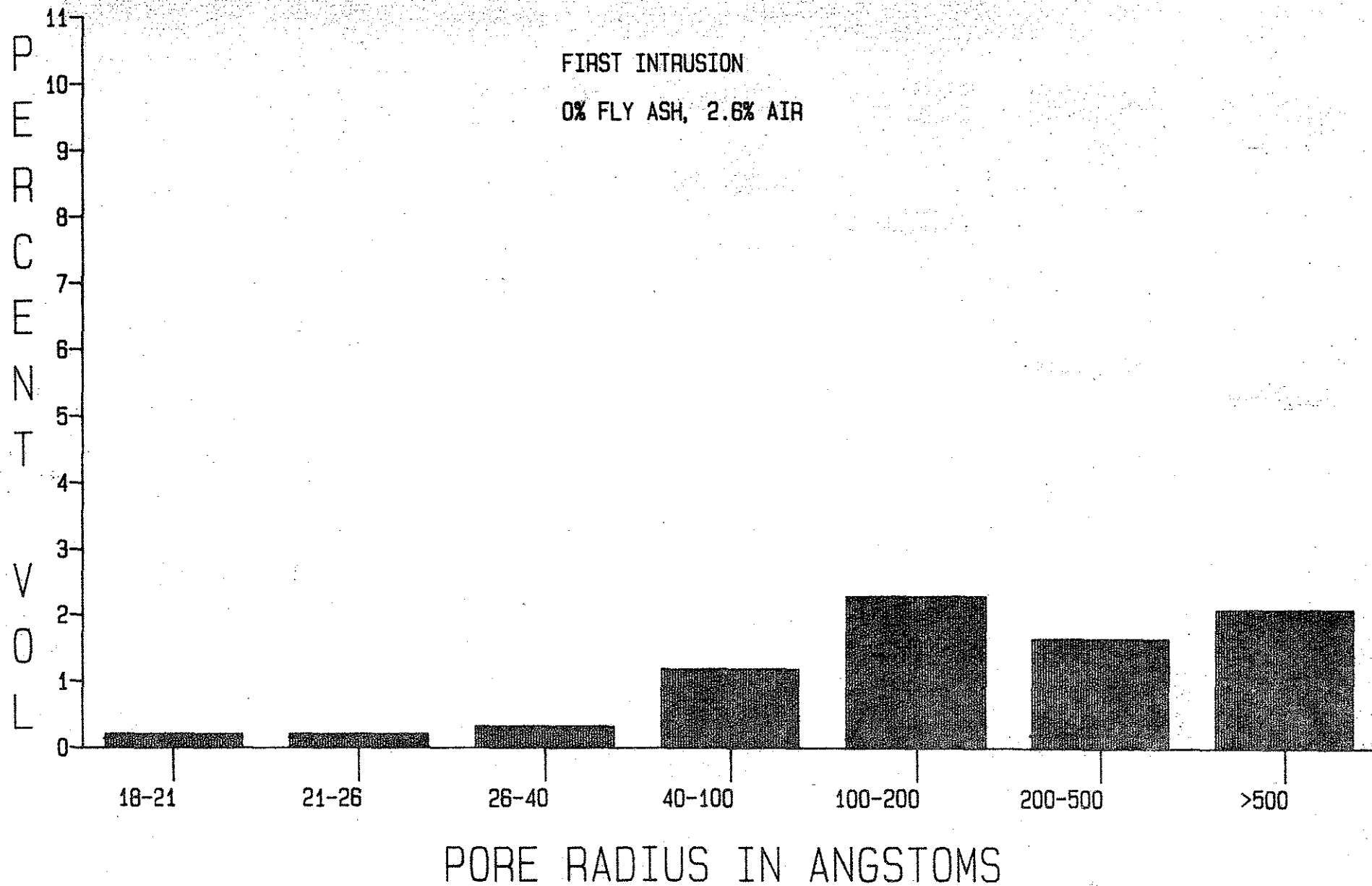
MONTOUR 3 DAY CURE

FIRST INTRUSION

0% FLY ASH, 2.6% AIR



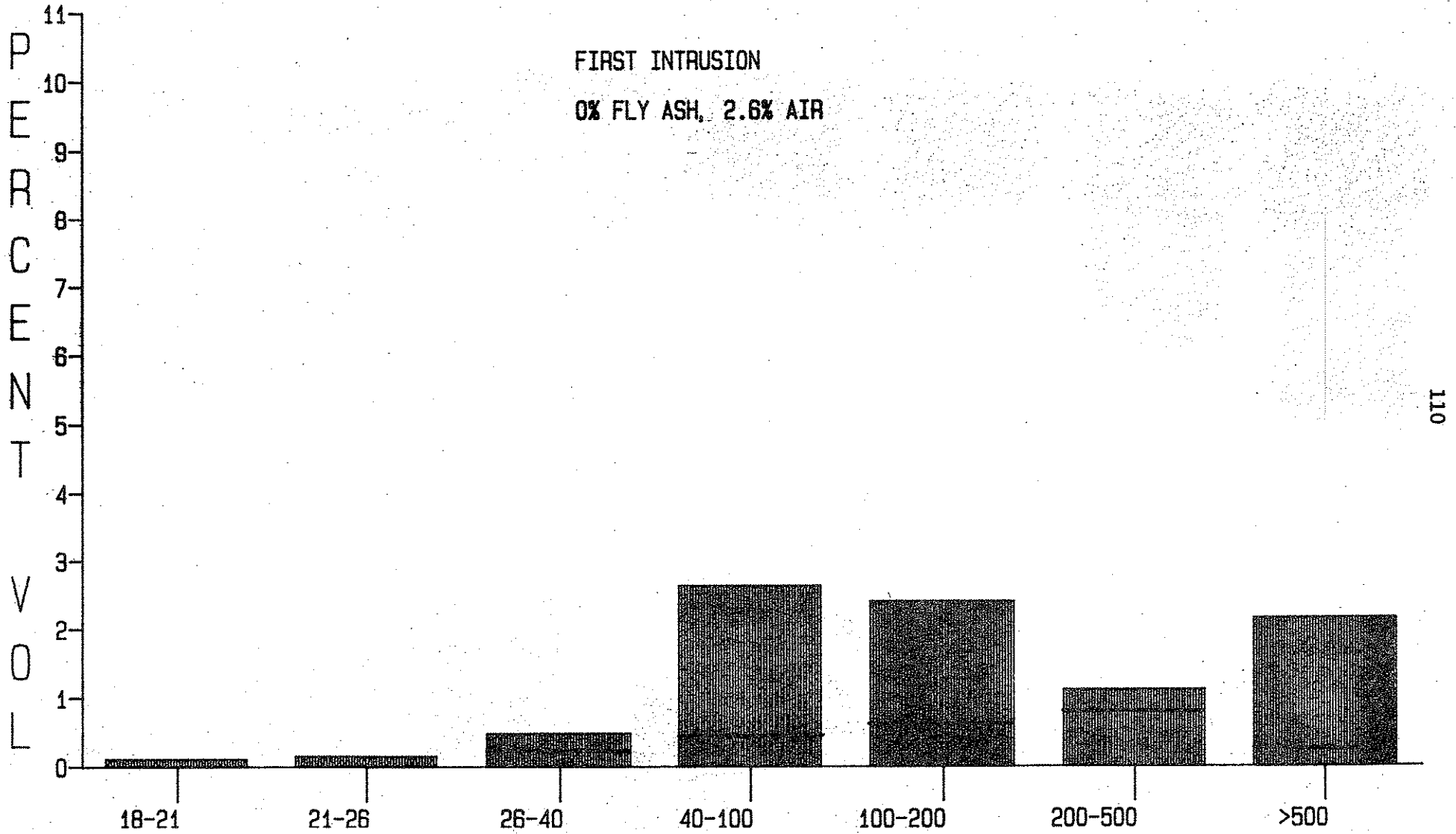
MONTOUR 7 DAY CURE



MONTOUR 28 DAY CURE

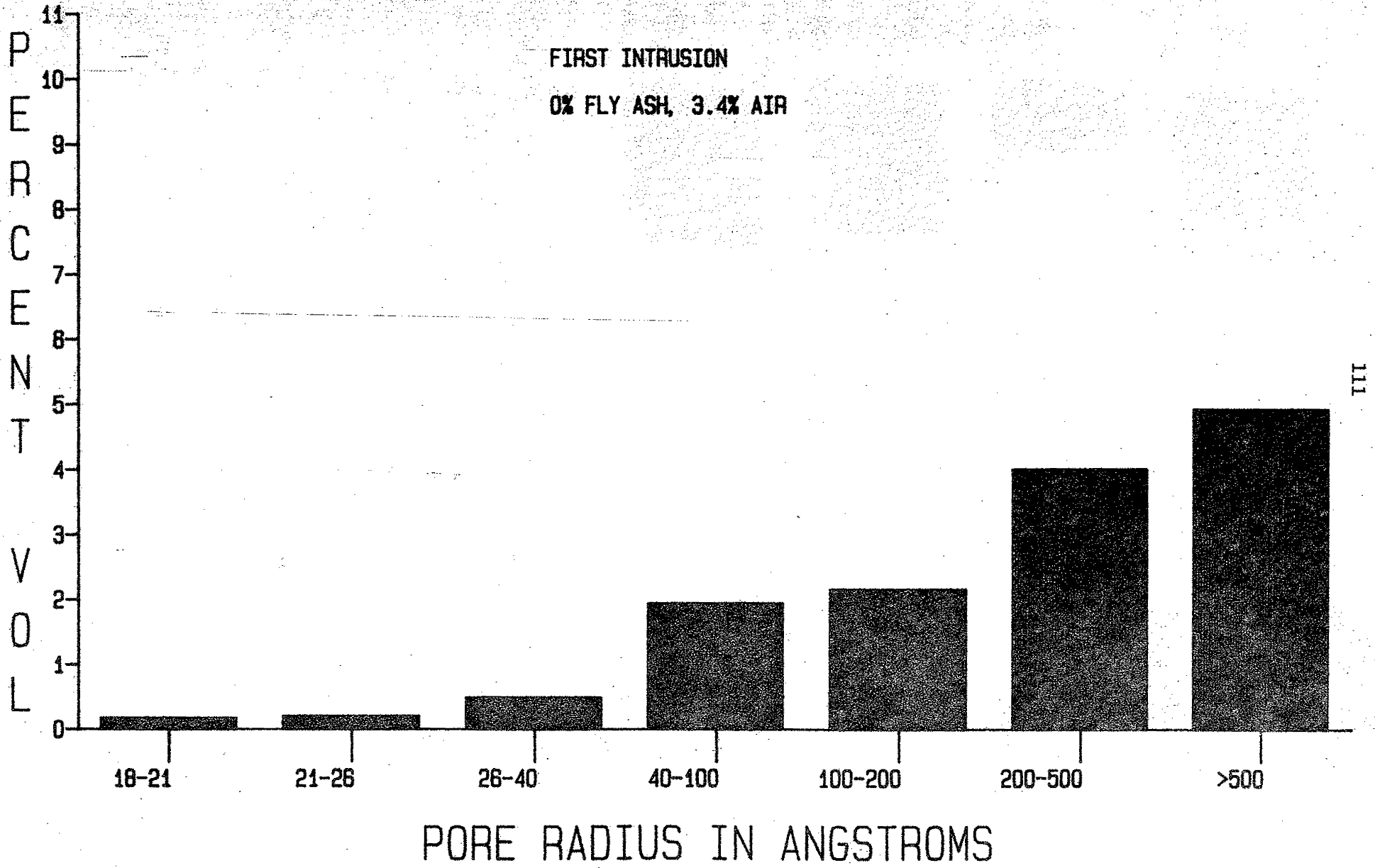
FIRST INTRUSION

0% FLY ASH, 2.6% AIR



PORE RADIUS IN ANGSTROMS

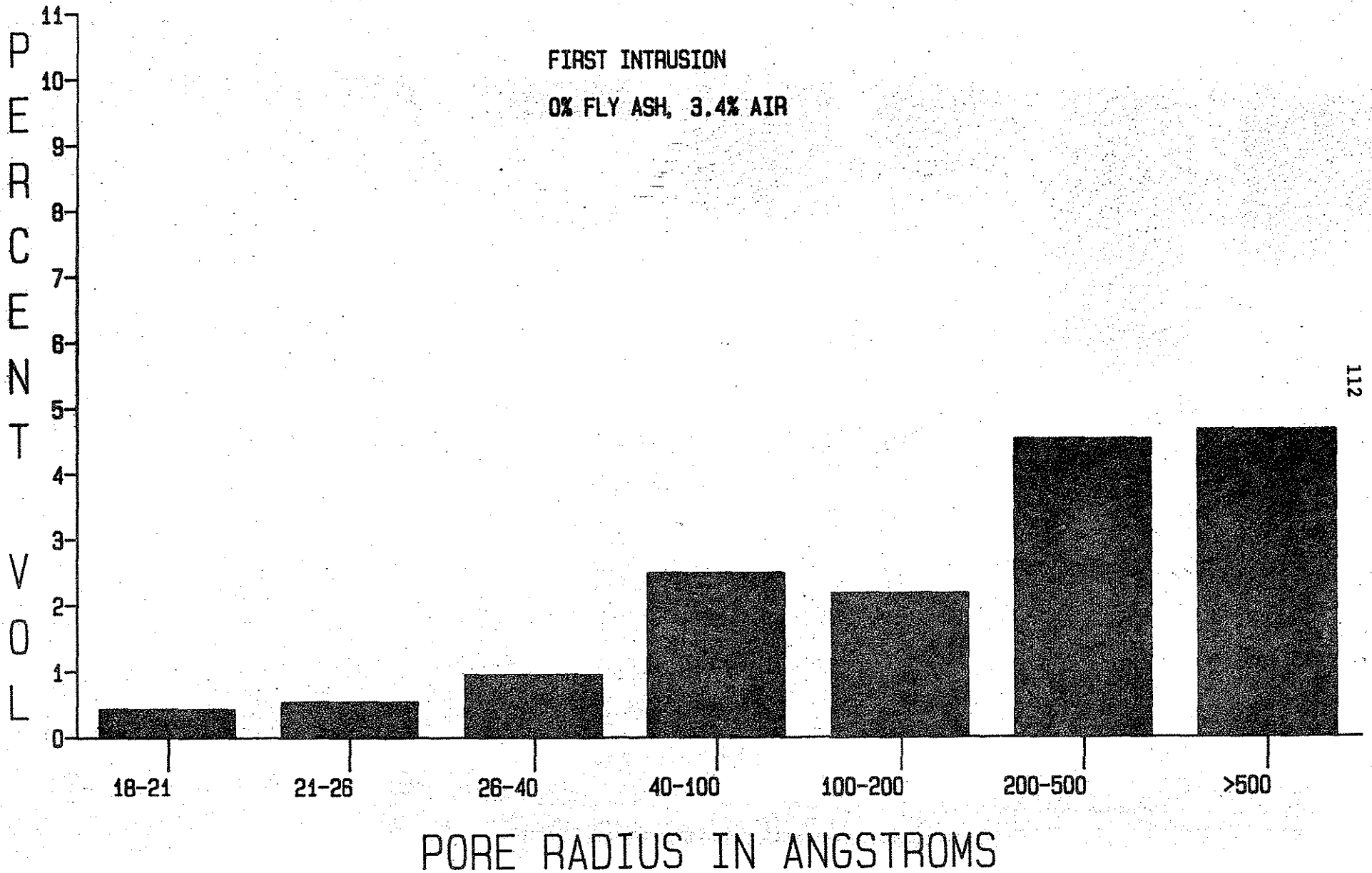
ALDEN 3 DAY CURE



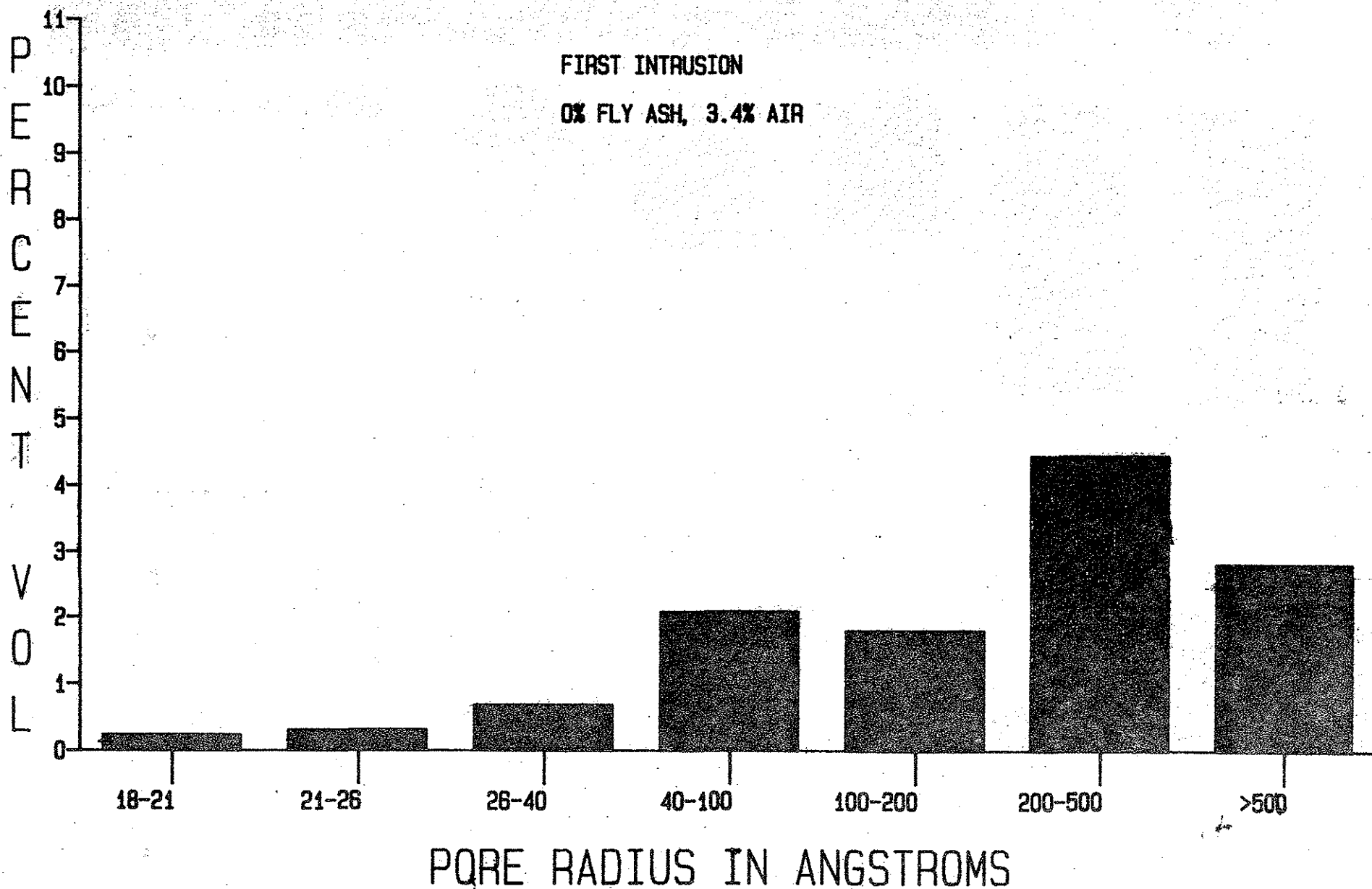
ALDEN 11 DAY CURE

FIRST INTRUSION

0% FLY ASH, 3.4% AIR



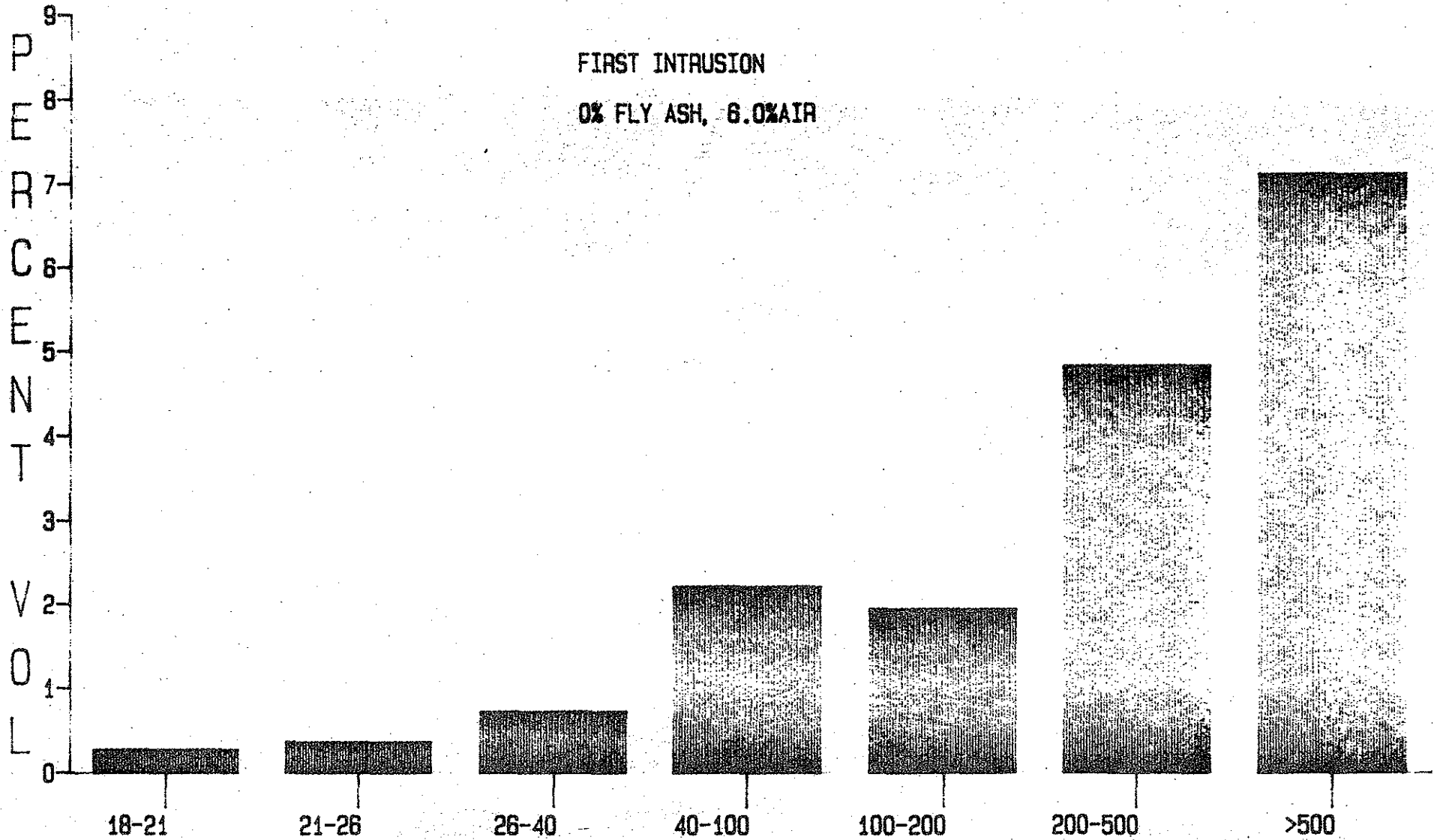
ALDEN 28 DAY CURE



MONTOUR 3 DAY CURE

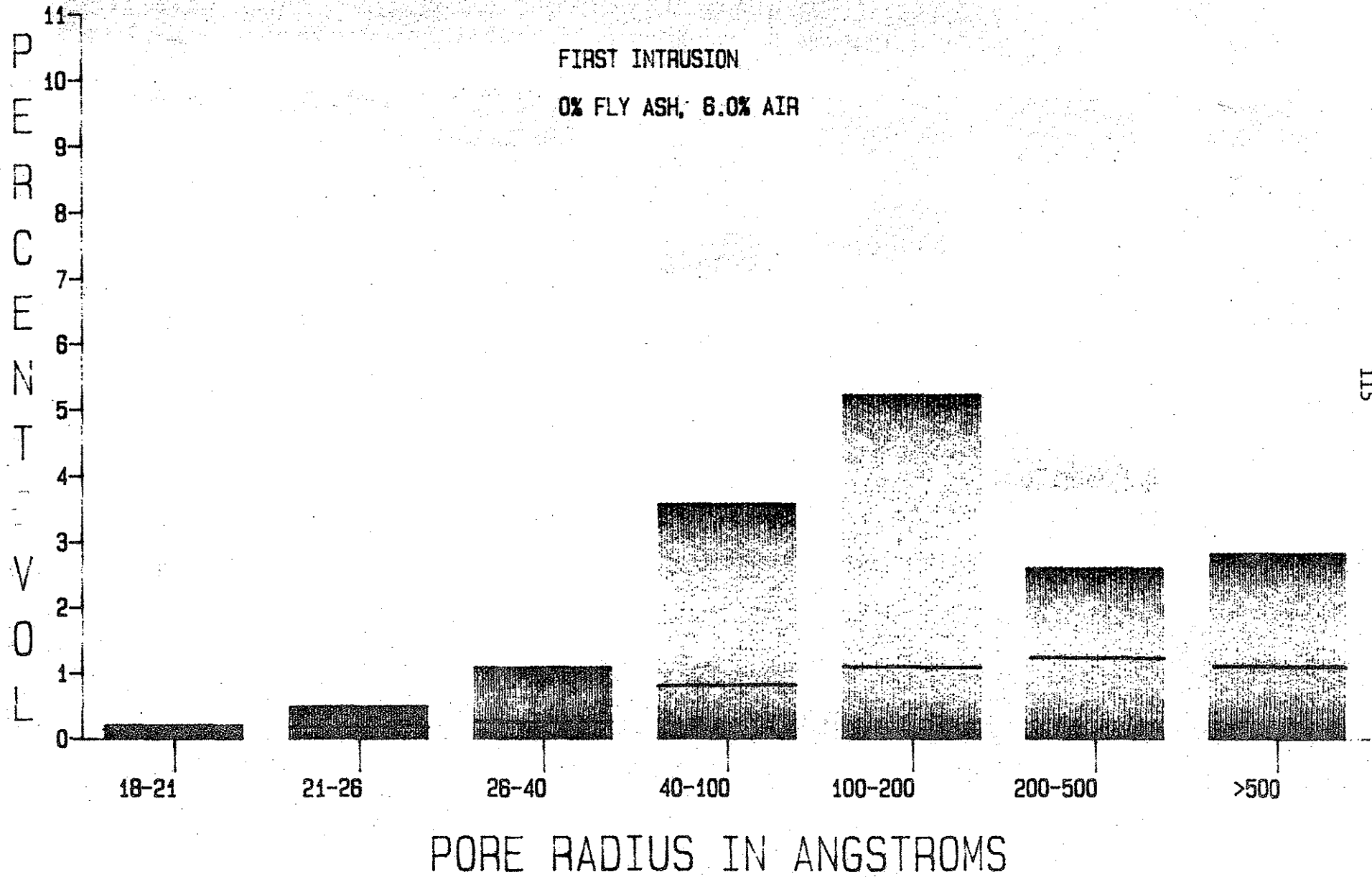
FIRST INTRUSION

0% FLY ASH, 6.0% AIR



PORE RADIUS IN ANGSTROMS

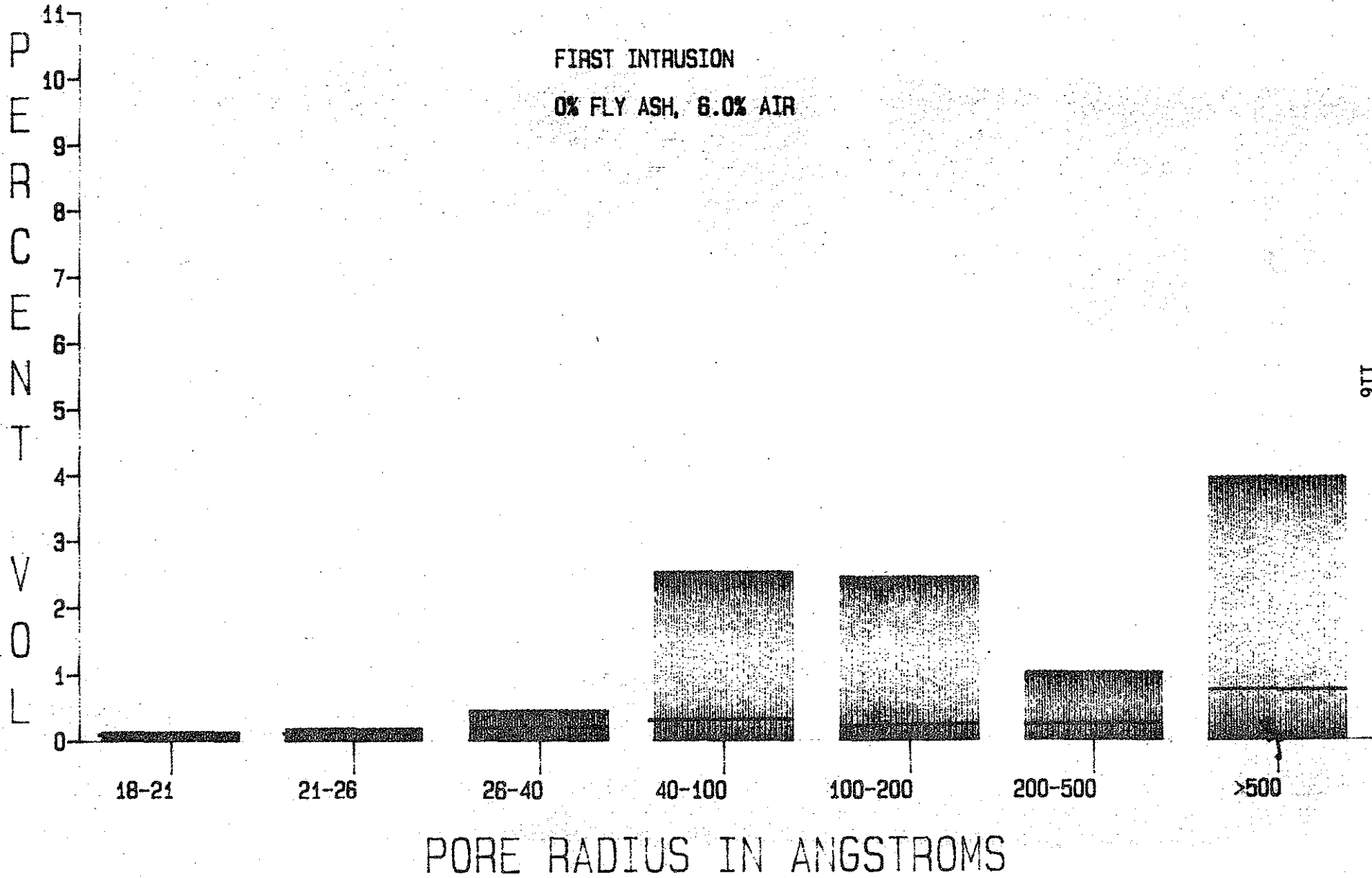
MONTOUR 7 DAY CURE



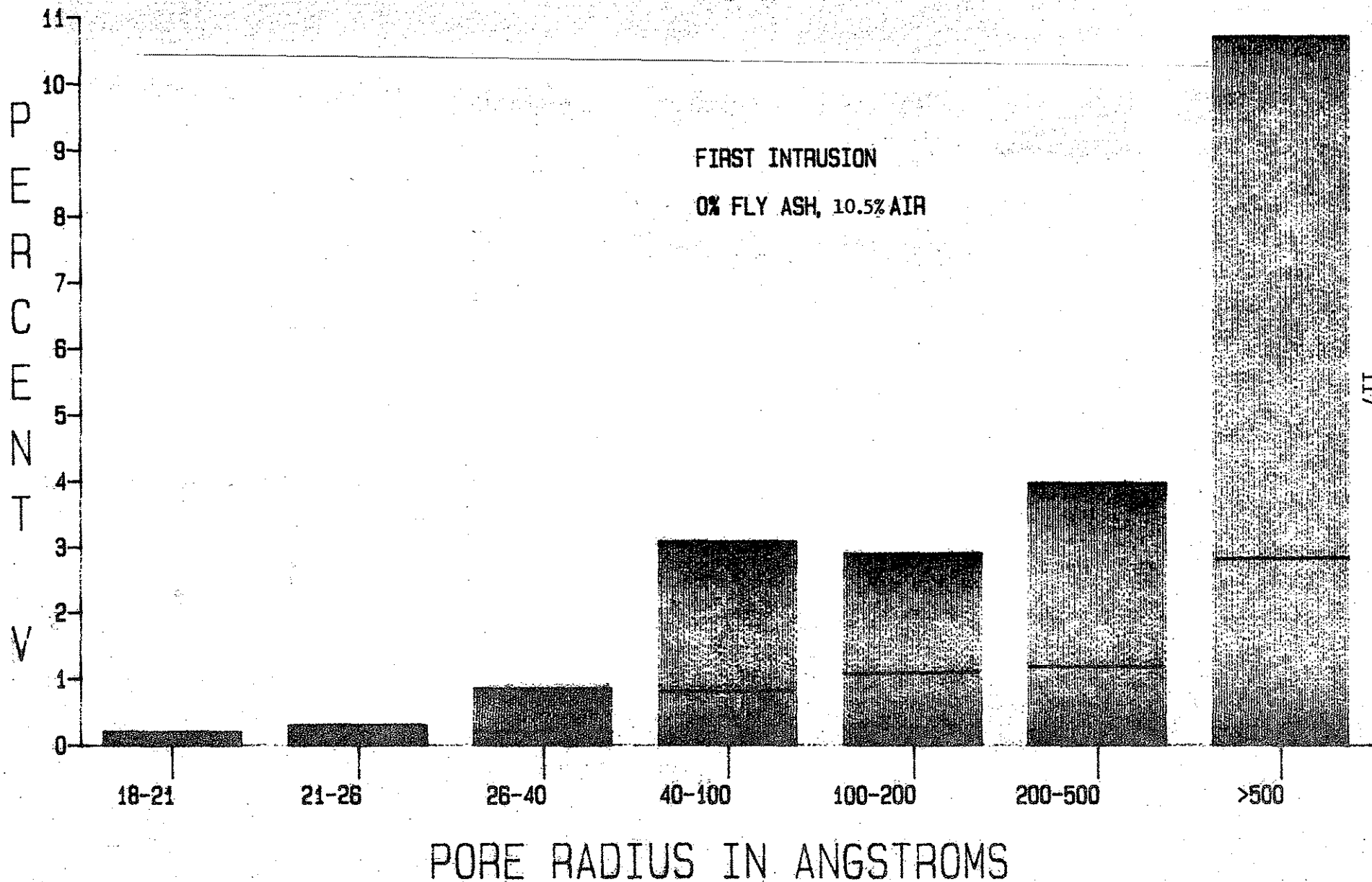
MONTOUR 28 DAY CURE

FIRST INTRUSION

0% FLY ASH, 6.0% AIR



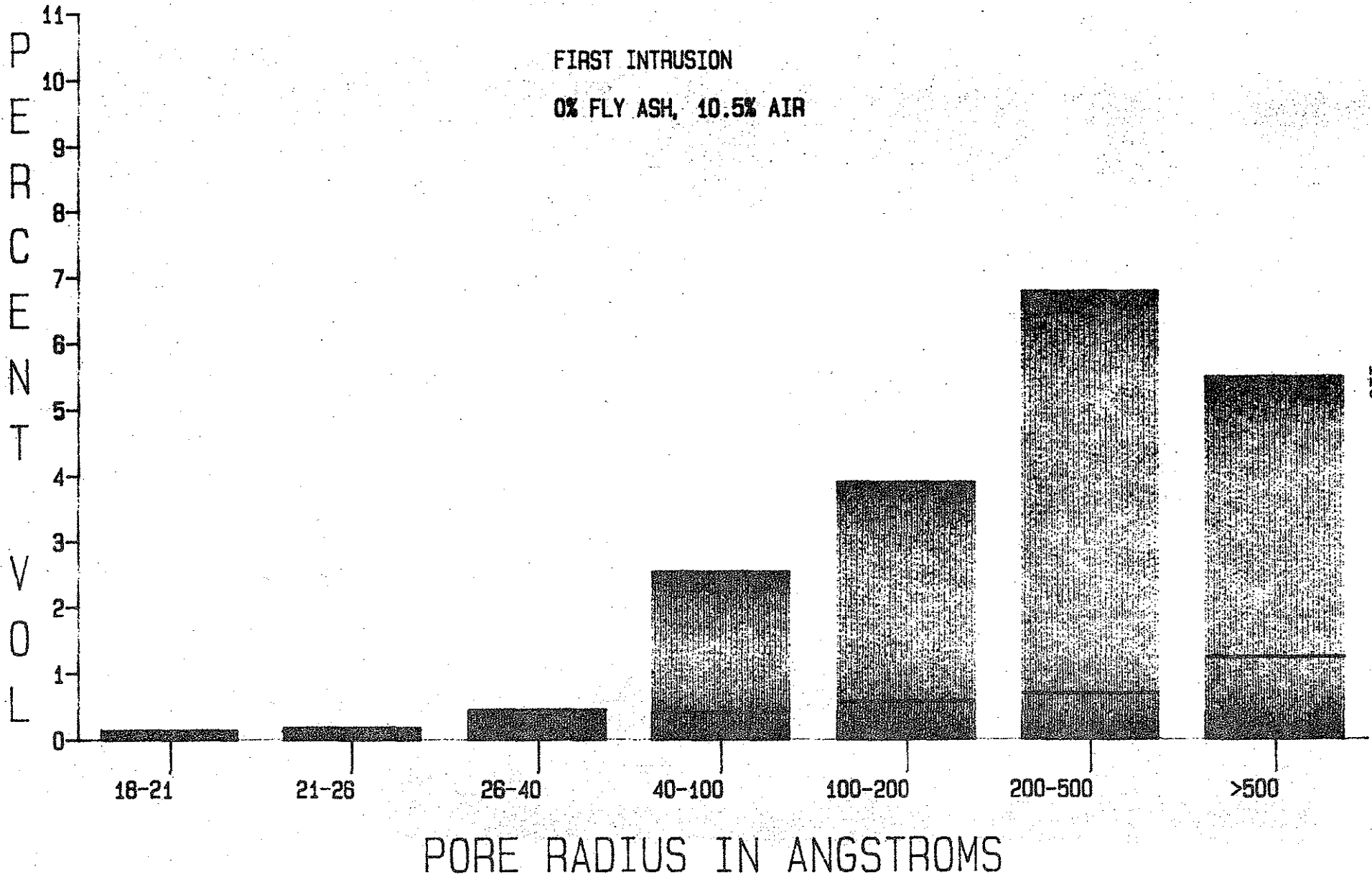
MONTOUR 3 DAY CURE



MONTOUR 7 DAY CURE

FIRST INTRUSION

0% FLY ASH, 10.5% AIR

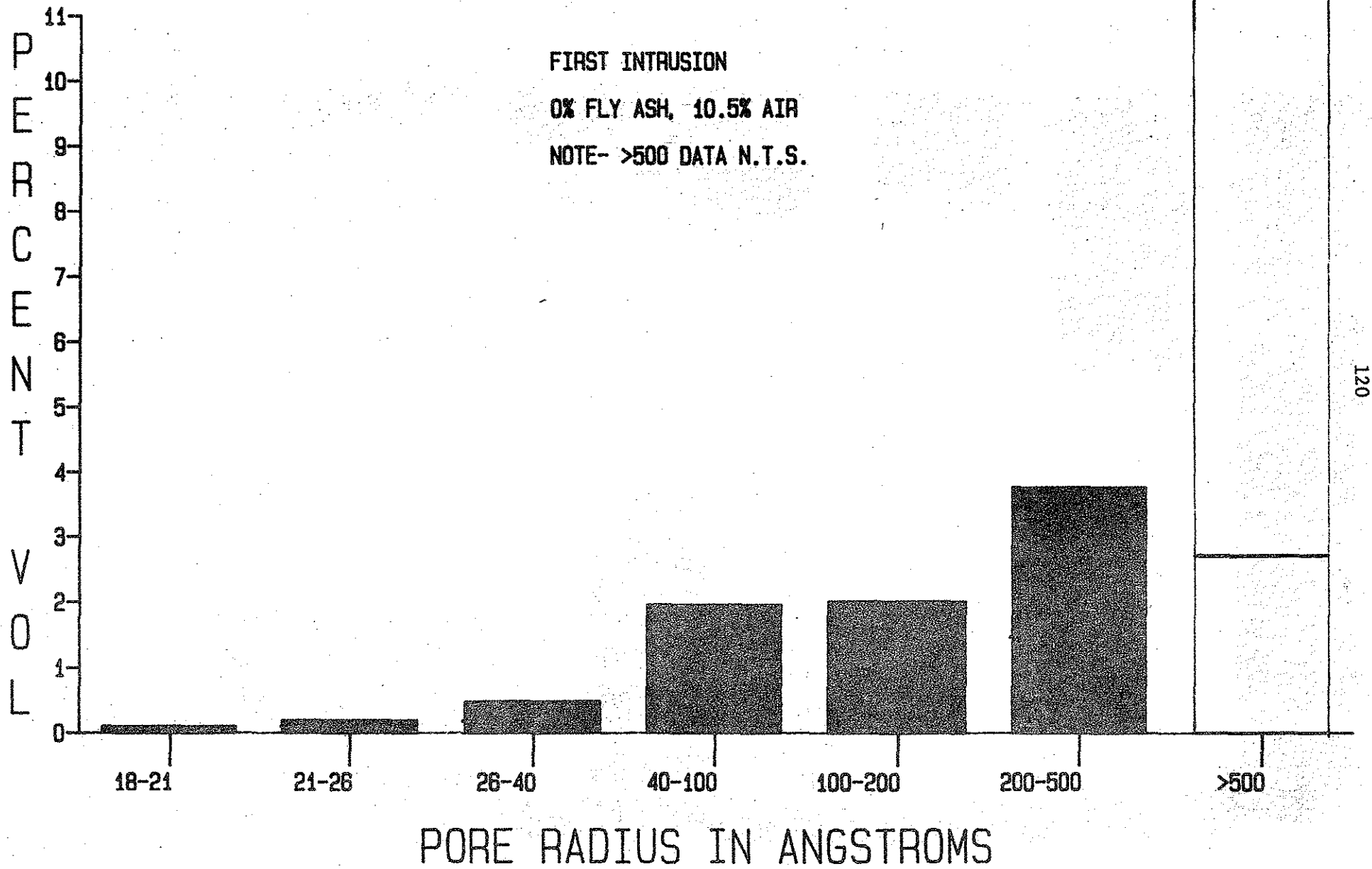


ALDEN 3 DAY CURE

FIRST INTRUSION

0% FLY ASH, 10.5% AIR

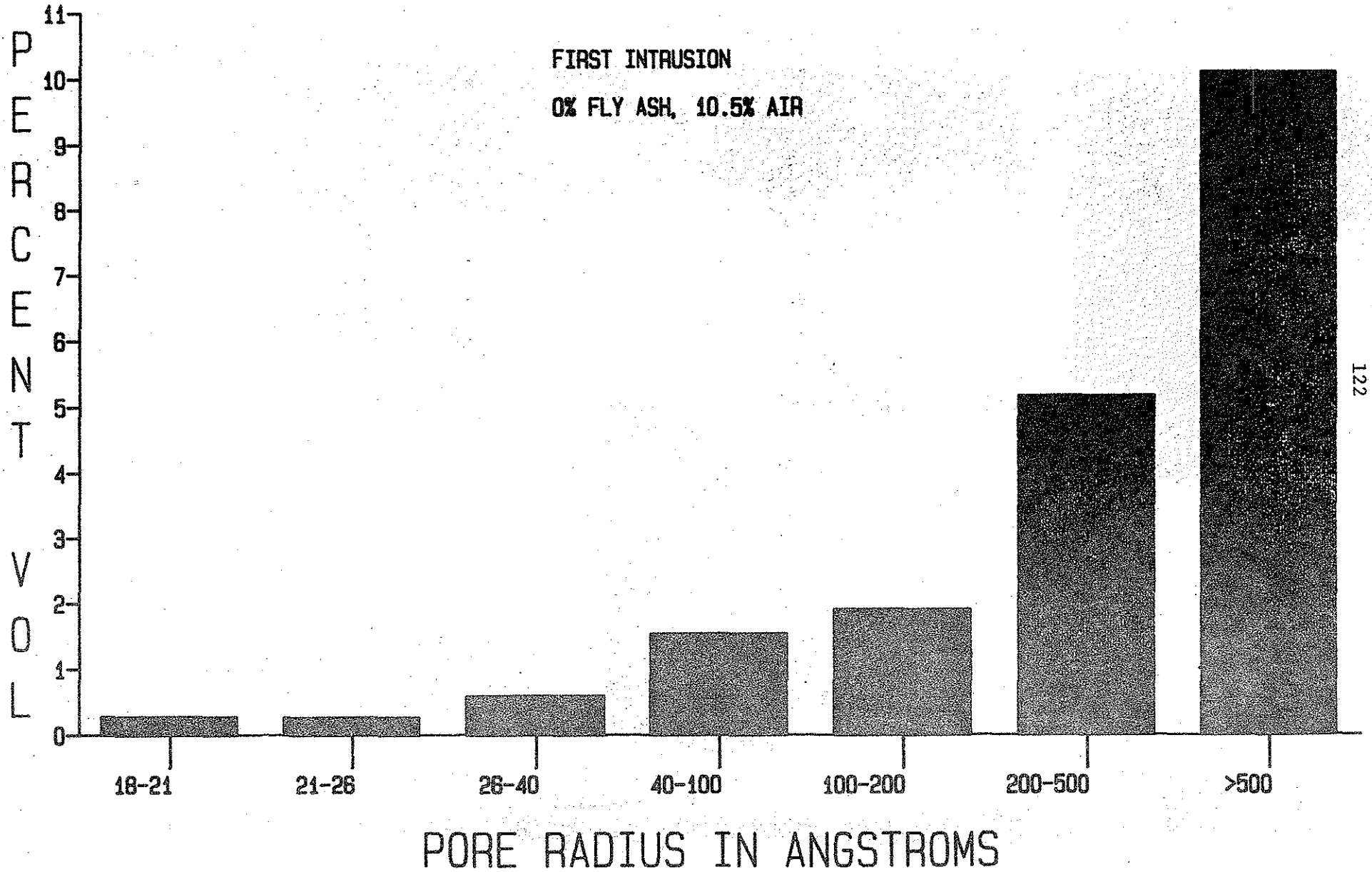
NOTE- >500 DATA N.T.S.



ALDEN 28 DAY CURE

FIRST INTRUSION

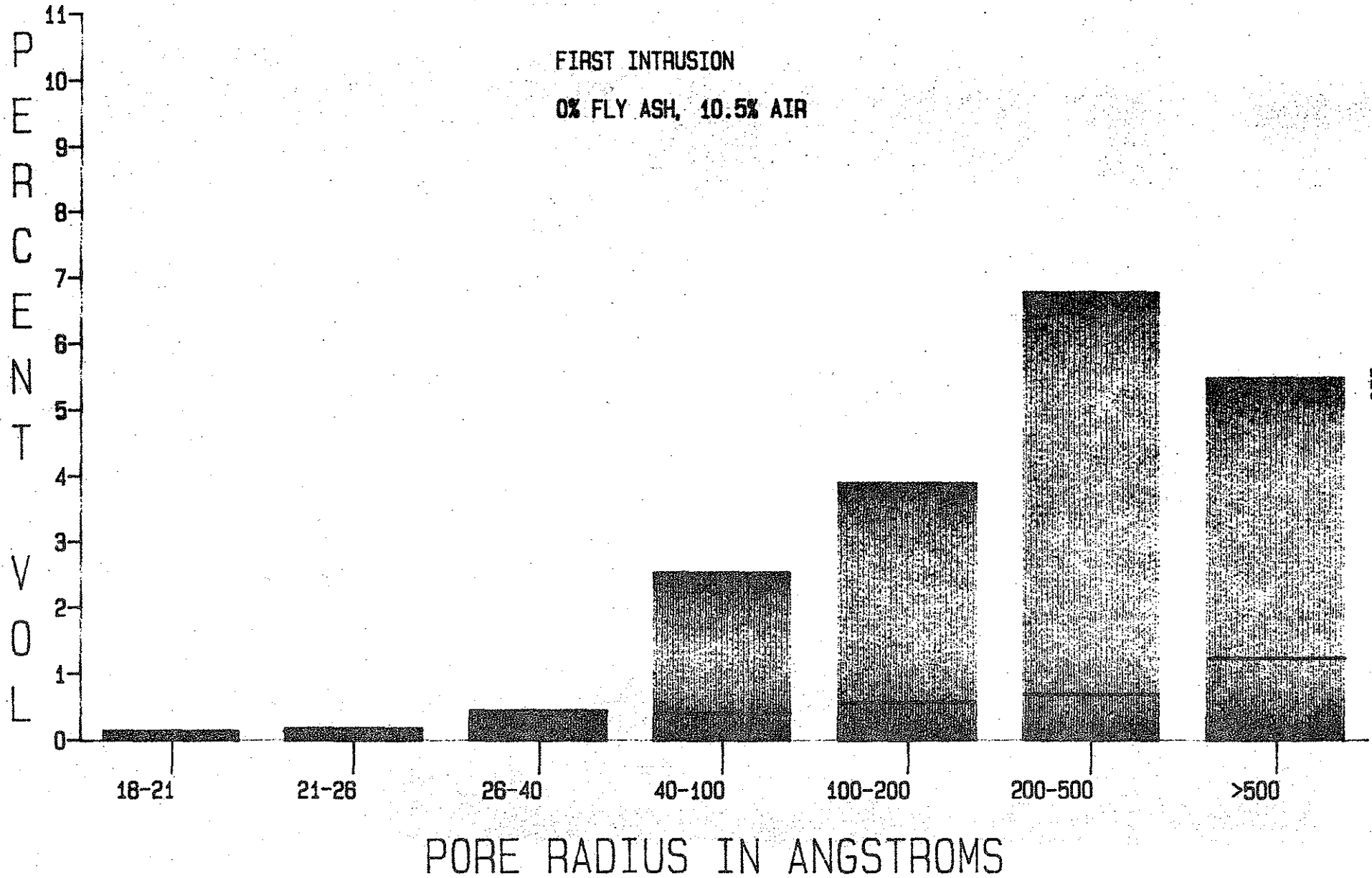
0% FLY ASH, 10.5% AIR



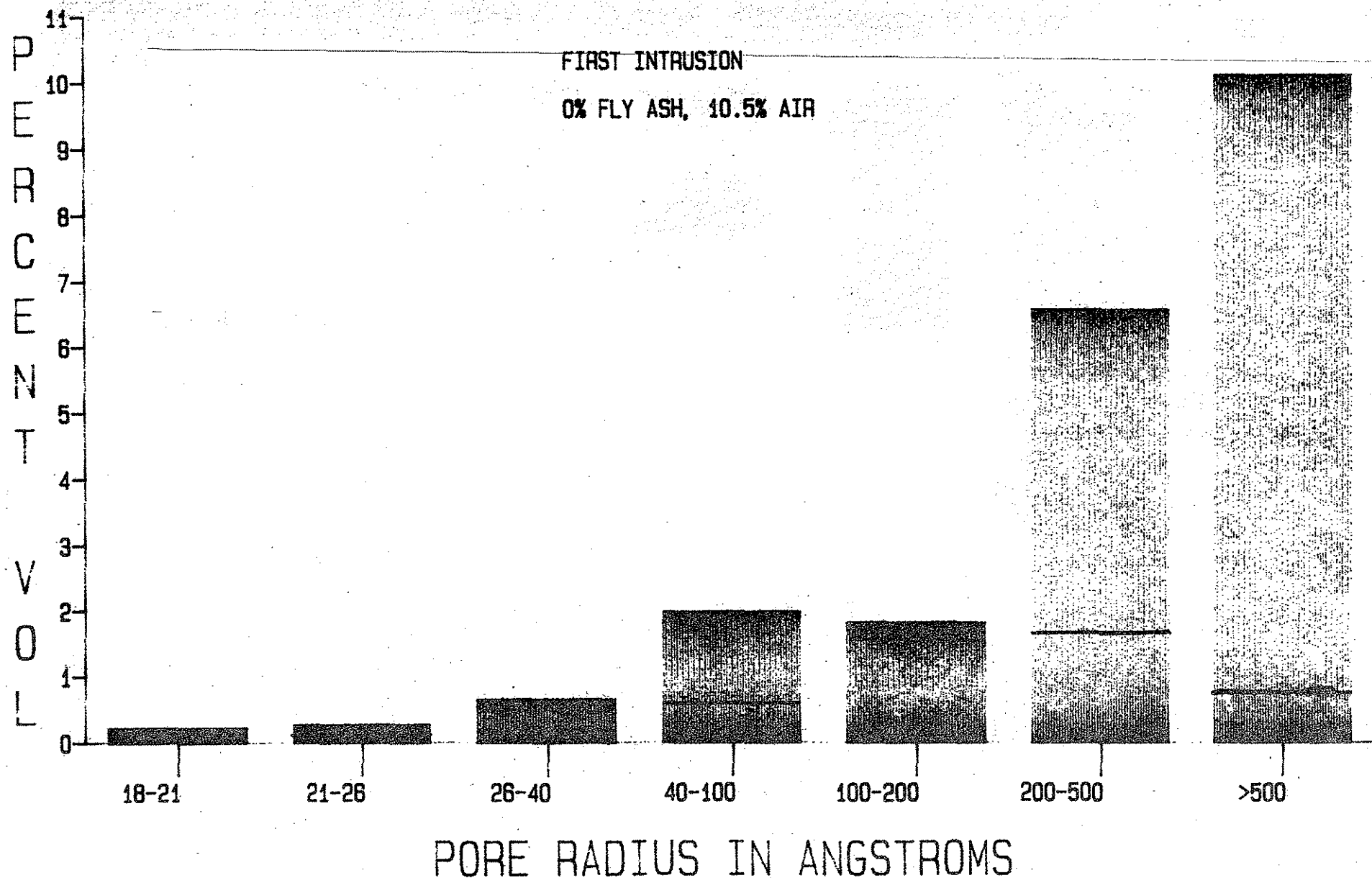
MONTOUR 7 DAY CURE

FIRST INTRUSION

0% FLY ASH, 10.5% AIR



MONTOUR 28 DAY CURE

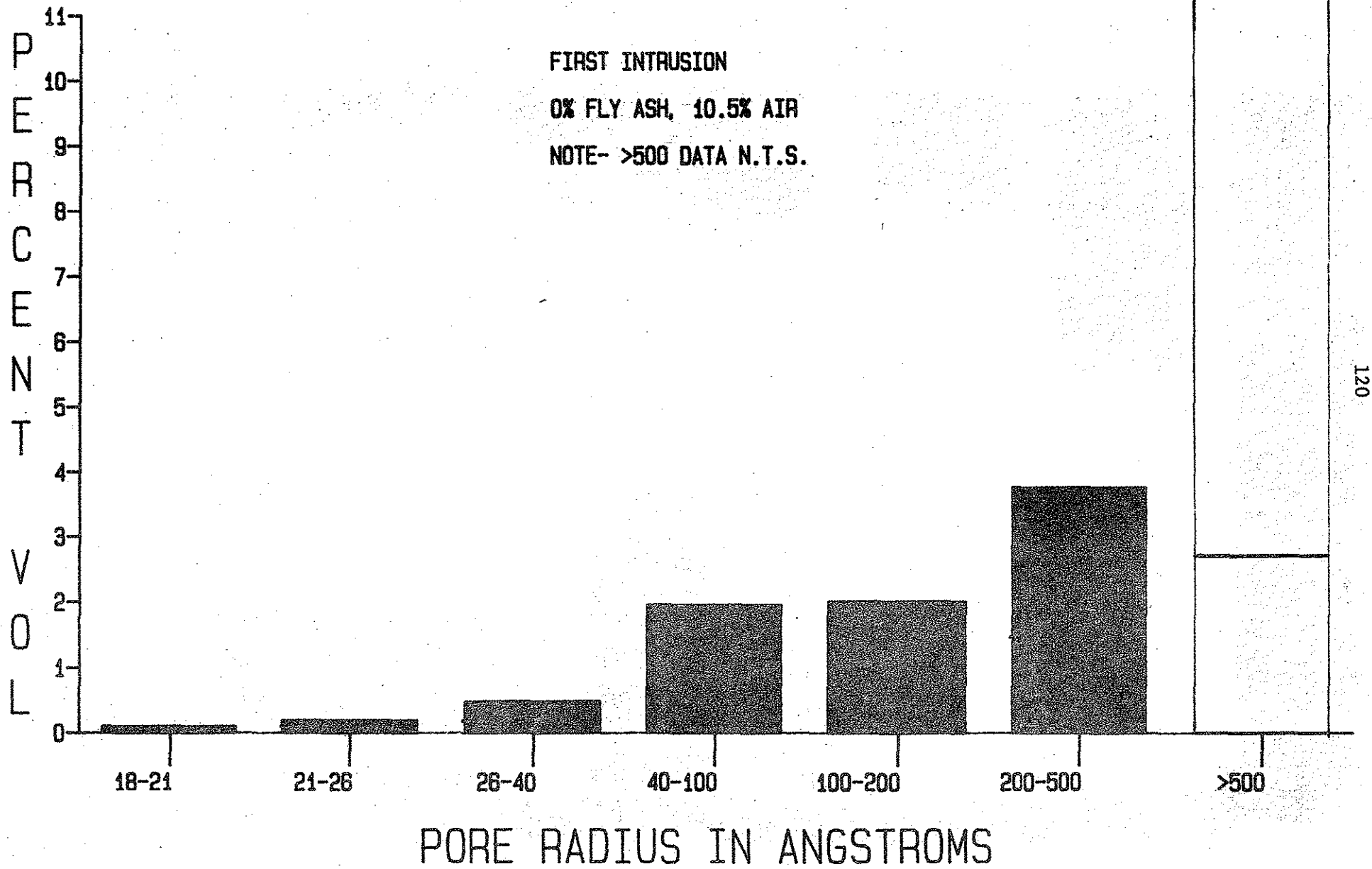


ALDEN 3 DAY CURE

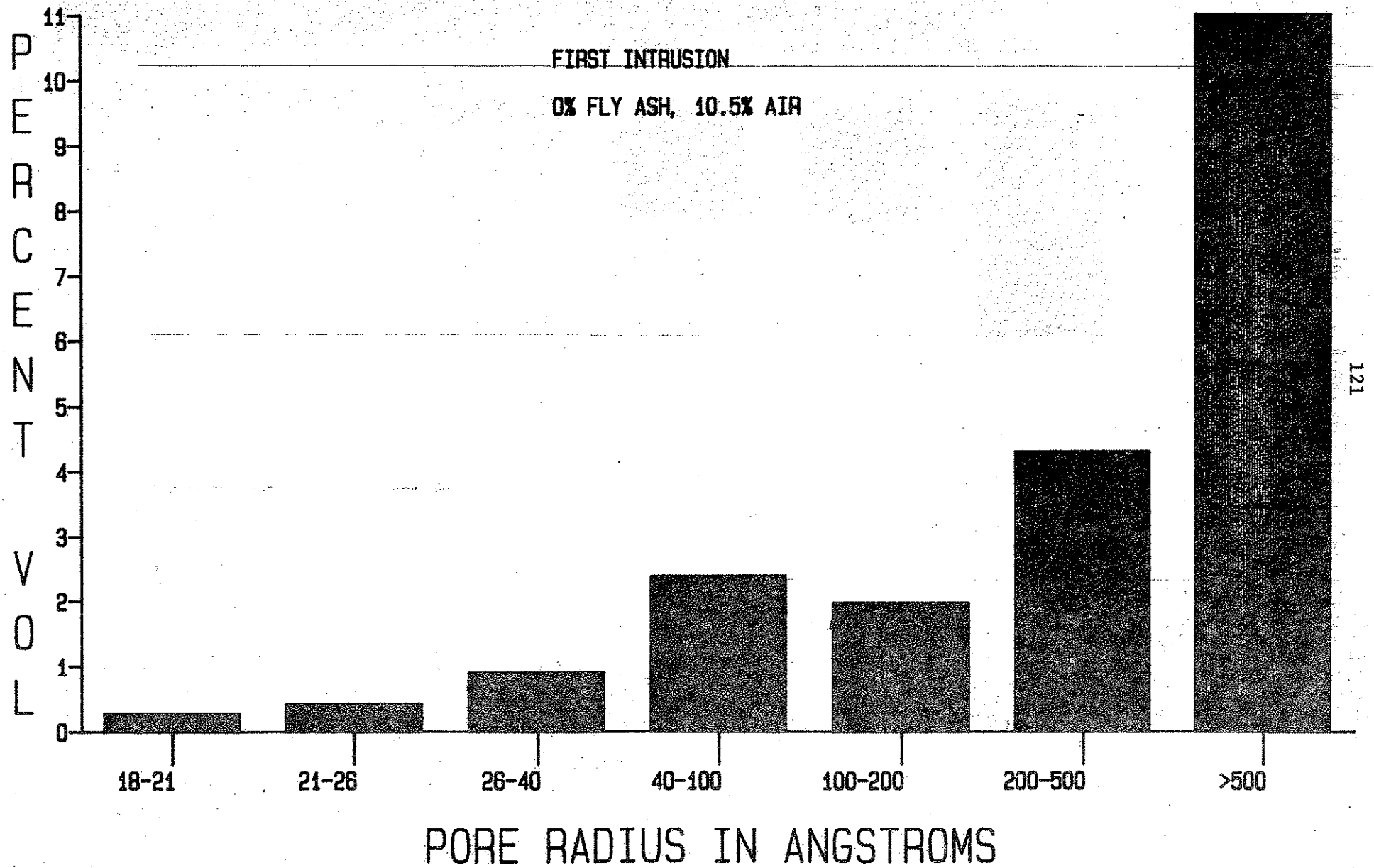
FIRST INTRUSION

0% FLY ASH, 10.5% AIR

NOTE- >500 DATA N.T.S.



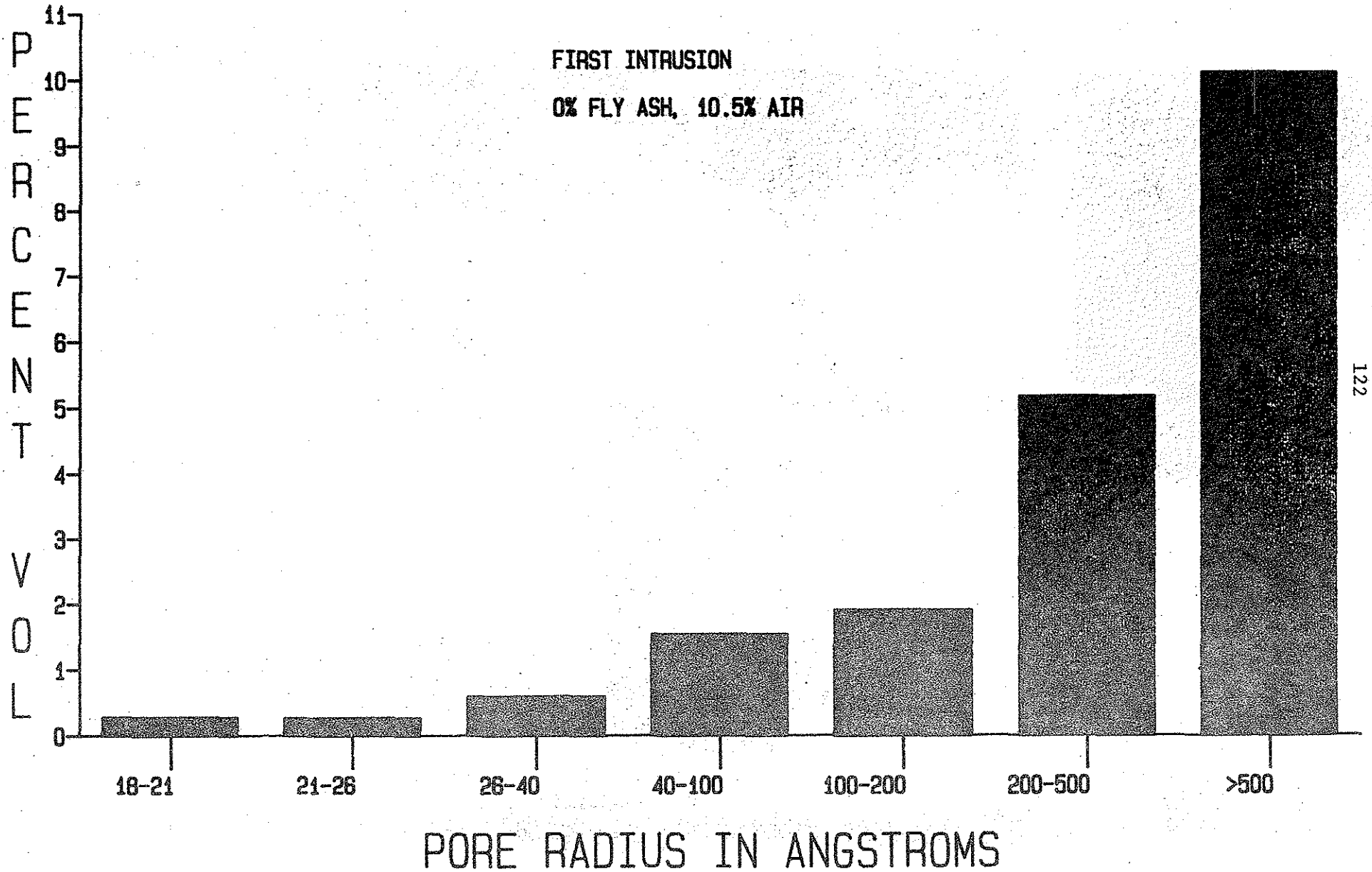
ALDEN 7 DAY CURE



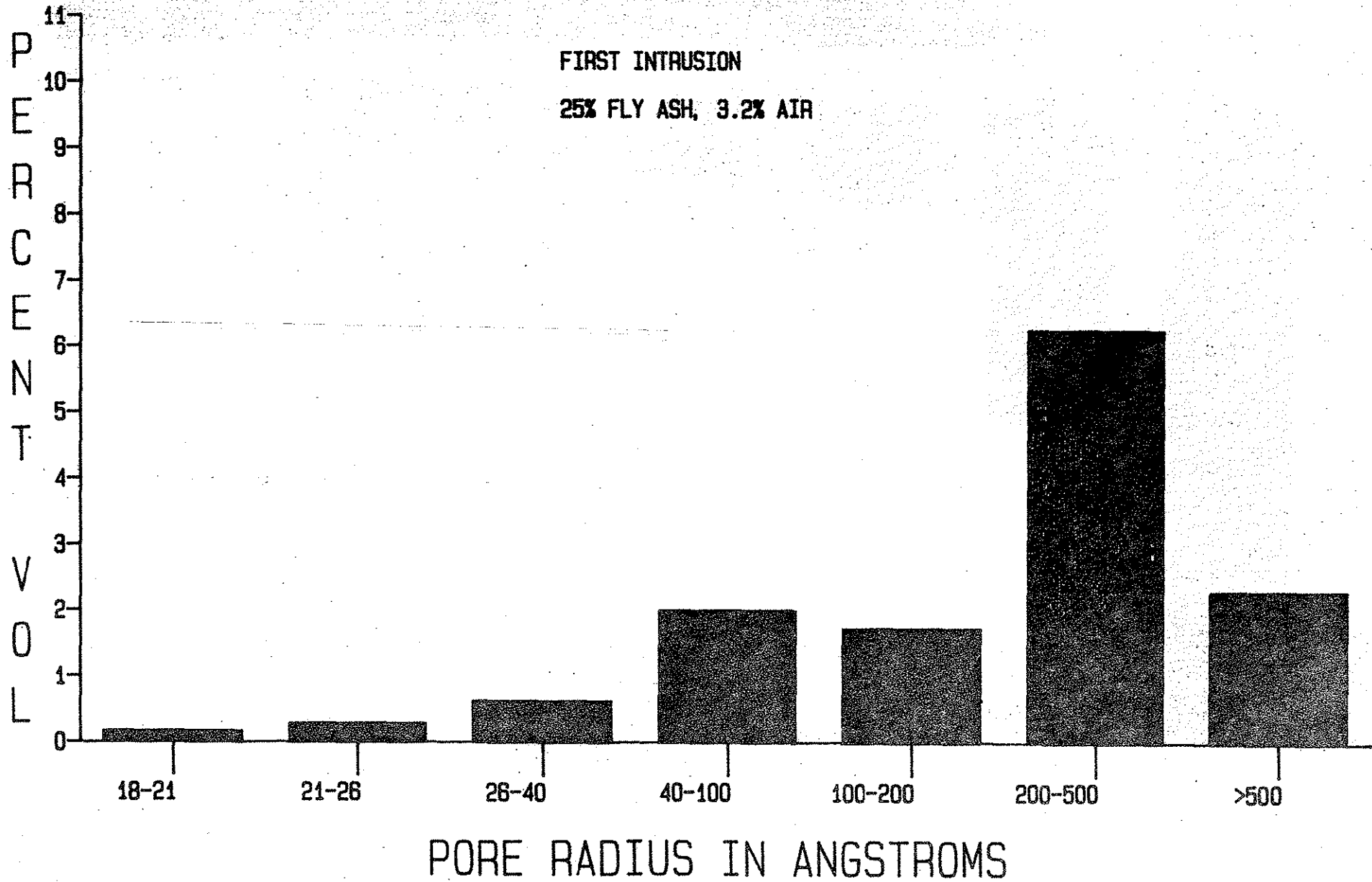
ALDEN 28 DAY CURE

FIRST INTRUSION

0% FLY ASH, 10.5% AIR

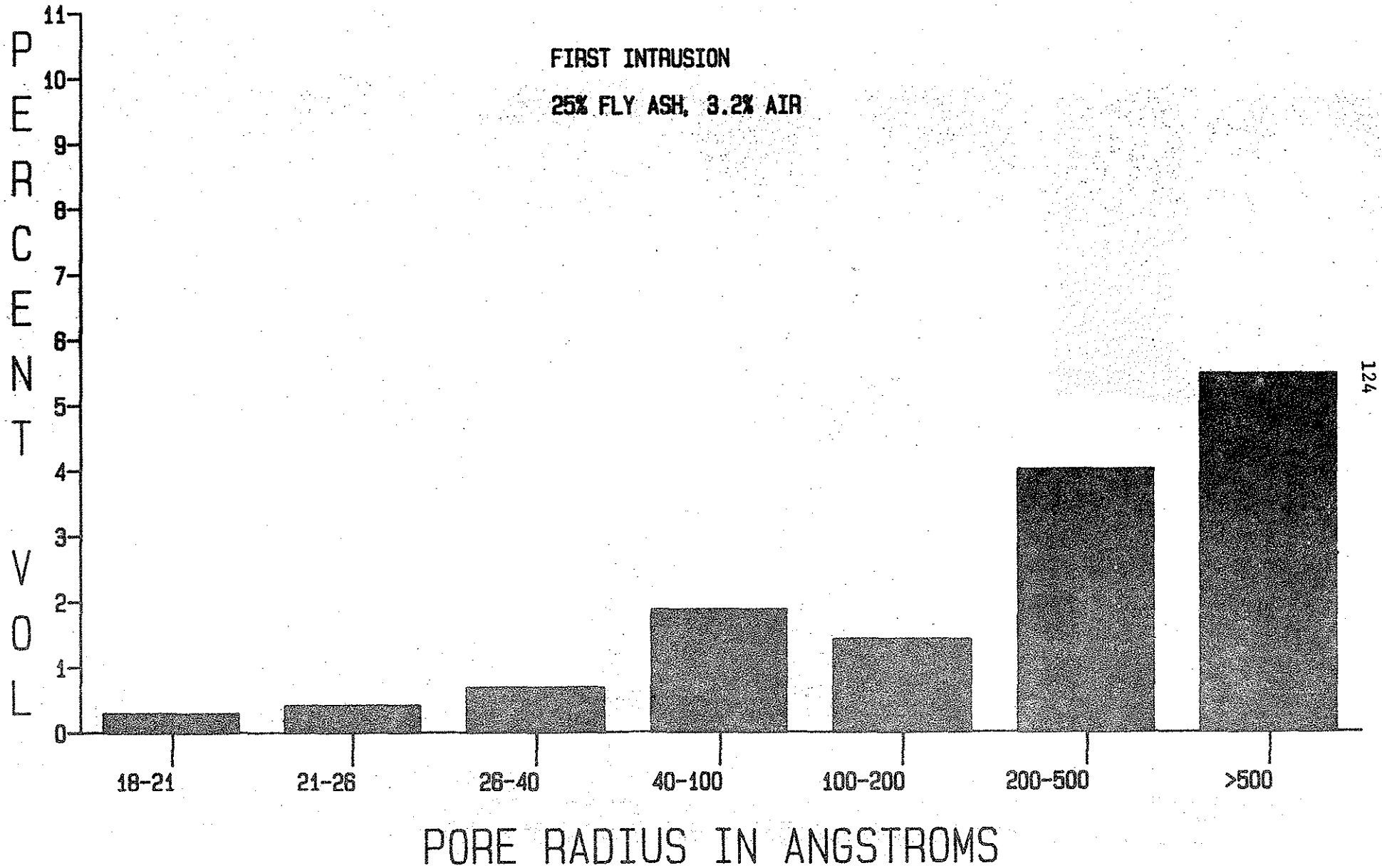


MONTOUR 3 DAY CURE

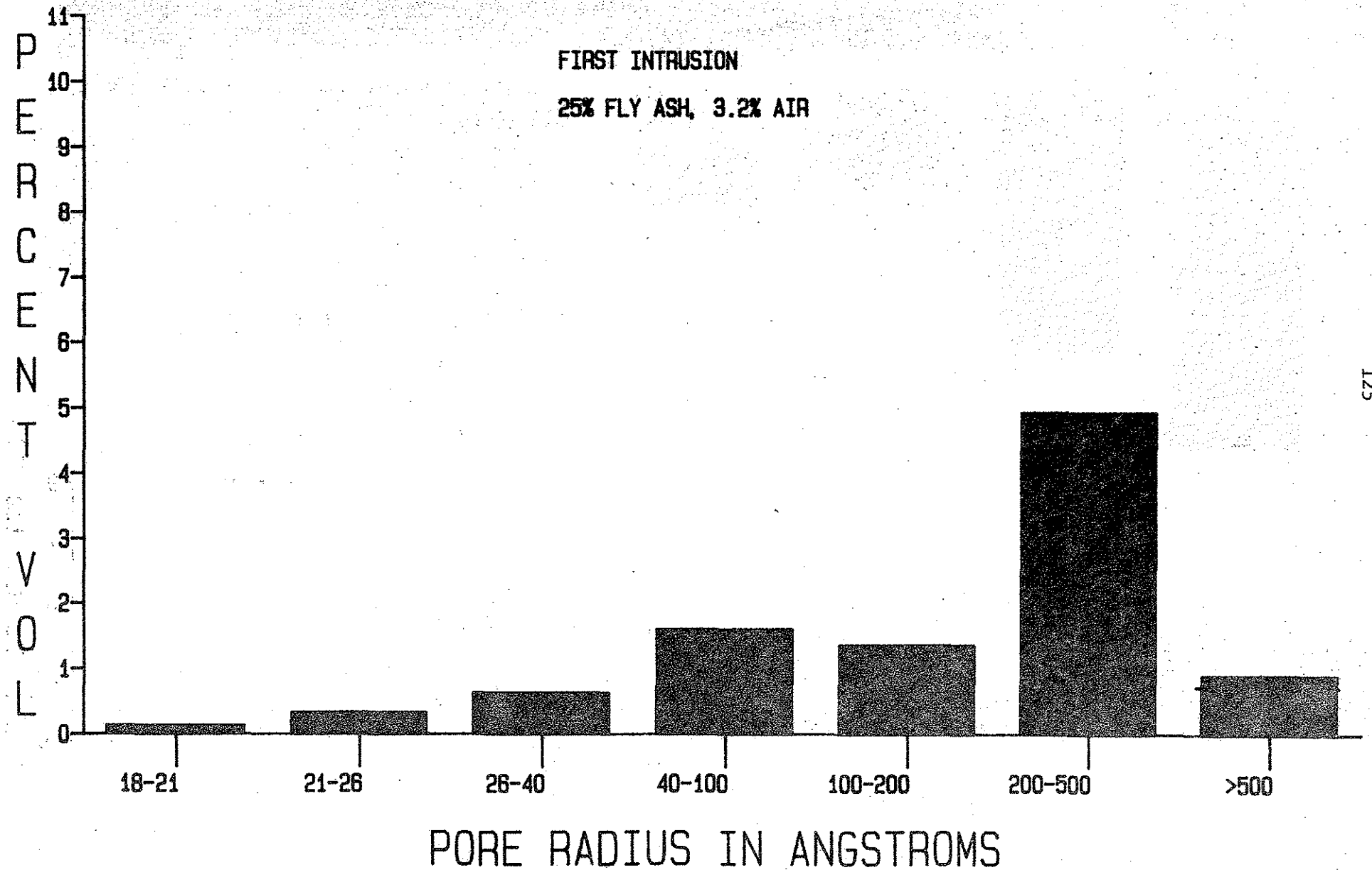


MONTOUR 7 DAY CURE

FIRST INTRUSION
25% FLY ASH, 3.2% AIR

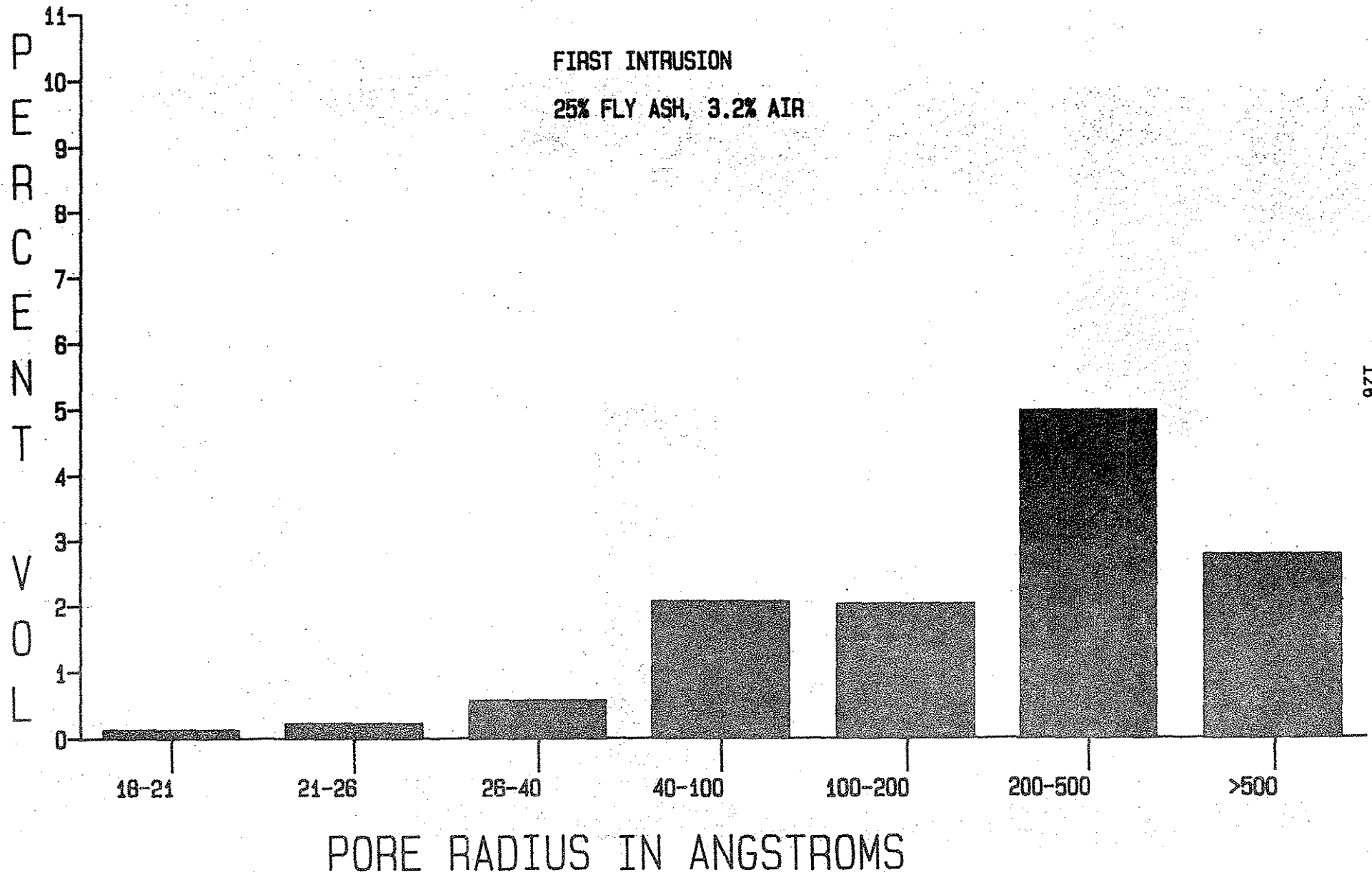


MONTOUR 28 DAY CURE

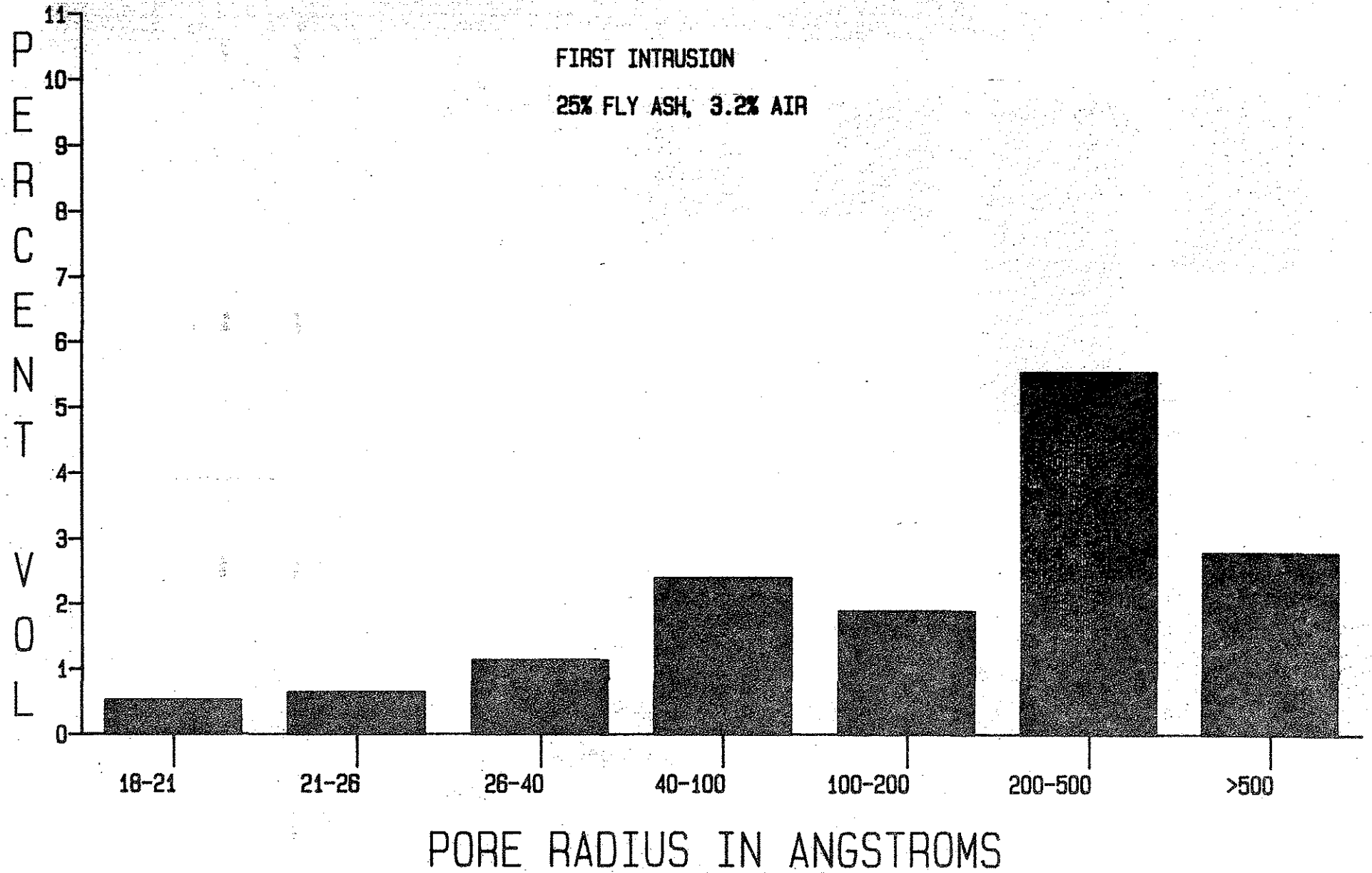


ALDEN 3 DAY CURE

FIRST INTRUSION
25% FLY ASH, 3.2% AIR



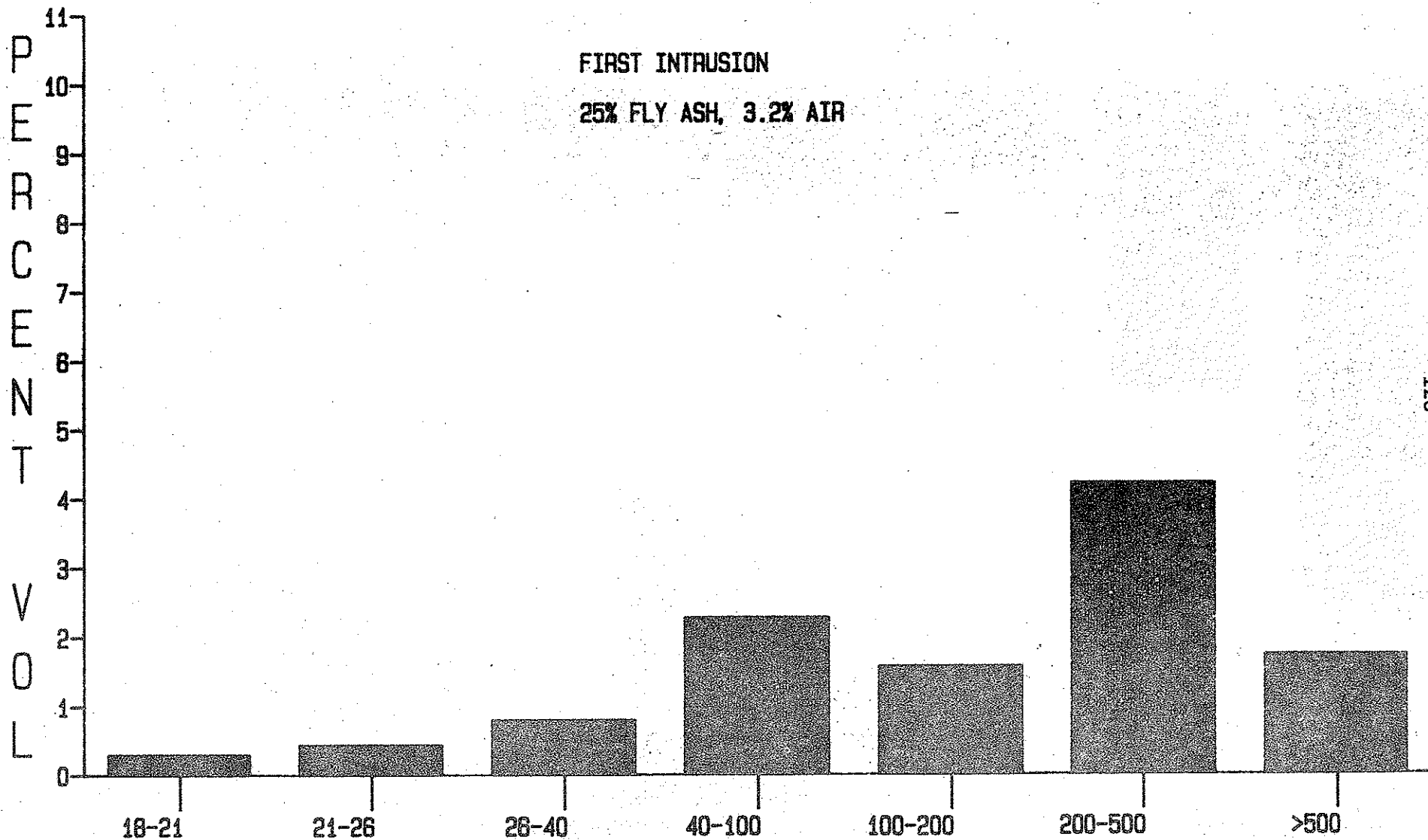
ALDEN 11 DAY CURE



ALDEN 28 DAY CURE

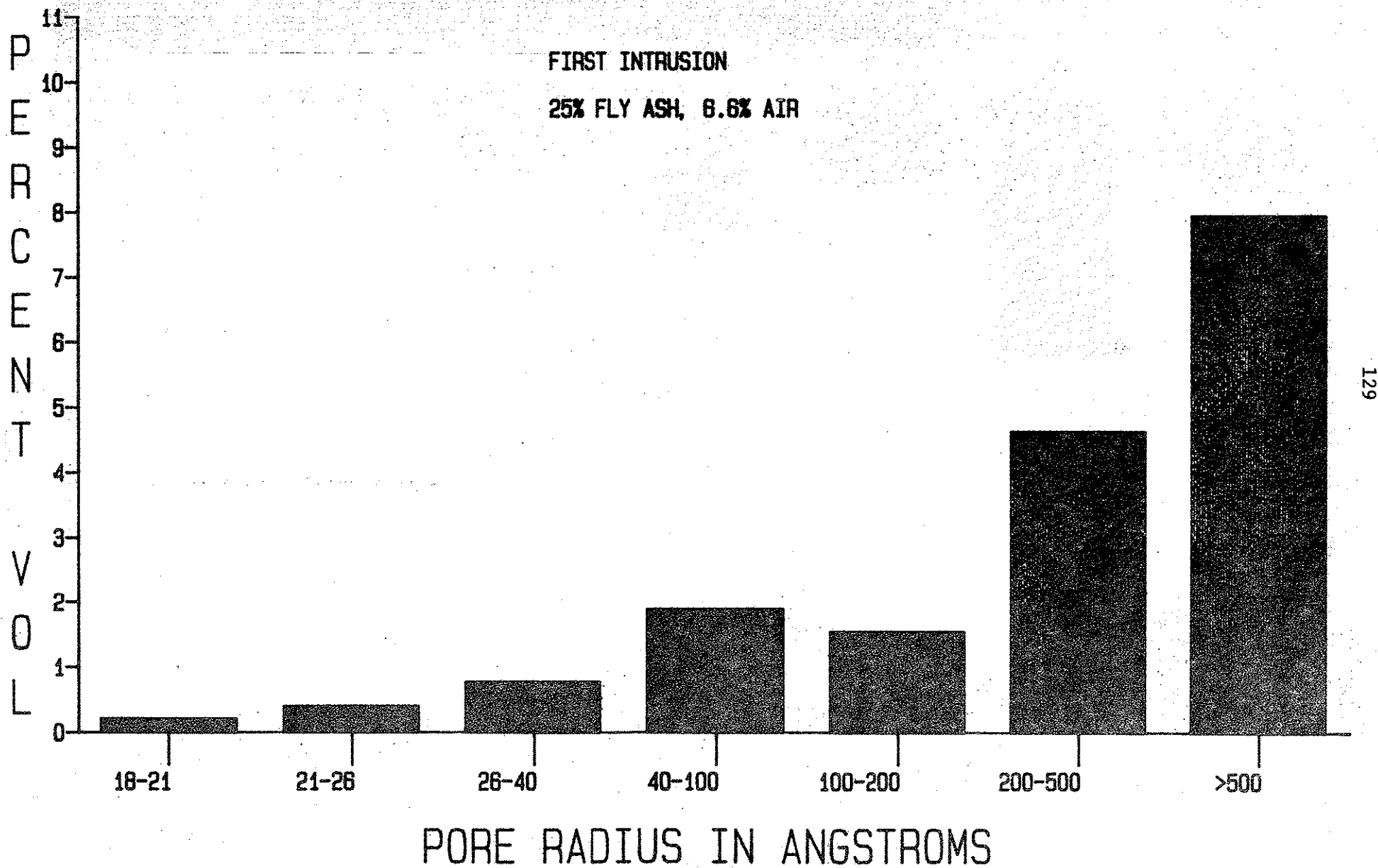
FIRST INTRUSION

25% FLY ASH, 3.2% AIR



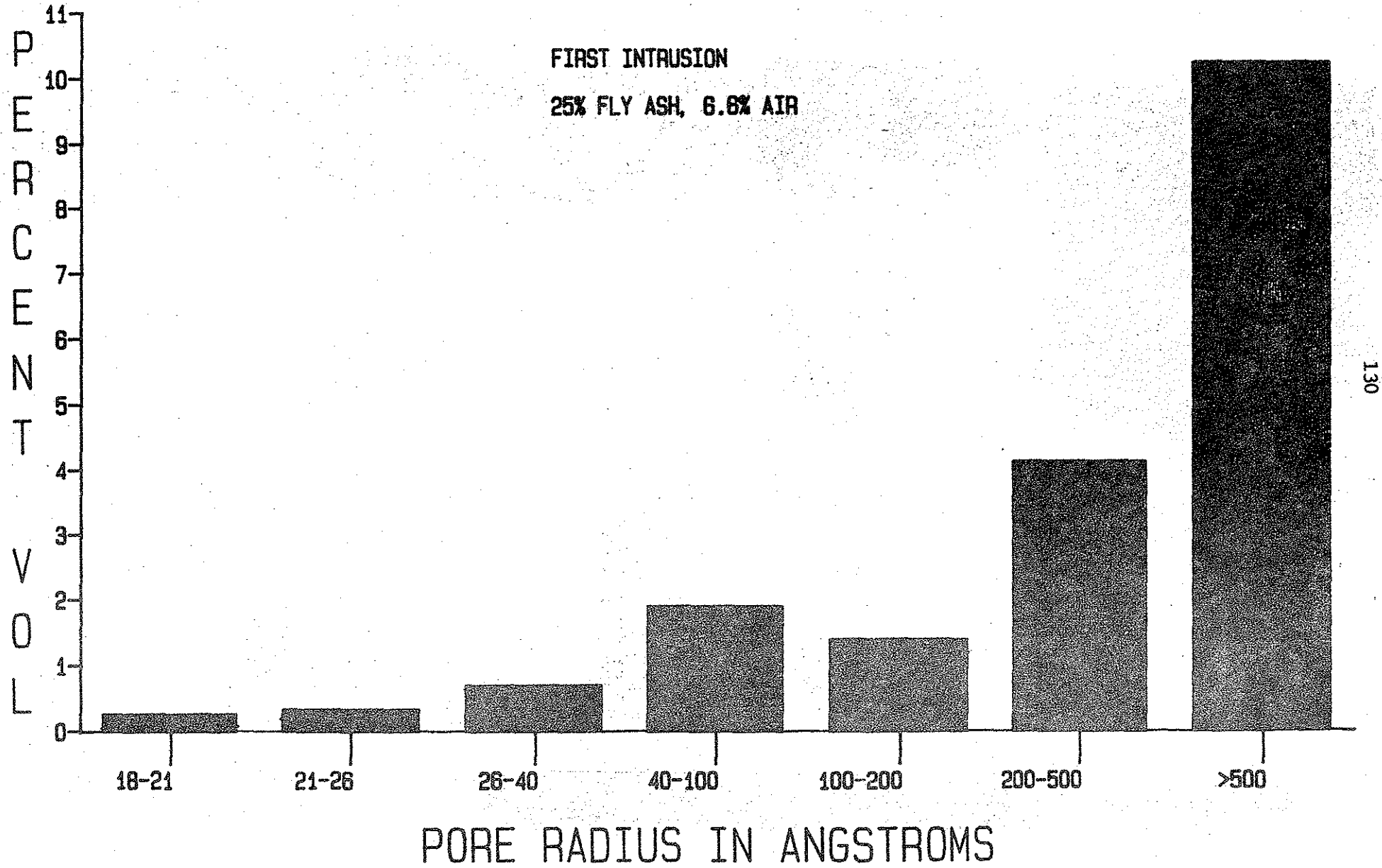
PORE RADIUS IN ANGSTROMS

MONTOUR 3 DAY CURE

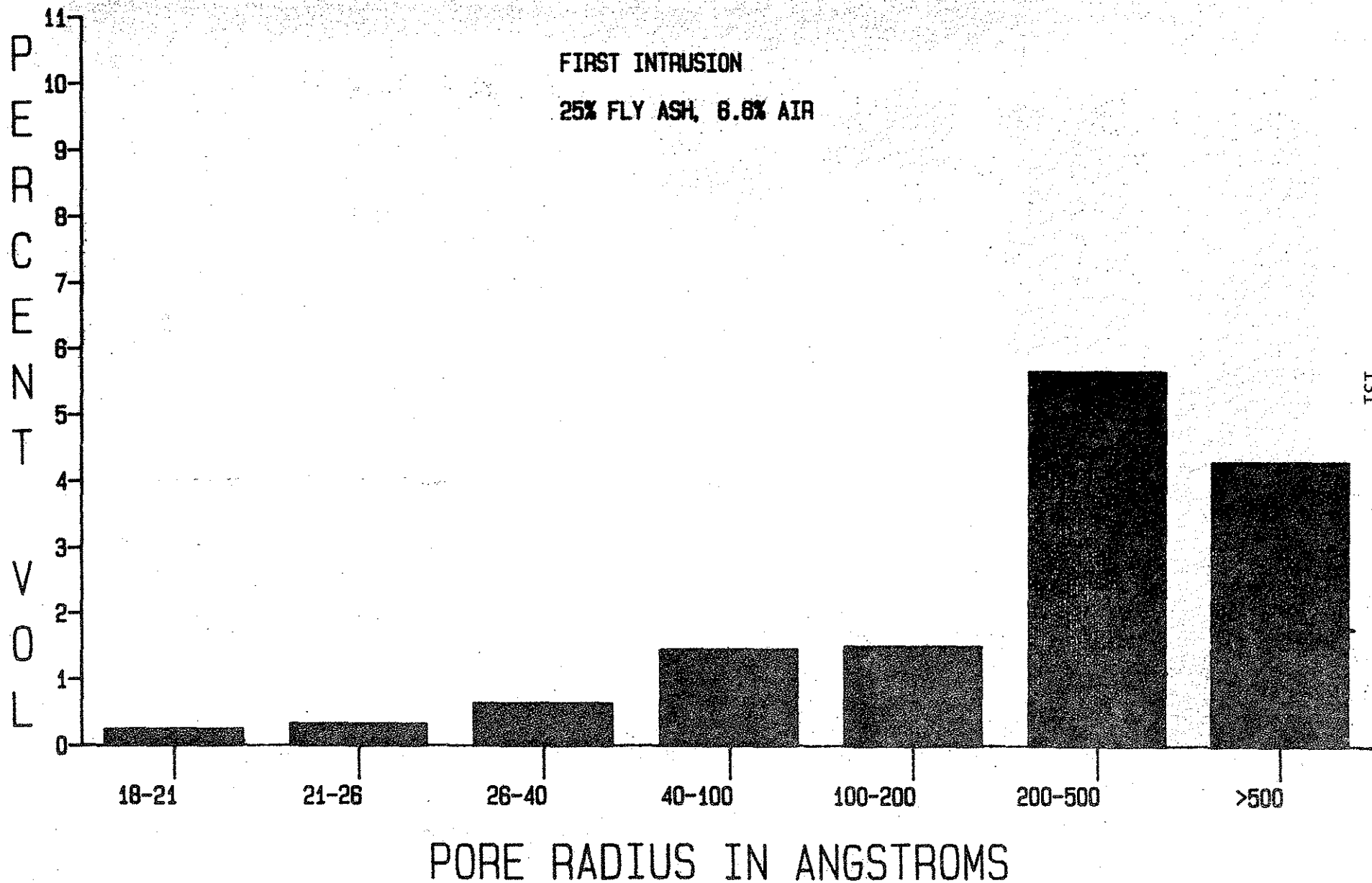


MONTOUR 7 DAY CURE

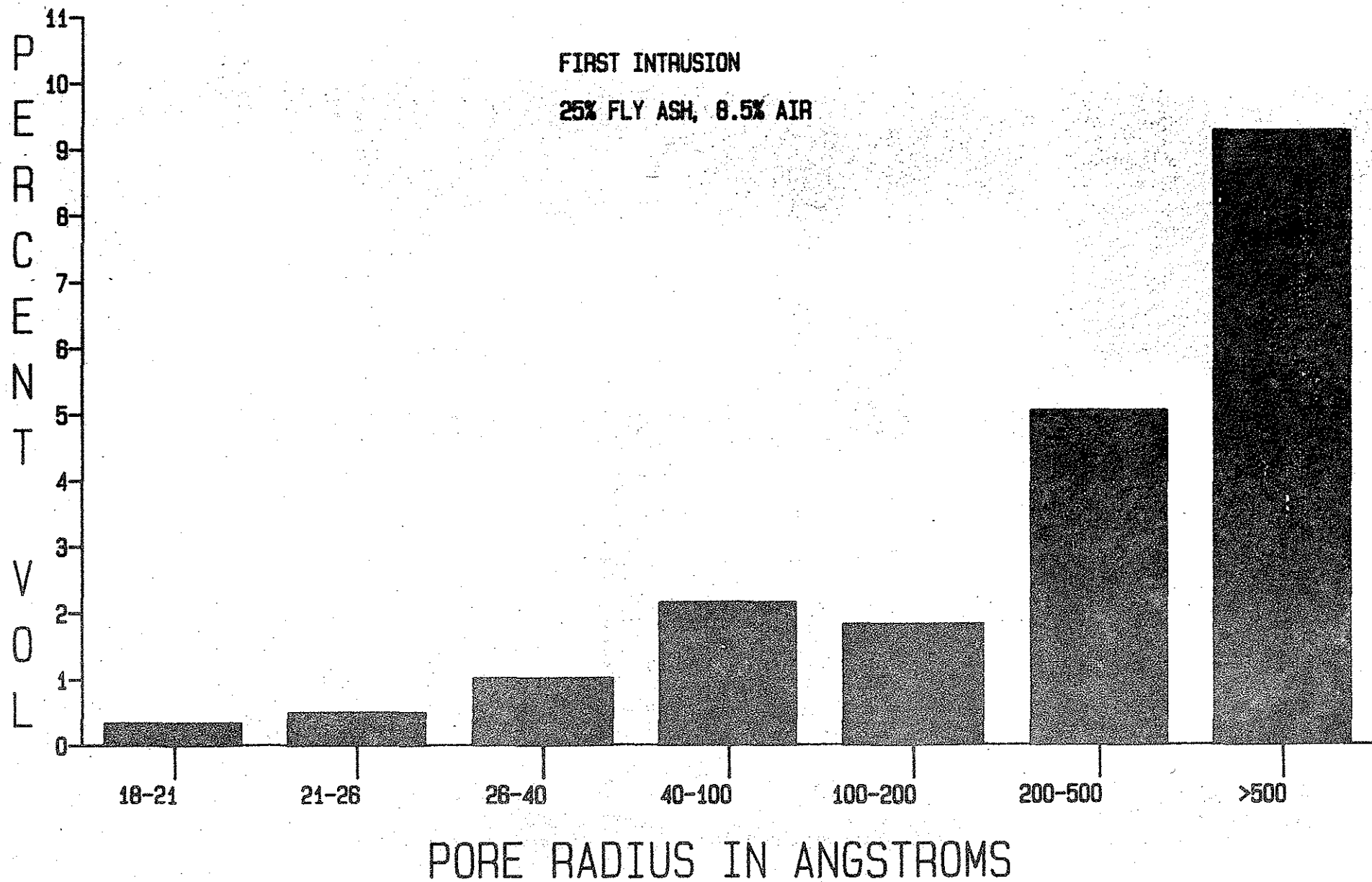
FIRST INTRUSION
25% FLY ASH, 6.6% AIR



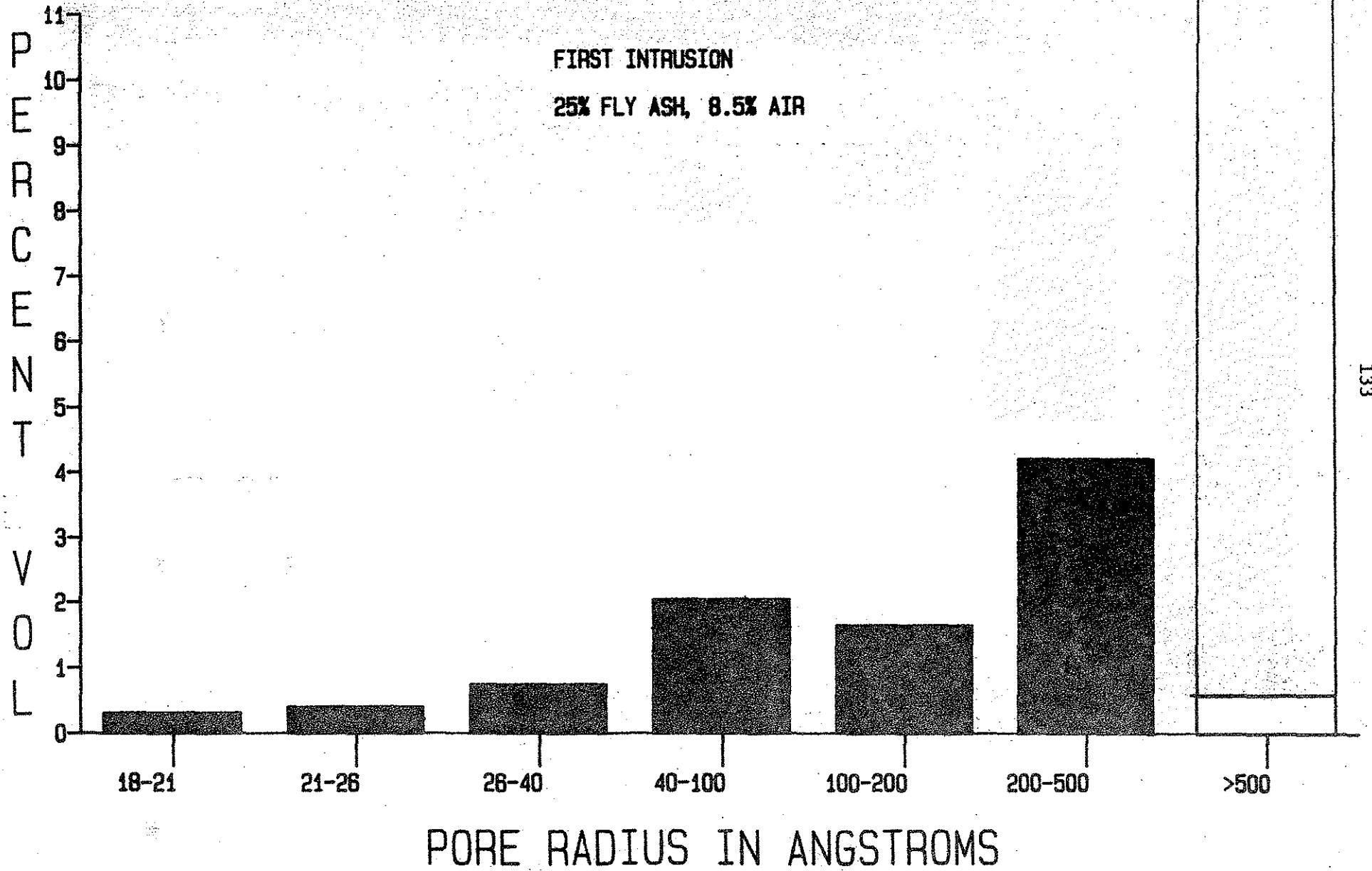
MONTOUR 28 DAY CURE



MONTOUR 3 DAY CURE



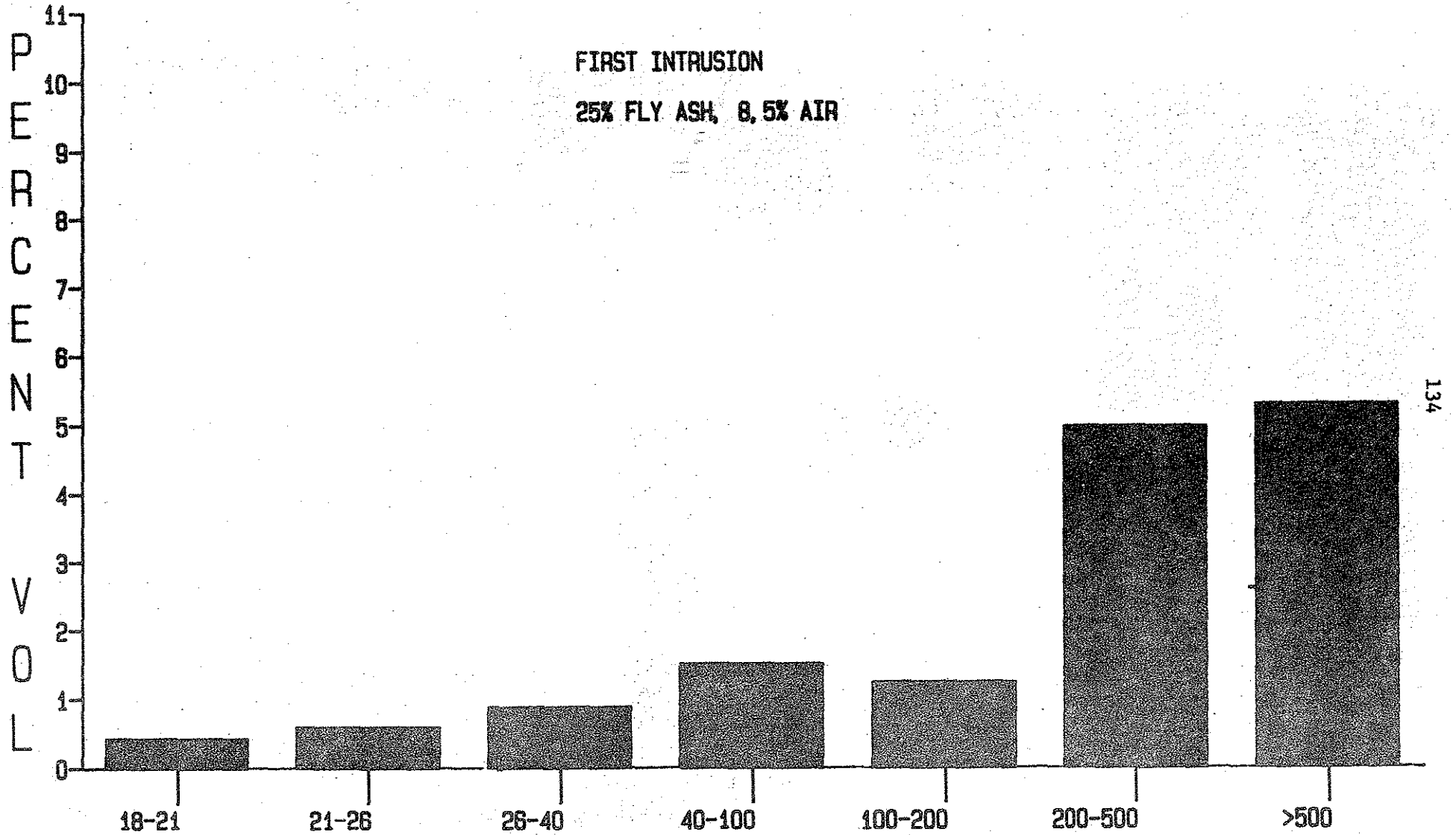
MONTOUR 7 DAY CURE



MONTOUR 28 DAY CURE

FIRST INTRUSION

25% FLY ASH, 8.5% AIR

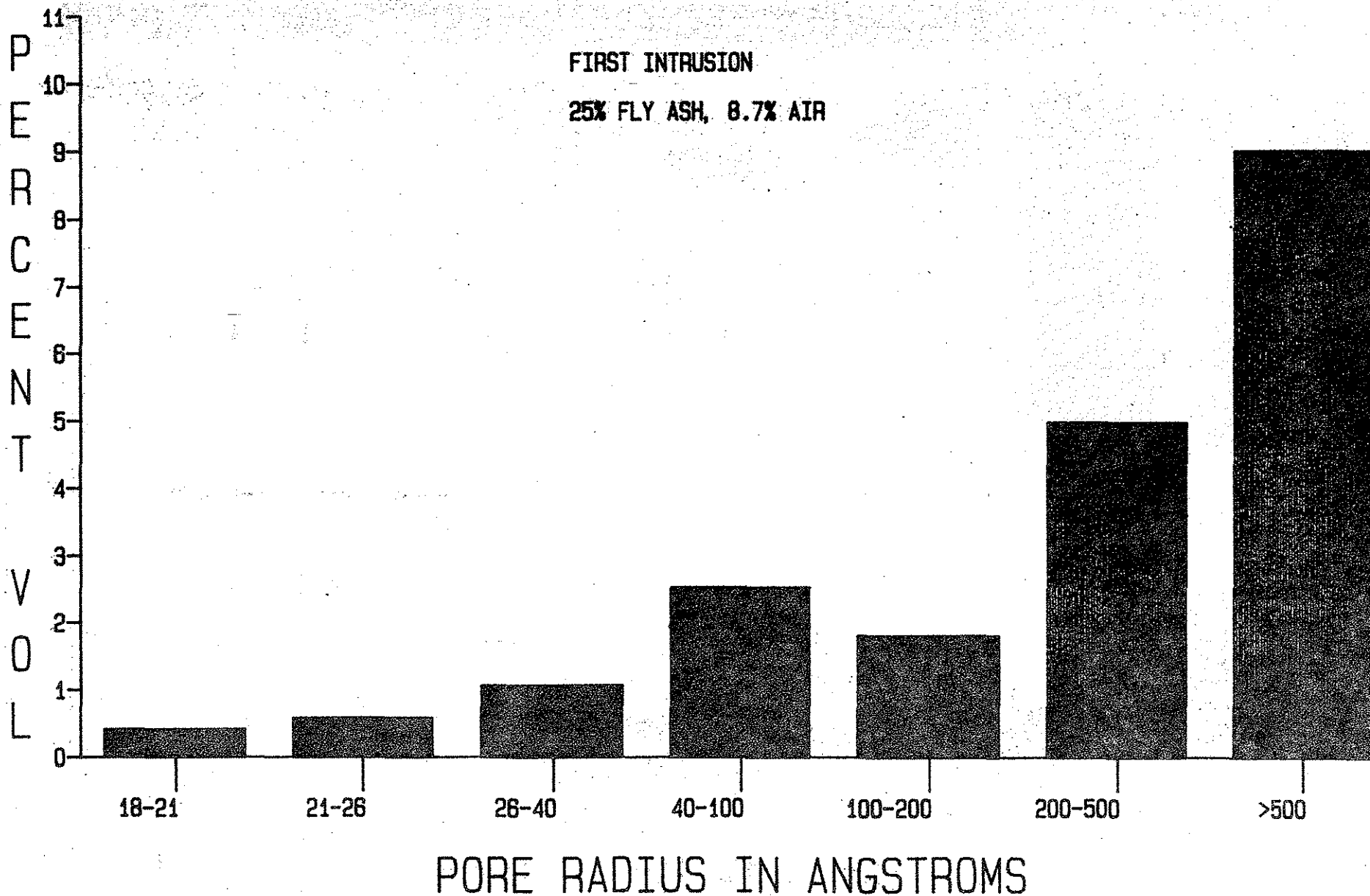


PORE RADIUS IN ANGSTROMS

ALDEN 3 DAY CURE

FIRST INTRUSION

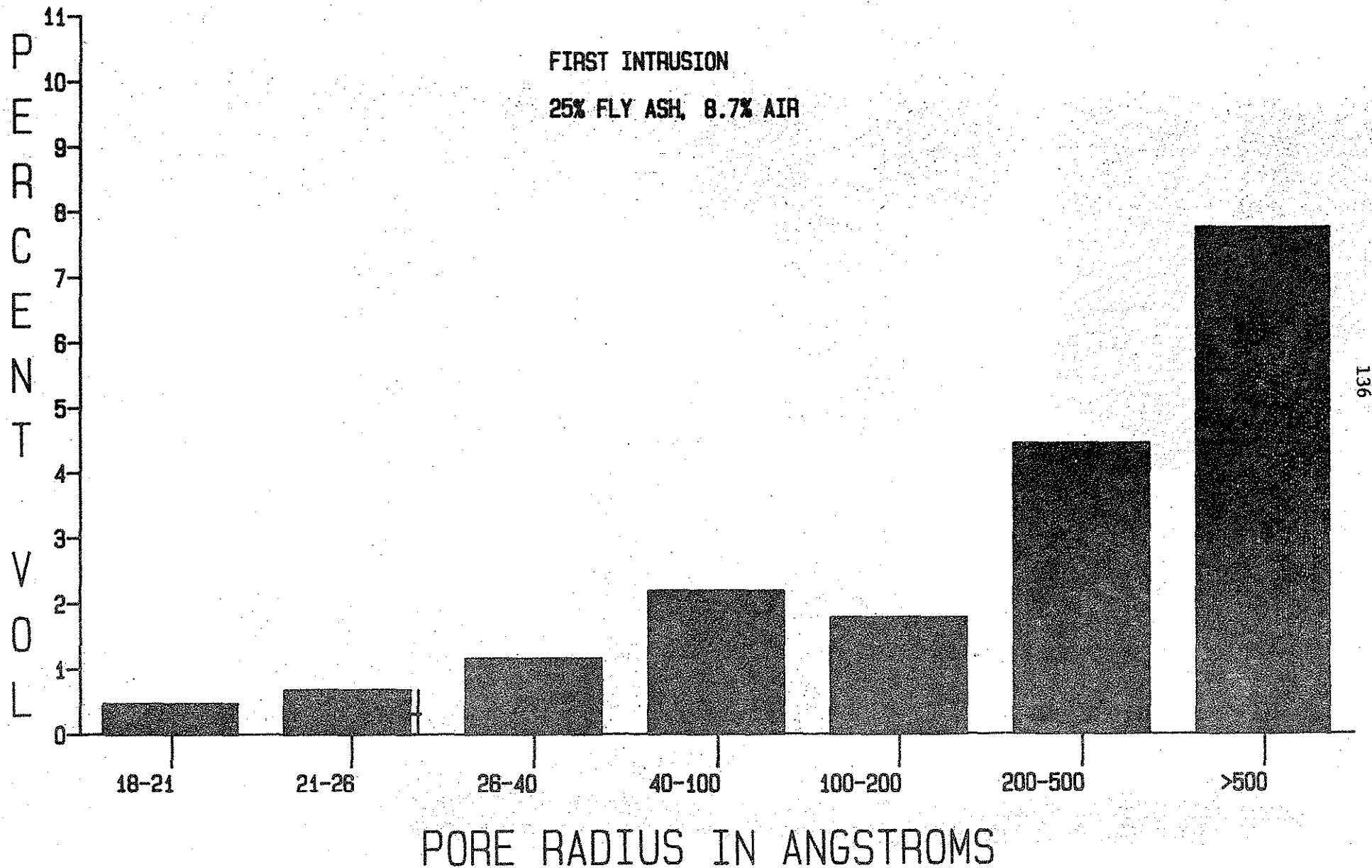
25% FLY ASH, 8.7% AIR



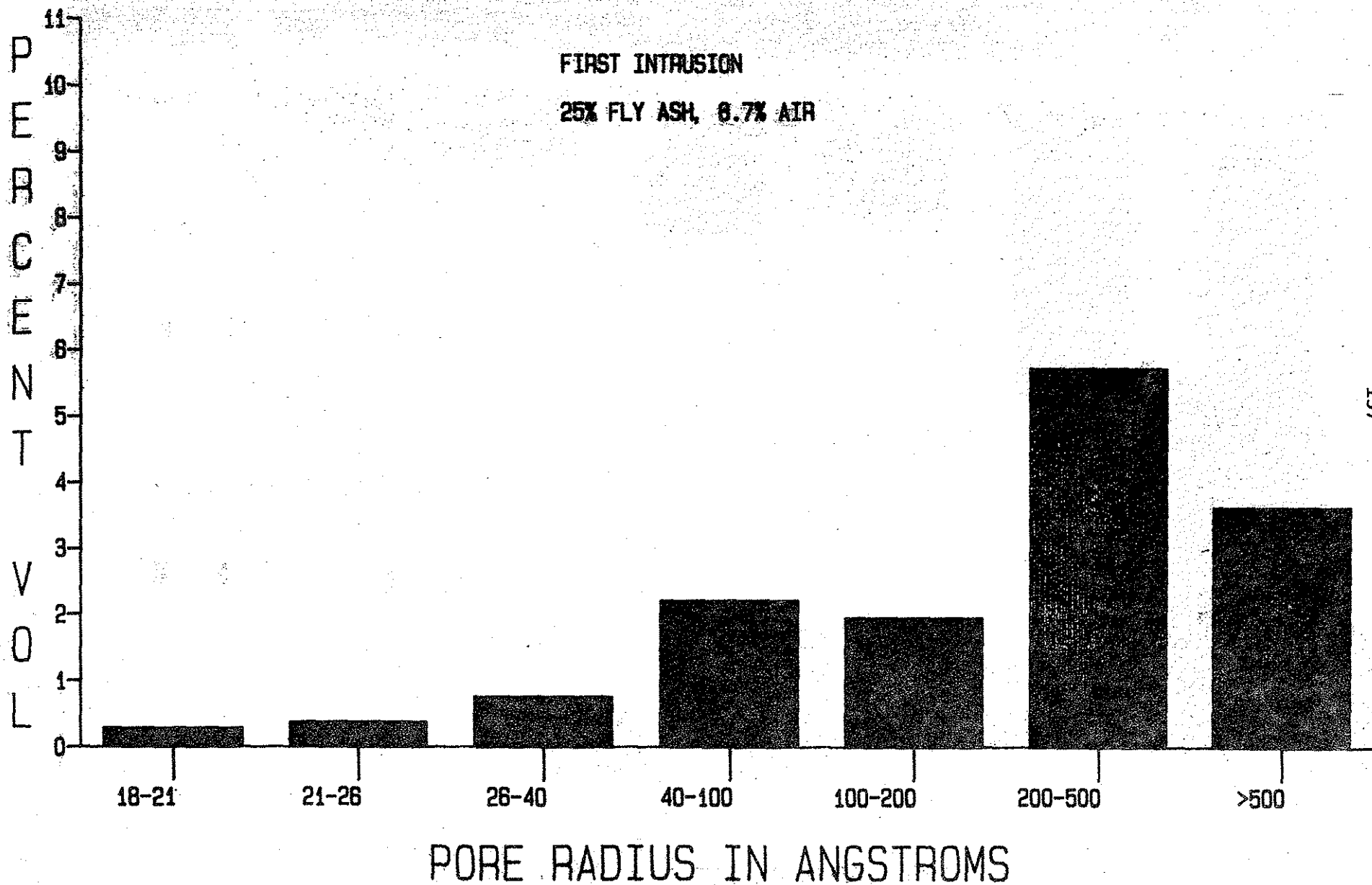
ALDEN 7 DAY CURE

FIRST INTRUSION

25% FLY ASH, 8.7% AIR



ALDEN 28 DAY CURE



MONTOUR 7 DAY CURE

FIRST INTRUSION

25% FLY ASH, 11.2% AIR

